TESIS DE DOCTORADO

MODELO DINÁMICO DE LA CIRCUITERÍA PUSH PULL DEL dNGL

Rubén Ferreiroa García

DEPARTAMENTO: ELECTRÓNICA Y COMPUTACIÓN

PROGRAMA: DOCTORAMIENTO EN NEUROCIENCIA

FACULTAD: BIOLOGÍA

SANTIAGO DE COMPOSTELA

ANO 2017

MODELO DINÁMICO DE LA CIRCUITERÍA PUSH PULL DEL dNGL
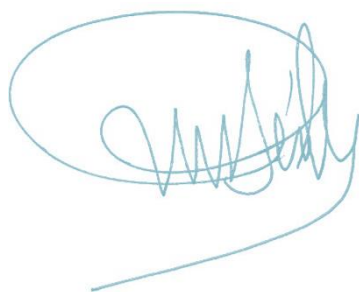
Asdo. ....

Rubén Ferreiroa García

DEPARTAMENTO: ELECTRÓNICA Y COMPUTACIÓN
PROGRAMA: DOCTORAMIENTO EN NEUROCIENCIA
FACULTAD: BIOLOGÍA

SANTIAGO DE COMPOSTELA
ANO 2017

A QUIEN CORRESPONDA:

D. Eduardo Sánchez Vila, profesor del Departamento de Electrónica y Computación de la Universidad de Santiago de Compostela (USC) y director de la presente tesis,

CERTIFICA

Que la presente tesis doctoral titulada "*Modelo Dinámico de la Circuitería Push-Pull del dLGN*" ha sido realizada bajo mi dirección por Rubén Ferreiroa García

Para que así conste y a los efectos oportunos, expide y firma el presente Certificado en Santiago de Compostela en Febrero de 2017

Fdo.: Eduardo Sánchez Vila

INSTITUTO DE NEUROCIENCIAS

En Alicante a 24 de Febrero de 2017

A QUIEN CORRESPONDA:

Luís Martínez Otero, Investigador Científico del CSISC en el Instituto de Neurociencias, centro mixto de la Universidad Miguel Hernández (UMH) y la Agencia Estatal de Consejo Superior de Investigaciones Científicas (CSIC) y codirector de la presente tesis,

CERTIFICA

Que la presente tesis doctoral titulada "*Modelo Dinámico de la Circuitería Push-Pull del dLGN*" ha sido realizada bajo mi codirección por Rubén Ferreiroa García.

Para que así conste y a los efectos oportunos, expide y firma el presente Certificado en San Juan de Alicante en Febrero de 2017

Fdo.: Luís Martínez Otero

Para Marta y Poe

AGRADECIMIENTOS

A Marta y Poe, simple y llanamente, porque me hacen feliz.

A mis padres, Mª Victoria y Rubén, por su interés y preocupación constantes durante todos estos años.

A Eduardo Sánchez y Luis Martínez. Solamente por el hecho de haberlos conocido ya ha merecido la pena realizar este doctorado. Ahora entiendo a qué se refieren cuando dicen que la temática de un doctorado es importante, pero más importante aún es la relación que mantienes con tus tutores.

ÍNDICE:

INTRODUCCIÓN

La información visual se procesa en el cerebro a través de múltiples vías que se originan en diferentes tipos de neuronas ganglionares de la retina y se mantiene relativamente bien segregada a través de núcleo geniculado lateral (dNGL) antes de alcanzar el córtex visual (V1).

El dNGL es la principal localización subcortical encargada de transportar la información visual a la corteza cerebral. En ausencia de esta vía la información visual desaparece. (Figura 1).
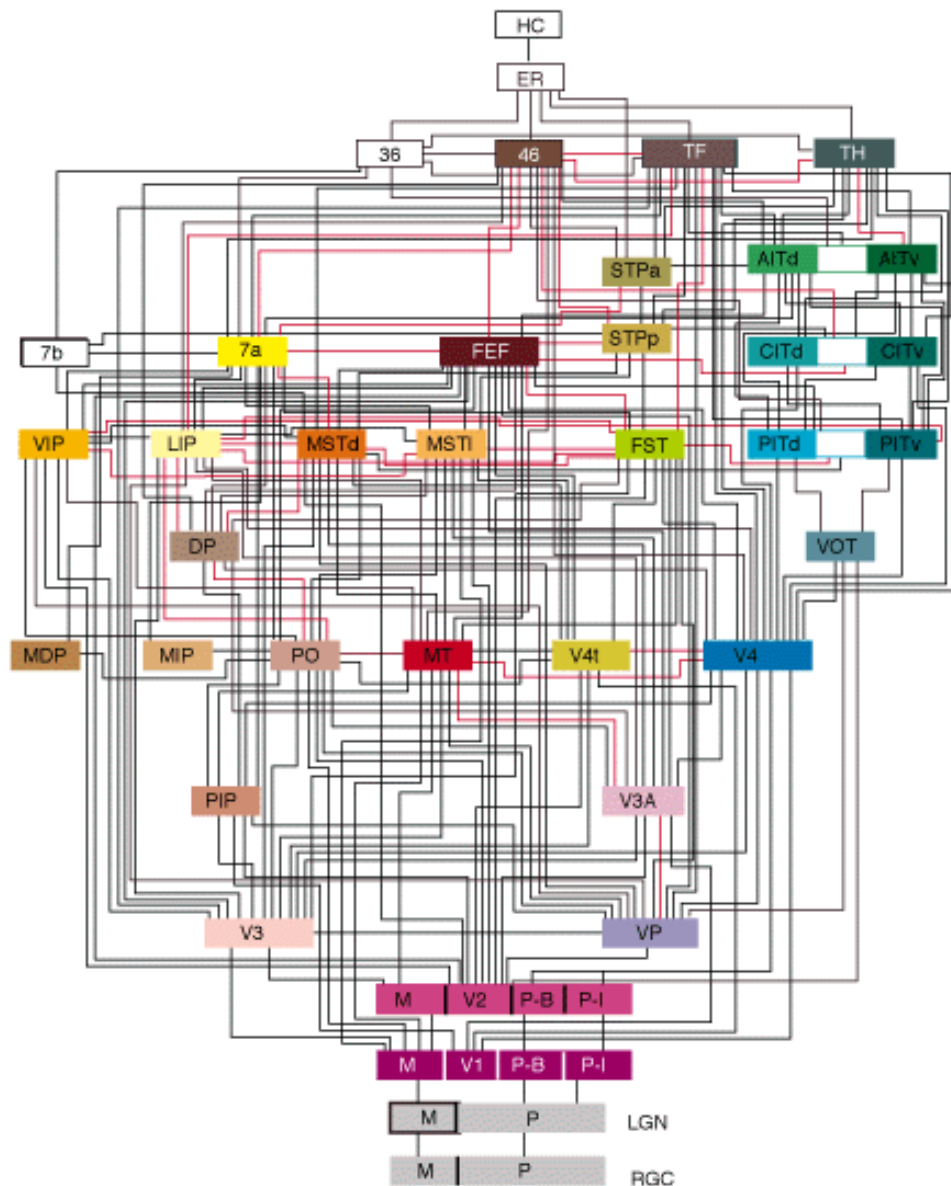

Figura 1. Diagrama de bloques sistema visual (Adaptado de Felleman y Van Essen, 1991).

En el gato, existen dos vías de comunicación entre la retina y el dNGL: la X (parvo celular) e Y (magno celular), que difieren en sus propiedades de respuesta y proyecciones axónicas.

Mientras la mayoría de las aferencias retinianas tipo X proyectan hacia la capa A del NGL, las aferencias retinianas tipo Y divergen en dos capas A y C (Figura 2).
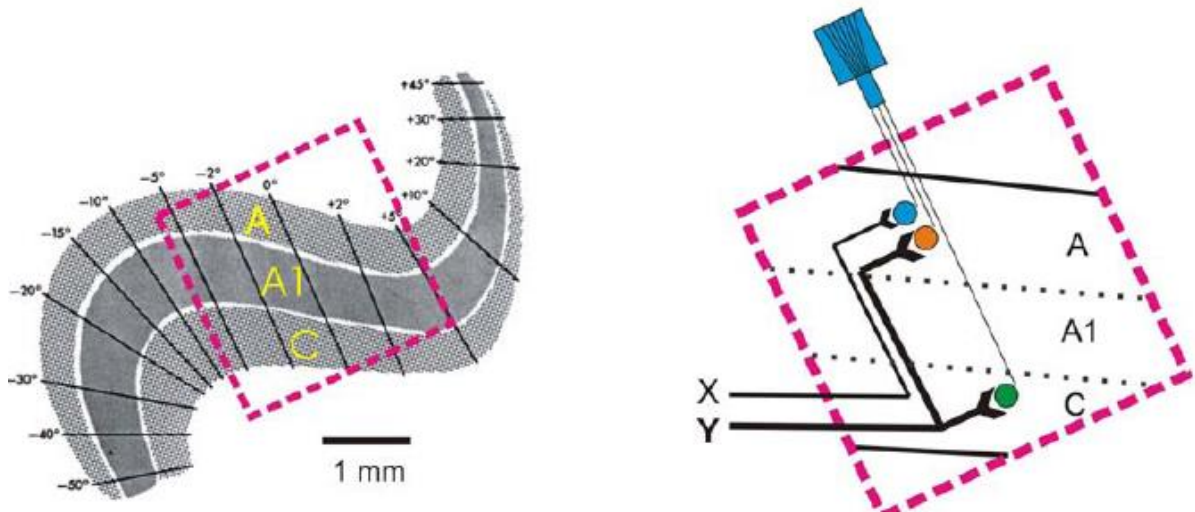

Figura 2. Mapa retinotópico del núcleo geniculado lateral del gato (adaptado de Sanderson 1971) y dibujo que ilustra las grabaciones simultáneas de 3 tipos de células diferentes: célula X de la capa A (XA en azul), célula Y de la capa A (YA en naranja) Y células Y de la capa C (YC en verde).

La presente tesis centra su estudio de la circuitería entre la retina y el dNGL procedente de las aferencias tipo X, las cuales se encuentran mayormente localizadas en la fóvea formando mosaicos con un empaquetamiento hexagonal (Wassle et al., 1981b; Eglen et al., 2005; Borghuis et al., 2008; Gauthier et al., 2009; Liu et al., 2009).

En gato la información de alta resolución es codificada por estas aferencias y enviada a la capa A del dNGL. Esta región está compuesta básicamente por dos tipos de neuronas: células de relevo e interneuronas.

Como se observa en la Figura 3, la estructura del dNGL es compleja puesto que las células de relevo están inervadas por muchas entradas adicionales a las entradas retinianas, que es la principal entrada que será transmitida.

Las entradas no retinianas, que representan aproximadamente el 90-95% de las entradas sinápticas sobre las células de relevo, proceden de neuronas GABAérgicas, células de retículo e interneuronas, más dos entradas exteriores procedentes del feedback de la capa 6 del córtex y proyecciones ascendentes de varios grupos de células dispersos de la formación reticular del tronco del encéfalo. Estas entradas corticales y del tronco además inervan células del retículo e interneuronas.
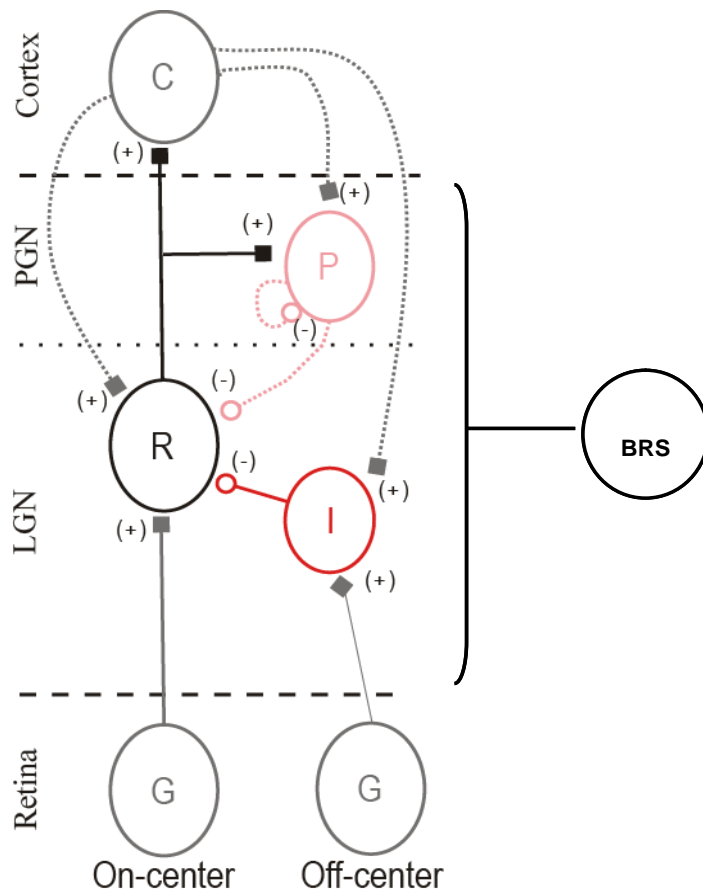
Figura 3. Circuito con la circuitería feedforward y feedback del dLGN.

En la presente tesis nos centramos en la circuitería feedforward que tiene como inputs las células ganglionares de retina y como outputs las células de relevo y las interneuronas del LGN. Hemos analizado tanto el efecto individual del centro del campo receptor (Figura 4) como la contribución conjunta del centro-periferia (Figura 10).

La función que siempre se ha atribuido al dNGL, es la de una mera estación de relevo, es decir el dNGL no realiza ningún tipo de procesamiento relevante de la información que procede de las células ganglionares de la retina. Se asume, por tanto, que los mosaicos de la retina configuran el límite máximo de resolución espacial. Pero el complejo esquema de la circuitería (Figura 10) y que las células de relevo del LGN superan en un factor 2 a las células ganglionares de la retina, (Madarasz et al., 1978; Peters and Payne, 1993) nos hace dudar de tal afirmación. Además en estudios previos se ha demostrado que las aferencias retinianas divergen hacia células de relevo del tálamo, de tal forma que estas reciben valores elevados de convergencia de las retinianas (Cleland et al., 1971a, b; Freund et al., 1985; Mastronarde, 1992; Peters and Payne, 1993; Usrey et al., 1999; Alonso et al., 2001; Yeh et al., 2009; Martínez et al., 2014). Todo esto nos hace pensar que el dLGN está transformando de forma sustancial el mensaje que la retina envía a la corteza visual primaria (V1).

OBJETIVOS

El objetivo general de la tesis es explorar como el núcleo geniculado lateral (dNGL) contribuye al procesamiento de la información visual.

A continuación mostramos una breve descripción de los objetivos particulares que se han tenido en cuenta durante su desarrollo:

1. Analizar el procesamiento de la información espacio-temporal que realiza la circuitería del dNGL (Functional properties of a realistic model of dLGN, Neurocomputing 114(2013)36–44).

    Para ello se ha desarrollado un modelo topológico realista del circuito retinotalámico donde se han tenido en cuenta los centros de los campos receptores con el objetivo de estudiar su dinámica y los efectos sobre los estímulos presentados.
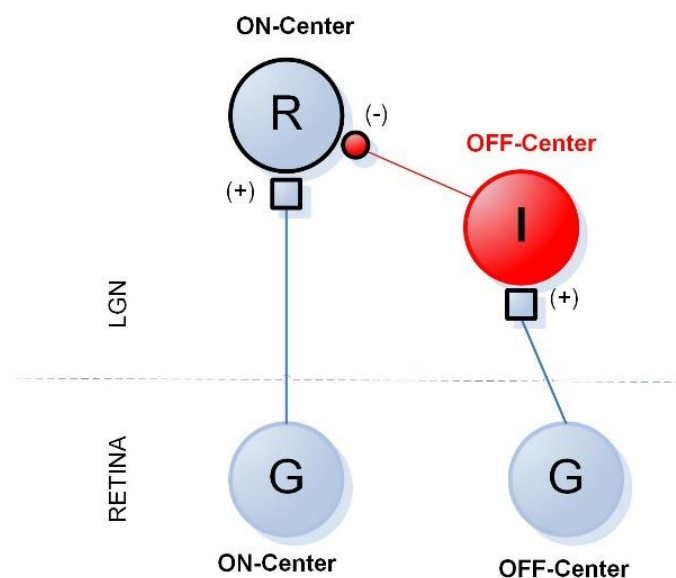

Figura 4. Circuito retinotalámico modelando el centro de los campos receptores.

En concreto nos planteamos responder a las siguientes preguntas:

1.1. ¿Cómo influye la ganancia centro-periferia de los campos receptores de las células ganglionares ON-OFF en el procesamiento del dNGL?

1.2. ¿Cuál es el impacto de la vía inhibitoria a través de la interneurona OFF en el procesamiento del dNGL?

1.3. ¿Cómo influyen los modos de actividad tónica y ráfaga de las células de relevo e interneuronas en el procesamiento del dNGL?

1.4. ¿Cómo influye la adaptación de las células de relevo e interneuronas en el procesamiento del dNGL?

2. Analizar el procesamiento de la información de nitidez y contraste que podría estar realizando la circuitería del dNGL (**Artículo 2:** *Sánchez, E., **Ferreiroa, R.**, Arias, A and Martínez LM. (2017). The indepence of image contrast and sharpness in the early visual pathway / Image sharpness and contrast tuning in the early visual pathway. International Journal of Neural Systems.* Aceptado para publicación con el título pendiente de modificación por el editor.)

Comprobaremos, si es cierta la hipótesis de que el dNGL debería preservar, o incluso mejorar, la de nitidez y el contraste de la representación de los estímulos visuales procedentes de la retina.

Para realizar este estudio dividimos el circuito retinotalámico en dos componentes PUSH y PUSH-PULL, teniendo en cuenta el centro y periferia de los campos receptores.

A continuación se plantean las preguntas abordadas en este estudio:

2.1. ¿Podría la componente PUSH estar realizando un proceso de upsampling?

2.2. ¿Podría el circuito completo recuperar/mejorar los detalles de su presentación retiniana, con el objeto de recobrar y mitigar el impacto del suavizado producido por el proceso de upsampling?

3. Analizar la codificación temporal que realiza el núcleo cuneatus para clasificar estímulos somatosensoriales (**Artículo 3:** *Navarro, J., Sánchez, E., Ferreiroa, R., & Canedo, A. (2015). Classification of somatosensory stimuli on the basis of the temporal coding at the cuneate nucleus. Neurocomputing, 151, 62-68.*)

Para ello, se han realizado cuatro experimentos de clasificación mediante una red feedfordward, entrenada bajo un algoritmo supervisado en el cual, la entrada es un vector que incluye la secuencia de salidas del núcleo cuneatus.

Los errores obtenidos en cada uno de los cuatro problemas de clasificación correlacionan con la complejidad del experimento. El error más bajo corresponde con la clasificación del tamaño del estímulo y el mayor con la identificación de los segmentos del estímulo. Un patrón común se observa en todos los experimentos: 1) el máximo error se obtiene con el vector de entrada más pequeño, 2) el error disminuye a medida que aumenta el tamaño del vector de entrada, 3) el error mínimo se alcanza con un tamaño intermedio del vector de entrada, 4) el error aumenta a medida que el tamaño del vector de entrada aumenta más allá de la longitud óptima. La clasificación óptima se lleva a cabo durante la ventana temporal en la cual, el modelo CN transmite una representación que combina las zonas de mayor contraste y una codificación progresiva de la superficie del estímulo.

Estas dos componentes son decisivas para reducir errores en el reconocimiento y clasificación de los estímulos, las cuales son el resultado del procesamiento que se lleva a cabo en la circuitería del núcleo cuneatus.

En resumen, el modelo predice que el CN crea un tipo de codificación espacio-temporal con el objetivo de realizar tareas de clasificación de estímulos somatosensoriales.

DISCUSIÓN Y CONCLUSIONES

Artículo: Functional properties of a realistic model of dLGN

En el presente artículo hemos demostrado que, efectivamente, el dNGL no es una mera estación de relevo de la información procedente de la retina, sino que participa activamente en el procesamiento del estímulo visual.

Nuestro modelo aporta una explicación a la funcionalidad de los canales ON y OFF del circuito PUSH-PULL (Figura 5). La estructura de los campos receptores centro-periferia del canal ON detecta cambios de contraste y por lo tanto detecta bordes de los estímulos. Efectivamente hemos comprobado que el canal ON está detectando bordes, y que la vía de la inhibición procedente del canal OFF está aportando una función de control de ganancia de los inputs retinianos procedentes del canal ON, con el objetivo de incrementar el contraste en los bordes del estímulo (Figura 5).
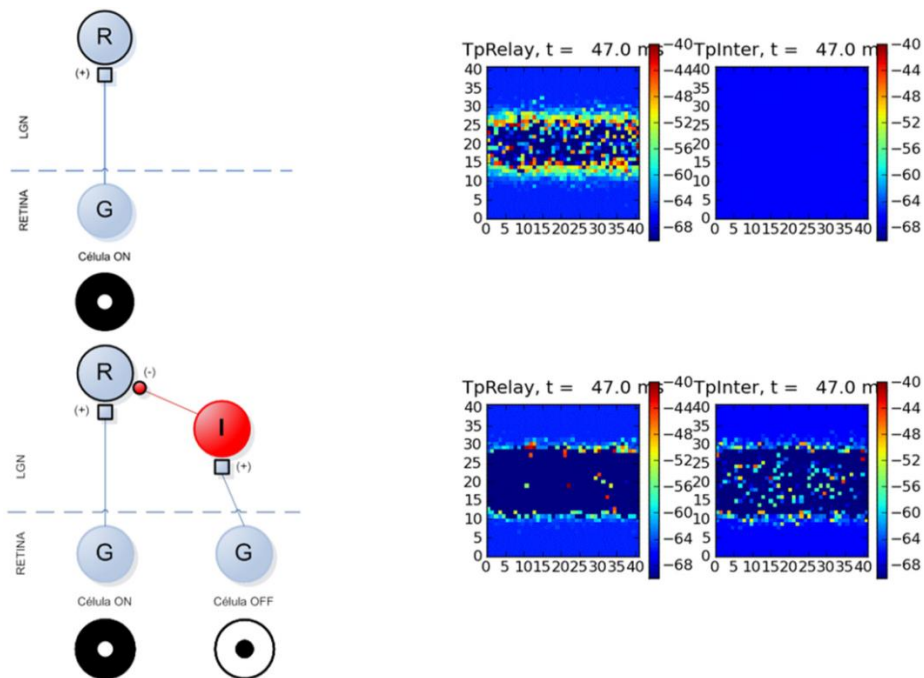
Figura 5. Procesamiento canal ON e impacto del canal inhibitorio OFF. Un estímulo barra horizontal se presenta en el canal ON (arriba izquierda) en t=47ms la actividad de las células del tálamo está centrada mayormente en los bordes del estímulo (arriba derecha). Cuando añadimos las conexiones inhibitorias procedentes del canal OFF (abajo izquierda), la actividad de las células del tálamo a t=47ms muestran una mayor definición en los bordes en relación a las diferentes zonas del estímulo (abajo derecha).

Hemos estudiado como influyen los modos tónico (Figura 6) y ráfaga de las células de relevo e interneuronas en el procesamiento del estímulo visual, descubriendo que:

- La configuración en la cual las células de relevo e interneuronas presentan modo tónico, es en la que obtenemos la mejor deteccion de bordes de nuestro estímulo (Figura 6).
- El tiempo de detección de bordes del estímulo se reduce a medida que el potencial de membrana de las células de relevo e interneuronas es más tónico.
- Cuando las células de relevo e interneuronas se comportan simultaneamente en modo ráfaga comprobamos que la detección de bordes es deficiente (Figura 7).
- Cuando las células de relevo y interneuronas se comportan en modo tónico/ráfaga y viceversa, la deteccción de bordes es más eficaz cuando las de relevo están en modo tónico y las interneuronas en modo ráfaga (Figura 7).
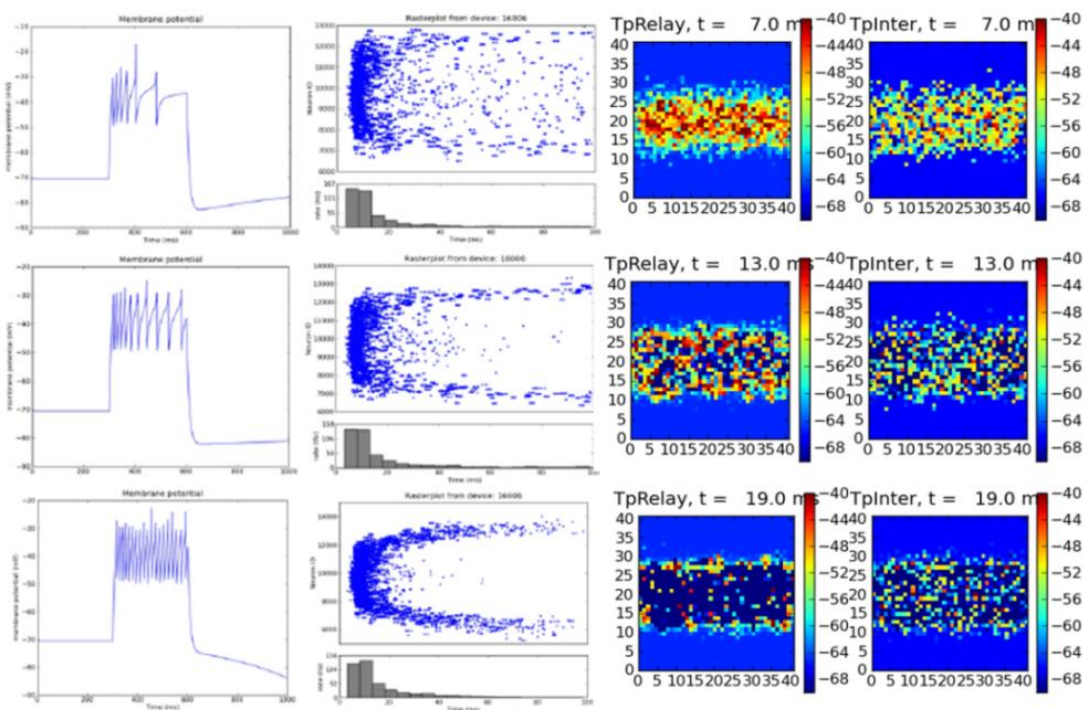
Figura 6. Impacto de la actividad tónica en el dNGL. La figura ilustra el potencial de membrana para una célula de relevo e interneurona (columna izquierda). La figura del raster nos indica la actividad de las células talámicas a lo largo de una sección longitudinal de la capa del tálamo (columna central). En la columna de la derecha tenemos la actividad de toda la población de las células de relevo para un instante de tiempo (columna derecha). A medida que el potencial de membrana de las células de relevo e interneuronas se vuelve más tónico conseguimos una mejor percepción de los bordes del estímulo tipo barra.
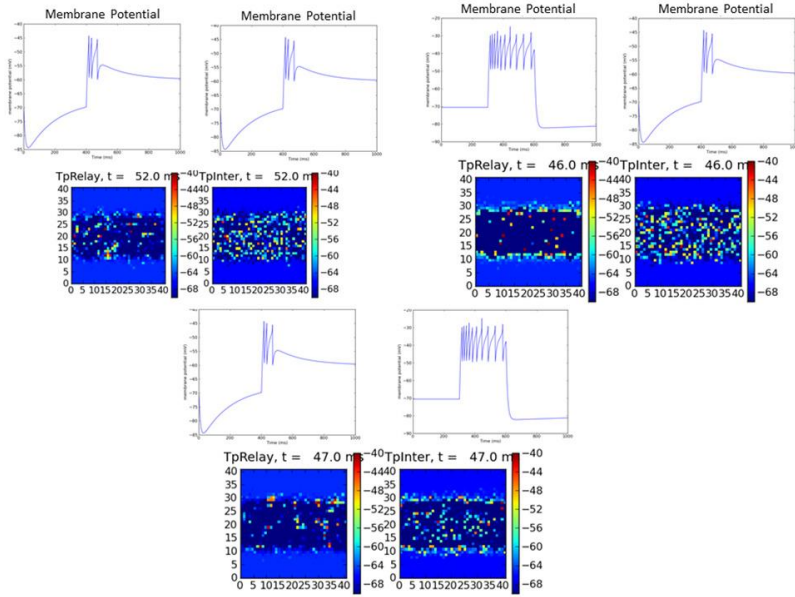
Figura 7. Impacto de la actividad modo ráfaga en el dNGL. La figura muestra distintas configuraciones del potencial de membrana para una célula de relevo e interneurona y la actividad de toda la población del dNGL cuando presentamos un estímulo tipo barra al circuito. Los bordes del estímulo se detectan mejor cuando el potencial de membrana de las células de las células de relevo se encuentra en modo tónico y las interneuronas en modo ráfaga (arriba derecha).

También hemos visto en el modelo, que el tamaño de la representación del estímulo en el dNGL varía en función del grado de contraste entre el estímulo y el fondo (Fig. 8). Para ello hemos presentado un estímulo circular con diferentes grados de contraste con respecto al fondo y medimos para cada uno de ellos el radio en pixels en su respectiva representación en el dNGL.
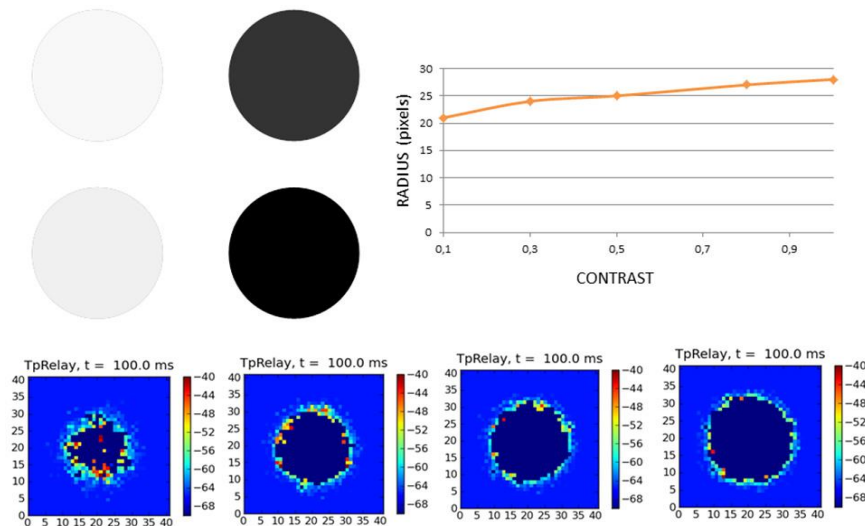
Figura 8. Procesamiento del dNGL depende del contraste. Incrementando los valores de contraste del estímulo (arriba-izquierda), conduce a incrementos de los valores del radio del estímulo percibido en el dNGL (arriba-derecha). La actividad a la salida del circuito del dNGL muestra como el dNGL percibe mejor el estímulo circular, cuando el contraste se incrementa de izquierda a derecha (abajo).

23

Hemos realizado, también, simulaciones del circuito PUSH-PULL del dNGL, modificando el desfase en la adaptación (parámetro b) del modelo de neurona AdEx (Adaptive exponential integrate-and-fire model) entre las células de relevo e interneuronas, observando una mejora en el tiempo de detección de los bordes del estímulo (Figura 8, articulo Functional properties of a realistic model of dNGL) .

Variando la contribución centro-periferia (funcion diferencia de gaussianas) de las células ganglionares, el circuito es capaz de detectar los bordes de los estímulos con mayor nitidez (Figura 4, articulo Functional properties of a realistic model of dLGN).

Algunas de las limitaciones al modelo se centran en que:

- No hemos considerado la dependencia temporal de los campos receptores. Hoy sabemos que la estructura de los campos receptores varia con el tiempo (Figura 9, Gregory C. DeAngelis).
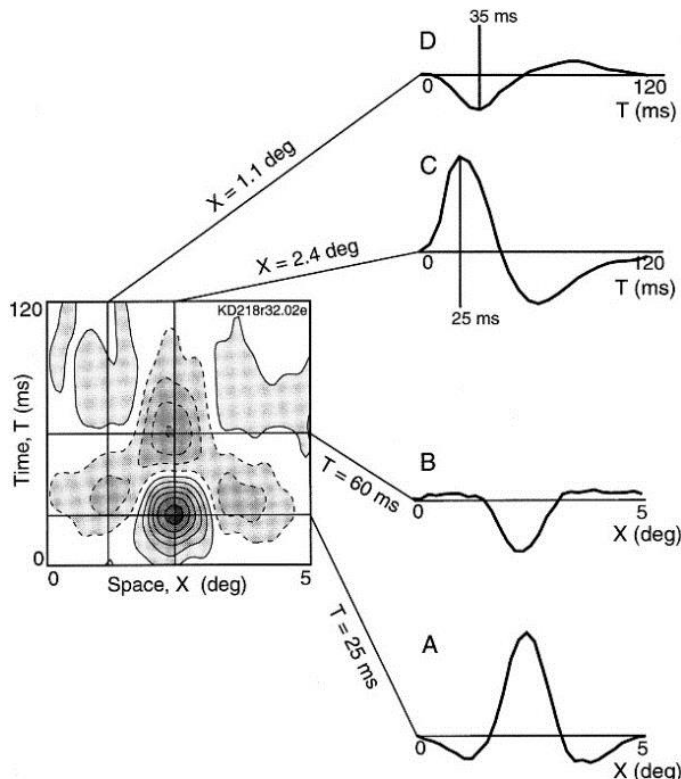
Figura 9. Construcción e interpretación de los perfiles de los campos receptores espacio-temporales. El panel A y B, perfiles campos receptores en diferentes instantes de tiempo. Panel C y D respuesta temporal obtenida cortando a través del eje espacial X (Daqing Cai, Gregory C. Deangelis, Ralph D. Freeman).

- El modelo pelota es una simplificación y presenta claras limitaciones al no incluir árbol dendritico, axón ni terminal presináptica.

- La activación del canal de sodio se asume instantanea. En el modelo Hodgkin-Huxley la activción de la corriente de sodio (mediante la variable m) es rápida pero retarda la evolucion del voltaje.
- El instante en el que se produce el descenso del potencial de acción es controlado por la corriente de potasio y parcialmente por la inactivación del canal de sodio, en el modelo no se ha considerado este comportamiento. El voltage desciende hacia un valor V_{reset} una vez se genera el potencial de acción.
- El tiempo refractario se representa mediante el reset del voltaje y las variables de adaptación, mientras que en las neuronas reales después del tiempo refractario se observa un incremento del umbral de disparo de la neurona.
- Hemos considerado una constante de tiempo de la corriente de adaptación. Esto es una enorme simplificación puesto que la adaptación ocurre en diferentes escalas de tiempo.

Los parámetros del modelo se pueden ajustar a las respuestas de las células de relevo e interneuronas del dNGL utilizando simples protocolos electrofisiológicos que son descritos en (Brette and Gerstner, 2005).

Los siguientes pasos a seguir en el estudio serían, la comparacion entre los resultados que predice el modelo y la actividad observada experimentalmente en el laboratorio. Para facilitar esta comparación se podría incorporar al circuito un modelo de neurona mas realista, definiendo las corrientes de los canales iónicos particulares para las células de relevo e interneuronas del dNGL.

Artículo: Image sharpness and contrast tuning in the early visual pathway

Los mosaicos estereotipados que forman las células ganglionares de la retina codifican información de alta resolución de la escena visual para su posterior procesamiento en V1, previo paso por la estación de relevo dNGL. Como las células del dNGL superan en gran número a sus inputs retinianos, el dNGL podría estar generando un mapa de interpolación más denso y empaquetado que mejoraría la representación espacial del estímulo visual en presencia de ruido (Martinez et al., 2014).

La interpolación introduce un compromiso entre la imagen borrosa y la calidad en la percepción de los bordes. Utilizando un simple modelo topológico de las conexiones retinotalámicas se ha descubierto una disposición específica de excitación e inhibición entre los centros de los campos receptores de las células de relevo que puede contrarrestar los efectos de la interpolación, aumentando la pendiente de las transiciones de luminancia en los bordes (Martínez et al., 2014).

En nuestros trabajos previos (Functional properties of a realistic model of dLGN) considerábamos solamente la estructura sináptica de los centros de los campos receptores talámicos, sin embargo los campos receptores del tálamo son espacialmente complejos, mostrando una estructura con doble oponencia. Tanto el centro como la periferia, estímulos de polaridades opuestas evocan respuestas de signo opuesto. Por tanto cuadrados blancos en el centro del campo receptor de una célula ON-center evoca una despolarización mientras que cuadrados negros presentados en la misma localización evocan inhibición (operando como un mecanismo PUSH-PULL), y tendremos la situación opuesta si el estímulo es presentado en la periferia. Una disposición espacial complementaria de la excitación e inhibición aparece también en las células OFF-center (Hirsch et al., 2015).
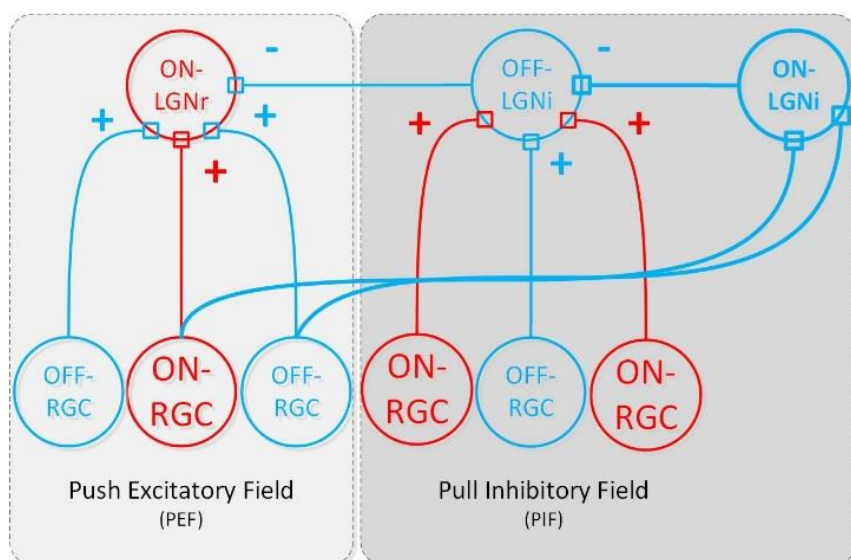

Figura 10. Circuito retinotalámico completo con el campo excitador Push y el campo inhibidor Pull. Se han incluido las periferias de ambos campos para completar el circuito de la Figura 4.

Los inputs excitatorios en cada compartimento del dNGL proceden de células de la retina (RGCs) del mismo signo (On u Off) mientras que la inhibición es enrutada a través de las interneuronas locales por las células de la retina (RGCs) de centro de signo opuesto (Figura 10).

Utilizando un modelo de dinámico que simula la respuesta en espigas de potencial de las neuronas, nos preguntamos cómo los diferentes componentes celulares del circuito retinotalámico, con sus campos centro-periferia podrían contribuir al procesamiento de la información de alta resolución de la escena visual.

El modelo de neurona utilizado es el de Izhikevich (Izhikevich, 2003) con este modelo en función de los parámetros podemos reproducir diferentes comportamientos del potencial de acción tanto para la células de relevo como para las interneuronas.

Nuestros resultados muestran que el dNGL utiliza análogamente técnicas que se utilizan en el procesamiento de imágenes, para mejorar los detalles finos que podrían perderse durante el proceso de interpolación.

En primer lugar un proceso de sharpening o resalte de bordes y en segundo lugar un proceso de contrast stretching con el fin de amplificar la diferencia de los niveles de luminancia en ambas caras de un borde. Curiosamente hemos encontrado que la mejora de la nitidez y contraste son producidas independientemente por diferentes componentes del campo receptor talámico. El campo excitador PUSH provocaría una mejora de la nitidez, mientras el campo inhibidor PULL, como previamente estudiaron Martínez et al. (2014) y Hirsch et al. (2015), ampliaría el contraste incrementando el rango dinámico de las respuestas visuales (Figura 11).

- **Salida retina**: de acuerdo con la hipótesis de código eficiente, la función de la retina es transformar la correlación espacial en un conjunto de salidas decorrelacionadas (Barlow, 1961; Srinivasan et al, 1982; Atick and Redlich, 1992; Dan et al., 1996; Wang et al., 2010). Por tanto la mejor discretización de la función diferencias de gaussianas continua será la opción, Medium-gain DoG Kernel descrita en Sánchez et al. (2017). La vía visual temprana debe maximizar la fiabilidad con la que transmite el mensaje a la corteza visual aumentando la información mutua entre el estímulo visual y la respuesta que evoca (Linsker, 1987; Van Hateren, 1992). Teniendo en cuenta esto, el mejor Kernel será aquel que preserve una respuesta lo más similar posible al estímulo de entrada, en este caso la mejor discretización es Zero-gain DoG kernel descrita en Sánchez et al. (2017). Dado este compromiso entre eficiencia y fiabilidad del mensaje, las propiedades del kernel retiniano podrían cambiar dinámicamente dependiendo de las propiedades de la entrada (señal-ruido, luminancia media, contraste, etc.) y podría hacerlo en diferentes regiones de la imagen visual.

- **Contribución del cableado del dNGL en la codificación de la imágen**: el proceso de upsampling entre la retina y el dNGL, en combinación con la operación de interpolación a través de la agregación ponderada de pesos de las salidas de la retina, determina el mensaje que cada célula ganglionar envía a un número de unidades del

dNGL. Esta disposición distribuye el mismo mensaje a través de diferentes canales, añadiendo por tanto redundancia y aumentando la fiabilidad del código generado por el dNGL. Sin embargo un aumento de la redundancia está limitado por el cableado estadísticamente aleatorio del circuito retino-talámico que favorece la diversidad de campos receptores del dNGL, reduciendo así la dependencia entre las unidades del dNGL (Martínez et al., 2014) y mejorando por tanto la eficiencia del código. Curiosamente en línea con el procesamiento que se realiza en la retina, discutido anteriormente, el circuito retino-talámico parece estar sujeto a un compromiso entre fiabilidad y eficiencia.

- **Sharpening a través de la excitación de signo opuesto en las células de relevo**: Sharpening es una técnica popular en fotografía digital y procesamiento de señales para detectar y resaltar los bordes de una imagen. Varios operadores y algoritmos se han propuesto para llevar a cabo esta operación (González and Woods, 2008): derivadas de primer y segundo orden, filtros unsharp masking, el operador Canny, etc. Sin embargo ninguno de ellos incluye interacciones excitadoras laterales de signo opuesto. El método más conocido es probablemente el algoritmo Marr-Hildreth que utiliza el Laplaciano de una función Gaussiana como kernel para detectar bordes o transiciones de luminancia. La versión discreta de esta función es una matriz con coeficientes positivos en el centro y negativos en la periferia. Esta disposición de coeficientes positivos y negativos se asemeja al perfil de una distribución espacial de una diferencia de Gaussianas, el paradigma utilizado para modelar los campos receptores de la retina y el tálamo. Esta similitud apoya la idea de que las neuronas en la vía visual temprana realizan operaciones de detección de bordes. En nuestro modelo el circuito retino-talámico, sin embargo, el sharpening es implementado de manera diferente por la interacción de un centro excitador y una periferia excitadora de signo opuesto en lo que denominamos circuito PUSH. Este resultado inesperado se explica por el hecho de que la periferia excitadora se origina a partir de las respuestas originadas por las células ganglionares tipo OFF.

- **Independencia de la nitidez y contraste en el dNGL**: el mecanismo de sharpening o nitidez podría ser una forma de mejora de la nitidez local. Por otro lado, resultados previos (Martínez et al., 2014) nos muestran que la inhibición de signo opuesto (pull) del centro del campo receptor, cubre una región del espacio visual mayor que la excitación del centro procedente del PUSH, reflejando así una mayor convergencia de la entradas retinianas hacía las interneuronas del tálamo (Montero, 1981; Van Horn et al., 2000). Nuestros resultados actuales con la versión dinámica del modelo corroboran que la estructura PUSH-PULL de los centros de los campos receptores permiten la interacción entre los canales ON y OFF en el dLGN, incrementando así el rango dinámico del circuito (Barlow, 1981; Pouille et al., 2009; Martínez et al., 2014), eliminando a la vez la redundancia introducida en el proceso de interpolación y realzando el contraste local alrededor de las transiciones de luminancia. Es importante saber que las operaciones de mejora de nitidez y contraste se realizan a nivel local e independiente una de la otra. La naturaleza local de estas operaciones permitiría ajustar la nitidez de forma independiente en diferentes zonas de la imagen visual. Esta

posibilidad es muy interesante por dos motivos: primero porque las transiciones de luminancia pueden diferenciarse notablemente en las imágenes naturales dada la independencia entre luminancia y contraste (Mante et al., 2005); segundo, porque la estructura y la densidad relativa de los mosaicos de la retina y el dNGL, y por tanto grado del proceso de interpolación, puede variar sustancialmente en diferentes localizaciones de circuito retino talámico (Ringach, 2007; Martínez et al., 2014). Además, la independencia de las operaciones de mejora de nitidez y contraste hacen posible la aplicación de ventanas temporales diferentes. Si asumimos que la parte del circuito PUSH se activa antes que la PULL, la corteza visual recibirá una primera versión del input visual con mejora de la nitidez seguida por una representación con mejora del contraste. Curiosamente ambas formas de mejora no pueden ajustar a la vez en el dLGN puesto que el circuito PIF-Center-Alone (Figura 11) tiende a suprimir los picos negativos y positivos introducidos por el circuito PEF-Center-Surround (Figura 11) alrededor de las transiciones de luminancia (Sánchez et al., 2017). Debe existir entonces una relación entre la retina y el dNGL con el fin de optimizar el comportamiento de ambos circuitos.
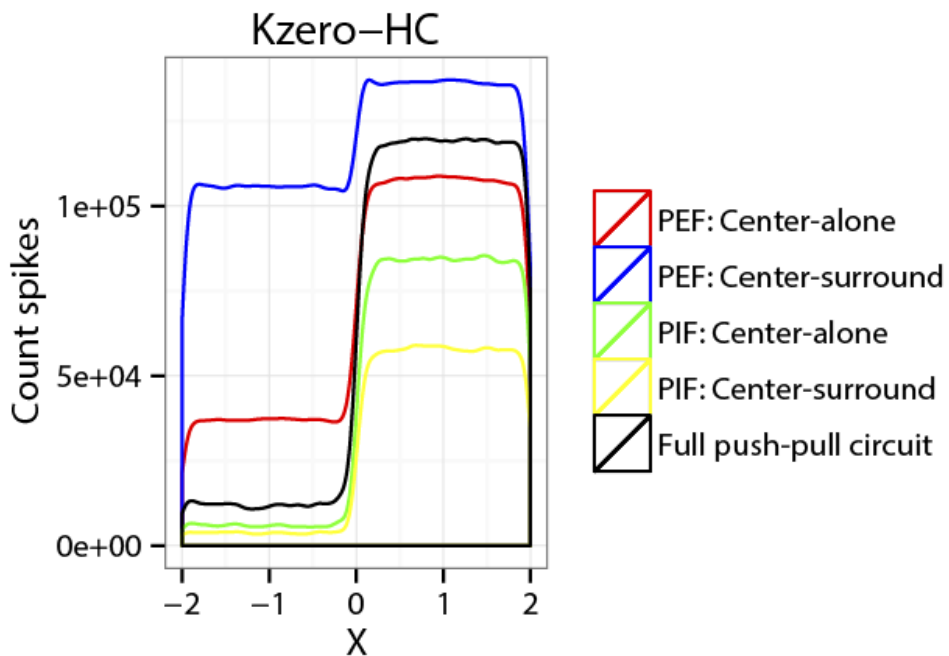
Figura 11. Resultados circuito push-pull completo para Kzero-HC (Image sharpness and contrast tuning in the early visual pathway)

En conclusión, las imágenes requieren de una alta nitidez y resolución para ser percibidas con mayor calidad y parece plausible que la vía visual temprana, a través de una distribución espacial precisa de circuitos excitatorios e inhibitorios, podría estar diseñada para tal fin.

Artículo: Classification of somatosensory stimuli on the basis of the temporal coding at the cuneate nucleus

Hemos analizado el procesamiento espacio temporal del estímulo visual y somatosensorial que se realizan en los núcleos dNGL y CN (núcleo cuneatus).

Para el análisis del dNGL se ha utilizado un modelo más realista de las neuronas que el CN. El modelo de neuronas utilizado para el CN es basado en unidades McCulloch–Pitts, sin embargo en el dNGL el modelo de neuronas es Adaptative Exponential Integrate and Fire (AEIaF) lo cual implica un mayor grado de detalle en la descripción del comportamiento del potencial de acción.

Los resultados obtenidos de la codificación temporal progresiva en el núcleo cuneatus ante un estímulo somatosensorial se muestran en la Figura 3 del artículo de Navarro et al. (2015) en los paneles A1 y A2. Ambos estímulos son cuadrados que incluyen un patrón con diferentes grados de regularidad: el primero es ligeramente suavizado por la media de un filtro Gaussiano, el segundo preserva el mismo perfil de intensidad. La respuesta temporal del CN antes estos estímulos se muestran en el panal A1 y A2. Lo que se observa es una codificación progresiva empezando por las zonas de baja regularidad y progresivamente avanzando hacia zonas de alta regularidad. Es interesante enfatizar que las zonas de baja regularidad en A1 son las zonas del perímetro del cuadrado, mientras que en A2 están localizadas en el interior del estímulo. En resumen parece que el circuito del núcleo cuneatus (CN) transmite la información en dos fases, la primera sería una fase en la se aprecia un efecto de relleno y una segunda fase donde se transmite una representación más estable del estímulo. El modelo del CN genera una codificación espacio-temporal, la cual tiene bastante similitud con la propuesta para el dNGL.

BIBLIOGRAFÍA

Ferreiroa, R., & Sánchez, E. Functional properties of a realistic model of dLGN Neurocomputing 114 (2013) 36–44

Navarro, J., Sánchez, E., Ferreiroa, R., & Canedo, A., Classification of somatosensory stimuli on the basis of the temporal coding at the cuneate nucleus. Neurocomputing 151 (2015) 62–68.

Sánchez, E., Ferreiroa, R., Arias, A.,& Martínez, L.M., (2017). The indepence of image contrast and sharpness in the early visual pathway / Image sharpness and contrast tuning in the early visual pathway. International Journal of Neural Systems. Aceptado para publicación con el título pendiente de modificación por el editor.

E.A.Allen, R.D.Freeman, Dynamic spatial processing originates in early visual pathways, J.Neurosci.26 (45) (2006)11763–11774.

J.M.Alonso, C.I.Yeh, C.Weng, C.Stoelzel, Retinogeniculate connections: a balancing act between connection specificity and receptive field diversity, Prog. BrainRes.154 (2006).

R.Brette, W.Gerstner, Adaptive exponential Integrate-and-Fire model as an effective description of neuronal activity, J.Neurophysiol.94 (5) (2005) 3637–3642.

C.I.Yeh, C.R.Stoelzel, C.Weng, J.M.Alonso, Functional consequences of neural divergence within the retinogeniculate pathway, J.Neurophysiol.101 (2009).

M.Madarasz, J.Gerle, F.Hajdu, G.Somogyi, T.Tömbol, Quantitative histological studies on the lateral geniculate nucleus in the cat.II.Cell numbers anddensitiesintheseverallayers, J.Hirnforsch.19 (2) (1978) 159–164.

L.M.Martinez, Q.Wang, R.C.Reid, C.Pillai, J.M.Alonso, F.T.Sommer, J.A. Hirsch, Receptive field structure varies with layer in the primary visual cortex, Nat.Neurosci.8 (3) (2005)372–379.

D.A.McCormick, J.Huguenard, A model of the electrophysiological properties of thalamocortical relay neurons, J.Neurophysiol.68 (1992) 1384–1400.

J.R.Huguenard, D.A.McCormick, Voltage clamp simulations of currents involved in rhythmic oscillations in thalamic relay neurons, J.Neurophysiol.68 (1992)1373–1383.

M.Molano, M.M.Rodrıguez, L.M.Otero, DEA. How the thalamus changes what the cat's eye tells the cat's brain, 2009.

M.O.Gewaltig, M.Diesmann, Nest (neural simulation tool), Scholarpedia 2 (4) (2007)1430.

D.L.Ringach, Haphazard wiring of simple receptive fields and orientation columns in visual cortex, J.Neurophysiol.92 (2007)468–476.

W.M.Usrey, J.B.Reppas, R.C.Reid, Specificity and strength of retinogeniculate connections, J.Neurophysiol.82 (1999)3527–3540.

Alonso, J. M., W. M. Usrey, et al. (2001) Rules of connectivity between geniculate cells and simple cells in cat primary visual cortex. J Neurosci 21:4002-4015.

Anishchenko, A., Greschner, M., Elstrott, J., Sher, M., Litke, A.M., Feller, M.B. and Chichilnisky, E.J. (2010) Receptive Field Mosaics of Retinal Ganglion Cells Are Established Without Visual Experience. J Neurophysiol. 103:18561864.

Arias, A., Sánchez, E., Martinez, L. (2015) Retinal DoG filters: effects of the discretization process. Artificial Computation in Biology and Medicine. Lecture Notes in Computer Science. 9107:249-257.

Barlow, H. B. (1961). Possible principles underlying the transformations of sensory messages. 217-234.

Blitz, D.M., and Regehr, W.G. (2005). Timing and specificity of feed-forward inhibition within the LGN. Neuron 45:917-28.

Carandini, M., Horton, J. C., and Sincich, L. C. (2007). Thalamic filtering of retinal spike trains by postsynaptic summation. Journal of Vision, 7(14), 20.

Cleland, B.G., Dubin, M.W., and Levick, W.R. (1971).Sustained and transient neurones in the cat's retina and lateral geniculate nucleus.J.Physiol.217:473-496.

Crunelli, V. Haby, M., Jassik-Gerschenfeld, D., Leresche, N., and Pirchio, M. (1988).Cl^- - and K^+ -dependent inhibitory postsynaptic potentials evoked by interneurons of the rat lateral geniculate nucleus. Physiol. 399:153-176.

Dan, Y., Atick, J.J., and Reid, R.C. (1996). Efficient coding of natural scenes in the lateral geniculate nucleus: experimental test of a computational theory.J. Neurosci.16:3351-62.

Eglen, S. J., Diggle, P. J., and Troy, J.B. (2005). Homotypic constraints dominate positioning of on- and off-center beta retinal ganglion cells. Vis. Neurosci. 22:859-71.

Enroth-Cugell C, Robson JG. (1966). The Contrast Sensitivity of Retinal Ganglion Cells of the Cat. JPhysiol. 187: 517-523.

Enroth-Cugell C, Robson JG. (1984). Functional characteristics and diversity of cat retinal ganglion cells. Basic characteristics and quantitative description. IOVS. 25: 250-67.

Freund, T. F., K. A. Martin, et al. (1985). Innervation of cat visual areas 17 and 18 by physiologically identified X- and Y- type thalamic afferents. I. Arborization patterns and quantitative distribution of postsynaptic elements.J. Comp. Neurol. 242:263-274.

Gauthier, J. L., Field, G. D., Sher, A., Greschner, M., Shlens, J., Litke, A. M., and Chichilnisky, E. J. (2009). Receptive fields in primate retina are coordinated to sample visual space more uniformly. PLoS biology, 7(4), 747.

Gonzalez R, and Woods R. (2008). Digital Image Processing. Prentice Hall.

Hamos, J.E., Van Horn, S.C., Raczkowski, D., Uhlrich, D.J., and Sherman SM. (1985).Synaptic connectivity of a local circuit neurone in lateral geniculate nucleus of the cat. Nature317:618-21.

Hirsch, J.A., Wang, X., Sommer, F.T. and Martinez, L.M. (2015) How inhibitory circuits in the thalamus serve vision.Annu. Rev. Neurosci. 38:309-329.

Hubel, D.H. and Wiesel, T.N. (1961) Integrative action in the cat's lateral geniculate body. J. Physiol.155:385-398.

Izhikevich, E. M. (2003). Simple model of spiking neurons. IEEE Transactions on neural networks, 14(6), 1569-1572.

Kuffler, S.W. (1953) Discharge patterns and functional organization of the mammalian retina. J. Neurophysiol.16:37-68.

LeVay, S., and Ferster D. (1979).Proportion of interneurons in the cat's lateral geniculate nucleus. Brain Res. 164:304-8.

Linsker, R. (1988). Self-organization in a perceptual network. Computer, 21(3), 105-117.

Liu, Y.S., Stevens, C.F., and Sharpee, T.O. (2009).Predictable irregularities in retinal receptive fields.Proc. Natl. Acad. Sci. USA. 106:16499-504.

Mante, V., Frazor, R.A., Bonin, V., Geisler, W.S. and Carandini, M. (2005) Independence of luminance and contrast in natural scenes and in the early visual system. Nat Neurosci. 8:1690-1697.

Martinez, L.M., Molano-Mazón, M., Wang, X., Sommer, F.T. and Hirsch, J.A. (2014) Statistical wiring of thalamic receptive fields optimizes spatial sampling of the retinal image. Neuron 81:943-956.

Mastronarde, D.N. (1992). Nonlagged relay cells and interneurons in the cat lateral geniculate nucleus: receptive field properties and retinal inputs. Vis.Neurosci. 8:407-41.

Montero, V.M. (1991).A quantitative study of synaptic contacts on interneurons and relay cells of the cat lateral geniculate nucleus. Exp. Brain Res. 86:7-270.

Peters, A. and B. R. Payne (1993).Numerical relationships between geniculocortical afferents and pyramidal cell modules in cat primary visual cortex.
Cereb Cortex 3:69-78.

Pouille, F., Marin-Burgin, A., Adesnik, H., Atallah, B.V., and Scanziani, M. (2009). Input normalization by global feedforward inhibition expands cortical dynamic range. Nat. Neurosci. 12:1577-85.

Ringach, D.L. (2007). On the origin of the functional architecture of the cortex. PLoS One 2, e251.

Srinivasan, M. V., Laughlin, S. B., and Dubs, A. (1982). Predictive coding: a fresh view of inhibition in the retina. Proceedings of the Royal Society of London B: Biological Sciences, 216(1205), 427-459.

Ruderman, D.L. and Bialek, W. (1992) Seeing beyond the Nyquist limit. Neural Comput. 4:682-690.

Stone, J., and Campion, J.E. (1978). Estimate of the number of myelinated axons in the cat's optic nerve.J. Comp. Neurol. 180:799-806.

Usrey, W. M., Reppas, J.B. and Reid, R.C. (1999). Specificity and strength of retinogeniculate connections.J Neurophysiol 82:3527-3540.

Van Hateren, J. H. (1992). A theory of maximizing sensory information. Biological cybernetics, 68(1), 23-29.

Van Horn, S.C., Erisir, A., and Sherman, S.M. (2000).Relative distribution of synapses in the Alaminae of the lateral geniculate nucleus of the cat.J. Comp.Neurol. 416:509-520.

Wang, X., Hirsch, J.A., and Sommer, F.T. (2010).Recoding of sensory information across the retinothalamic synapse. J. Neurosci. 30:13567-13577.

Wässle, H., Boycott, B.B., and IllingR.B. (1981a). Morphology and mosaic of on- and off-beta cells in the cat retina and some functional considerations. Proc. R. Soc. Lond. B Biol. Sci. 212:177-95.

Wässle, H., Peichl, L., and Boycott, B.B. (1981b). Dendritic territories of cat retinal ganglion cells. Nature 292:344-5.

Wiesel, T.N. (1959) Recording inhibition and excitation in the cats retinal ganglion cells with intracellular electrodes. Nature 183:264-265.

Yeh, C. I., Stoelzel, C.R., Weng, C. and Alonso, J.M. (2009).Functional consequences of neuronal divergence within the retinogeniculate pathway. J Neurophysiol 101:2166-2185.

J. Aguilar, C.Soto, C.Rivadulla, A. Cañedo, The lemniscal-cuneaterecurrent excitation is suppressed by strychnine and enhancedby GABAA antagonists in the anaesthetized cat, Eur.J.Neurosci.16 (2002)1697–1704.

K.J. Berkley, R.J.Badell, A.Blomqvist, M.Bull, Output systems of the dorsal column nuclei in the cat, BrainRes.Rev.11 (1986)199–225.

K.H. Britten, M.N.Shadlen, W.T.Newsome, J.A.Movshon, The analysis of visual motion: a comparison of neuronal and psychophysical performance, J.Neurosci. 12 (1992)4745–4765.

A. Canedo, L.Martinez, J.Marino, Tonic and bursting activity in the cuneate nucleus of the chloralose anesthetized cat, Neuroscience 84(2) (1998)603–617.

A. Canedo, J.Aguilar, J.Marino, Lemniscal recurrent and transcortical influences on cuneateneurons, Neuroscience 97(2) (2000)317–334.

H.G.J.M. Kuypers, J.D.Tuerk, The distribution of the cortical fibers within the nuclei cuneatus and gracilis in the cat, J.Anat.98 (1964)143–162.

J.H. Lue, S.M.Luai, T.J.Wang, J.Y.Shieh, C.Y.Wen, Synaptic relationships between cortico cuneate terminal sandglycine-immuno reactive neurons in the rat cuneate nucleus, BrainRes.771 (1997)167–171.

J. Navarro, E.Sánchez, A.Canedo, Spatio-temporal information coding in the cuneate nucleus, Neurocomputing 69(16–18) (2006)1946–1953.

J.Navarro, E.Sánchez, A.Canedo, Information coding in early stages of the somatosensory system, Nat.Comput.6 (2007)253–267.

A.Nunez, W.Buno, In vitro electrophysiological properties of rat dorsal column nuclei neurons, Eur.J.Neurosci.11 (1999)1865–1876.

A.Reboreda, E.Sánchez, M.Romero, A.Lamas, Intrinsic spontaneous activity and subthreshold oscillations in neurons of the rat dorsal column nuclei in culture, J.Physiol.551 (1) (2003)191–205.

D.E. Rumelhart, E.H.Geoffrey, R.J.Williams, Learning Internal Representations by Error Propagation, in: E.David, Rumelhart, JamesL.McClelland (Eds.), Parallel Distributed Processing: Explorations in the Microstructure of Cognition and the PDP Research Group, vol.1, MITPress, 1986.

E. Sánchez, J.Aguilar, C.Rivadulla, A.Canedo, The role of glycinergic interneurons in the dorsal column nuclei, Neurocomputing58–60(2004)1049–1055.

S.Shamma, Spatial and temporal processing in central auditory networks, in:
C. Koch, e.I.Segev (Eds.), Methods in Neuronal Modeling, 1998, pp.411–460.

S.J.Thorpe, J.Gautrais, Rank order coding: a new coding scheme for rapid Processing in neural networks, in: J.Bower (Ed.), Computational Neuroscience: TrendsinResearch,1998,113–119.

ANEXO 1

FUNCTIONAL PROPERTIES

OF

A REALISTIC MODEL OF dLGN

Ferreiroa R., Sánchez, E.
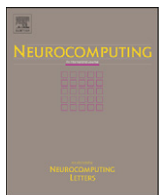
Functional properties of a realistic model of dLGN

Rubén Ferreiroa, Eduardo Sánchez *

Grupo de Sistemas Intelixentes (GSI), CITIUS, Universidade de Santiago de Compostela, 15782 Santiago de Compostela, Spain

ARTICLE INFO

ABSTRACT

In this work we propose a dynamic model of the push–pull circuitry of the lateral geniculate nucleus (dLGN) in order to study the spatio-temporal filtering being carried out. It is widely accepted that the thalamus preserves the retinal structure of the receptive field and thus works as a simple relay station. We believe, however, that this assumption may not be valid on the basis that the thalamus could perform a more relevant processing of information by means of its complex circuitry and functional response properties. To test this hypothesis, a computational model was developed with a retina-dLGN wiring configuration (convergence/divergence) derived from experimental evidences, and a realistic description of the dLGN's ON and OFF channels. Our findings suggest that responses of relay cells in the LGN are highly modulated by center-surround gain, response mode and adaptation.

© 2012 Elsevier B.V. All rights reserved.

1. Introduction

Visual information is processed through multiple pathways that originate in different types of retinal ganglion cells and remain relatively well segregated through the dorsal lateral geniculate nucleus (dLGN) until reaching the visual cortex [12]. In the cat's visual system, there are two main pathways (X and Y) that differ in their response properties and axonal projections. Whereas most X retinal afferents project to a single dLGN layer (layer A), Y retinal afferents can diverge into two dLGN layers (A and C). In our study, we are focused on X-type afferents located in the fovea, responsible for dealing with the details of the scene, and concretely on the dLGN's layer A. This region is constituted by two types of neurons: relay cells and interneurons. LGN relay cells receive retinal as well as non-retinal afferents coming from local sources (mostly GABAergic interneurons and Perigeniculate cells) and external ones (feedback projection from cortical layer 6 and an ascending projection from various scattered cell groups in the brainstem reticular formation). Moreover, inhibition in the dLGN does not come from the retina, but locally from the interneurons that receive inputs from retinal ganglion cells of the opposite sign.

The complexity of the retinothalamic circuitry is further increased when dealing with its topological features. The fact that the number of relay cells in the dLGN of the cat doubles the number of retinal ganglion cells and the number of interneurons is half the number of retinal ganglion cells [5], posed the question about how the thalamus contributes to analyze the visual image. This was addressed by different authors [6], who carried out whole cell recordings in the

cat's dLGN while stimulating with sparse-noise protocol. With this kind of recordings, it is possible to get a clear picture of the analysis performed by the center of the thalamic receptive fields but not by their surrounds, which is only mildly engaged by small stimuli. In addition, thalamic relay cells can operate in two main modes, burst and tonic, depending on functional state and behavioral context and, moreover, their activity undergoes profound adaptation in presence of sustained visual stimulation. Interestingly, the contribution of all these functional properties to the thalamic relay was never before explored in a topologically realist model of the dLGN. Thus, we built a retinothalamic computational model similar to Molano et al. [9] and Ringach [11], using data of retinothalamic divergence available in the literature to investigate responses of populations of thalamic relay cells to simple visual stimuli [4].

2. The problem

The goal of this paper is to analyze the spatio-temporal processing carried out by the dLGN. We have developed a realistic topological model of the retinthalamic circuit to analyze its dynamics and behavior. Concretely, we face the following questions: (1) What is the contribution of the different center-surround gains to processing of borders? (2) What is the impact of tonic and bursting activity? and (3) What is the contribution of spike adaptation to visual processing in the LGN?

3. Computational methods

3.1. Model composition

The retina is represented by two rectangular layers of 40×40 pixels, the first one representing the ON type ganglion cells, the

* Corresponding author.
E-mail addresses: rferreiroa@gmail.com (R. Ferreiroa),
eduardo.sanchez.vila@usc.es (E. Sánchez).
URL: http://citius.usc.es.

second one the OFF type ganglion cells. The lateral geniculate nucleus is modeled by a rectangular layer of 40×40 pixels, each point in the lattice having two neuron models, one for the relay neurons and the other for interneurons. The ratio of neurons per point is 1:4, meaning that for each interneuron there are four neighboring relay cells [9] (Fig. 1).

3.2. Coordinate system and topology

The retina and the thalamus are simulated by means of a lattice of size 40×40 pixels representing a patch with a parafoveal visual field of $8° \times 8°$. Each position in the layer corresponds to a node, each node defining subnets of neurons. In our model, a node of the thalamus layer has two subnets, one constituted by one interneuron and the other made up with four relay neurons.

3.3. Connectivity

The spatial arrangement of the receptive fields of retinal ganglion cells is captured by a difference-of-Gaussians model in which the spatial receptive field is expressed as

$$D(x,y) = \left(\frac{1}{2\pi\sigma_{cen}^2} e^{-(x-y)^2/2\sigma_{cen}^2} - \frac{B}{2\pi\sigma_{sur}^2} e^{-(x-y)^2/2\sigma_{sur}^2} \right) \qquad (1)$$

The first Gaussian function describes the excitatory center and the second one the inhibitory surround receptive field, the sizes of both fields being determined by the parameters σ_{cen} and σ_{sur}. Receptive field parameters for the ganglion cells, shown in Table 1, have been set in accordance with Allen and Freeman [1].

Each relay cell in the thalamus is initially connected to its nearest neighbor in the retinal lattice, i.e. the one from which its polarity is inherited. The probability of each thalamic cell, being connected to another retinal ganglion cell follows a Gaussian function of their relative distance [2]. The synaptic strength of the connections is also assumed to follow a Gaussian distribution of the distance between the receptive-field centers [2]. The function for both connection probability and strength is as follows (see Fig. 1):

$$P = p_{max}e^{-(x-y)^2/2\sigma_{cen}^2} \qquad (2)$$

3.4. Input and output models

The stimuli used in our simulations are simple geometric figures like bright circles, rectangles and bars. Stationary stimuli are mathematically represented by using bi-dimensional arrays of
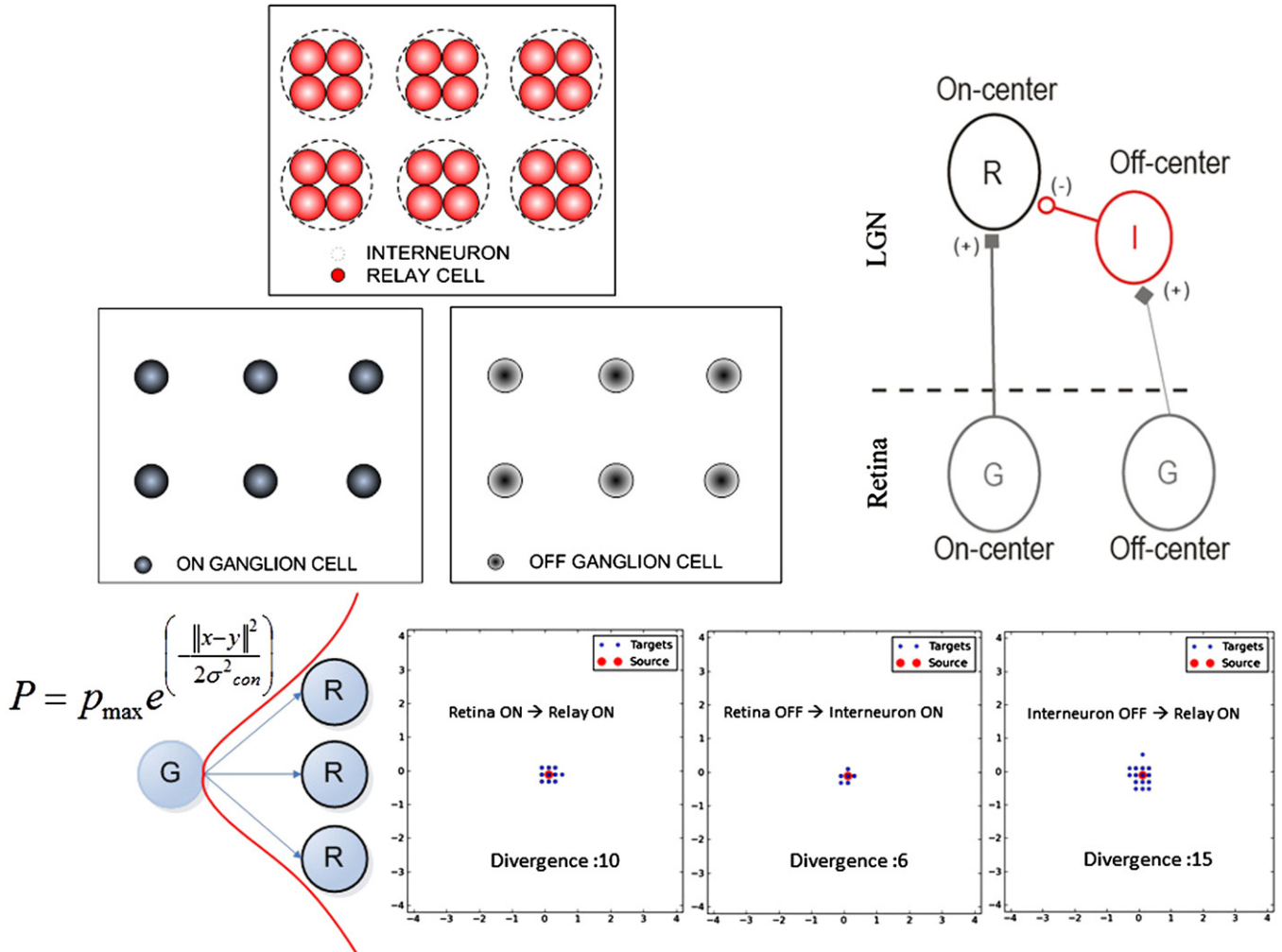

Fig. 1. Topology and spatial connectivity of the LGN model. Nodes and subnets of the thalamus layer (upper left inset). Those nodes are the basic elements of the retinothalamic circuit, which is constituted by the ON and OFF channels (upper right inset). The connections between retinal ganglion cells and thalamic relay cells follow a Gaussian distribution probability (lower left inset). The number of divergent connections between layers is derived from empirical studies (lower right inset).

size 40 × 40, where the coefficients represent either high or low light intensity.

Table 1
DoG parameters for ON and OFF retinal ganglion cells.

DoG	A	B	σ_{cen}	σ_{sur}
ON retinal ganglion cells	3	1	0.4	0.9
OFF retinal ganglion cells	1	3	0.4	0.9

The rate of the pulse train evoked by a stimulus in the ganglion cells is modeled with a 2D convolution function

$$r = r_0 + \int \int D(x,y)s(x,y) \, dx \, dy \qquad (3)$$

where r represents the firing rate evoked by a stimulus $s(x,y)$, r_0 is the background firing, and $D(x,y)$ the difference-of-Gaussians function representing the receptive field of ganglion cells.

Finally, the stochastic nature of the ganglion cell activity is modeled through a pulse train modulator, which is modulated by the firing rate r and follows the statistics of a homogeneous Poisson
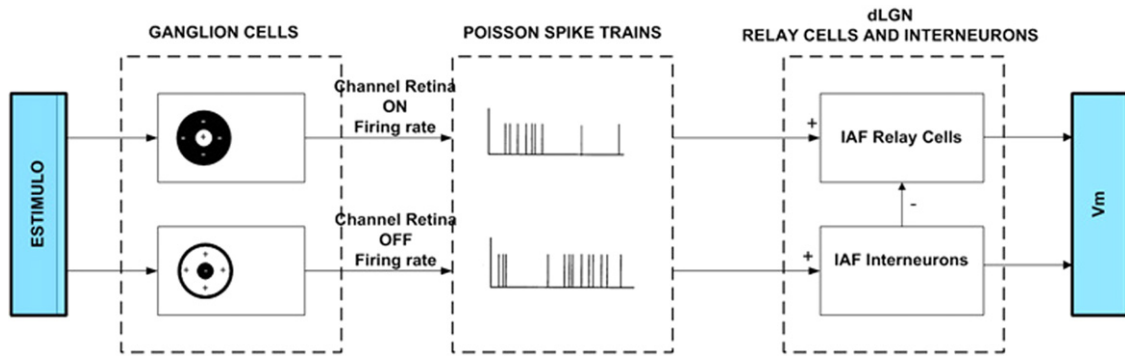

Fig. 2. General overview of the LGN model. The model includes the external stimuli, retinal ganglion cells, retinal Poisson generators, thalamic relay cells, and thalamic interneurons. Thalamic cells are modeled as Adaptive Exponential IAF neurons.
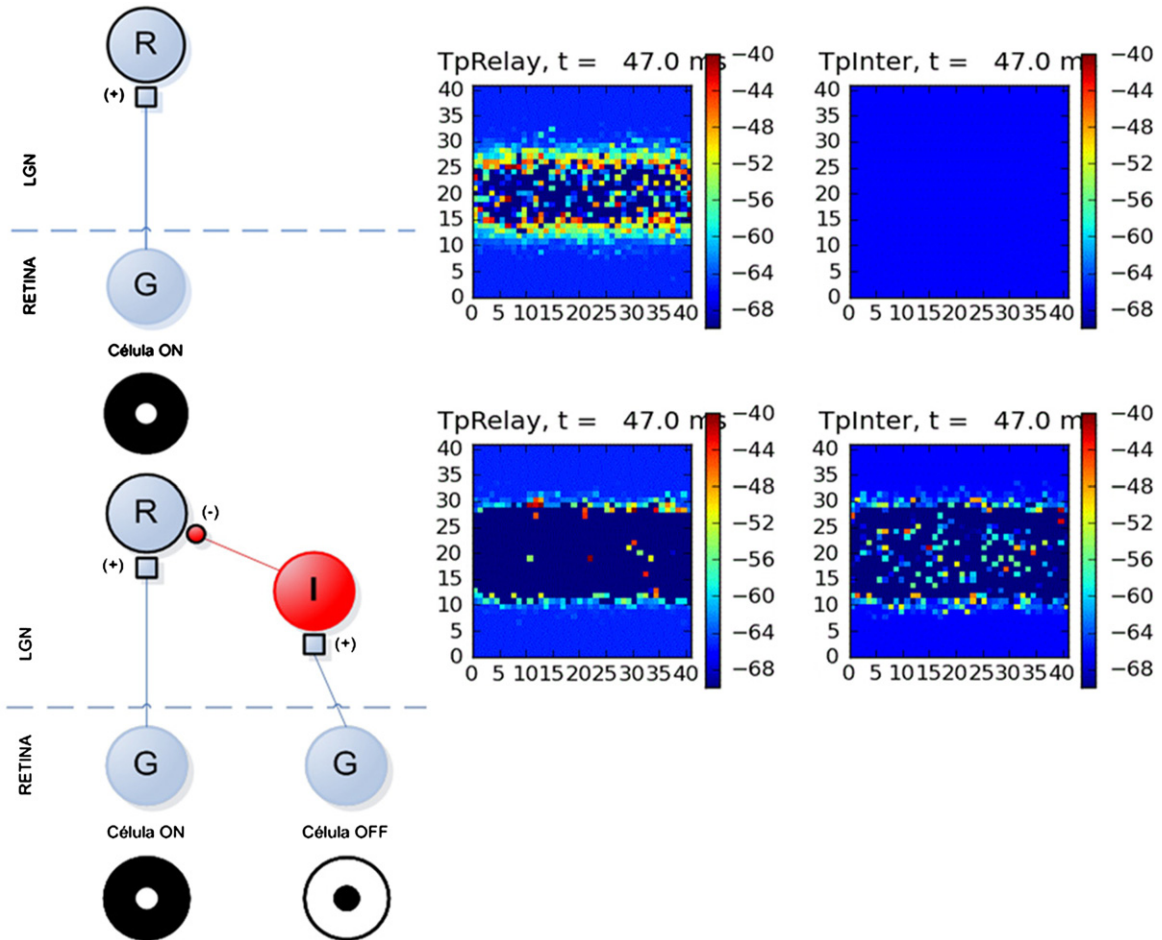

Fig. 3. ON channel processing and impact of OFF channel inhibition. A horizontal bar stimulus is presented to the ON channel circuit (upper left inset), and at $t=47$ ms, the activity recorded at the thalamic relay cells is mainly centered at the edges of the stimulus (upper right inset). When the inhibitory connections coming from the thalamic OFF channel are added (lower left inset), the activity recorded at the thalamic relay cells, also at $t=47$ ms, reveals a much clearer picture of the edges (lower right inset).

process

$$P_T(n) = \frac{rT}{n!} e^{-rT} \tag{4}$$

Fig. 2 provides an overview of all the components involved in our model.

3.5. Neuron model

We use an implementation of the Adaptative Exponential Integrate and Fire (AEIaF) neuron model of Brette and Gerstner [3] as implemented in the NEST simulator [10]. The AEIaF model is a conductance-based integrate and fire model with an exponential soft spiking threshold rather than a hard threshold, and with a second state variable that recreates both membrane potential and spike adaptation effects. With this generic model we can characterize neurons showing similar behaviors to those observed in relay cells and interneurons. The membrane potential is computed according to the following equation:

$$C_m \frac{dV}{dt} = -g_L(V-E_L) + g_s(t)(V-E_s) + g_L \Delta_T e^{(V-V_T)/\Delta_T} - w + \frac{I_e}{A} \tag{5}$$

where C_m is the capacitance, g_L is the leak conductance, E_L is the resting potential, and the exponential term creates a soft spiking threshold around V_T with softness determined by Δ_T, g_s, I_e.

The synaptic conductances are shaped by the alpha function with time constant τ_s

$$g_s(t) = \overline{g_s}\left(\frac{t}{\tau_s}\right)e^{-t/\tau_s} \tag{6}$$
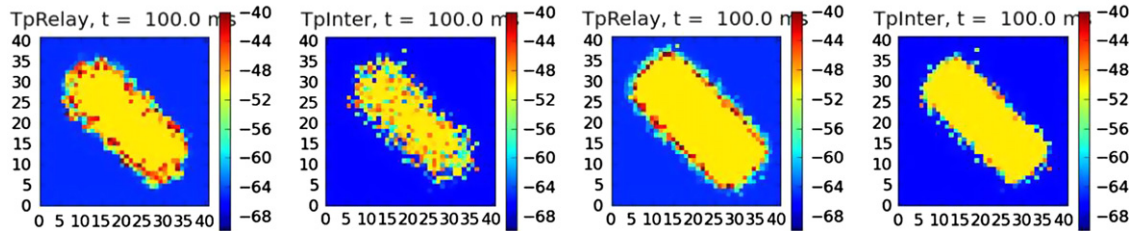

Fig. 4. Effect of parameter B on the efficacy of edge detection. Higher values of B (right inset), compared to the default value (left inset), favor the detection of the stimulus edges.
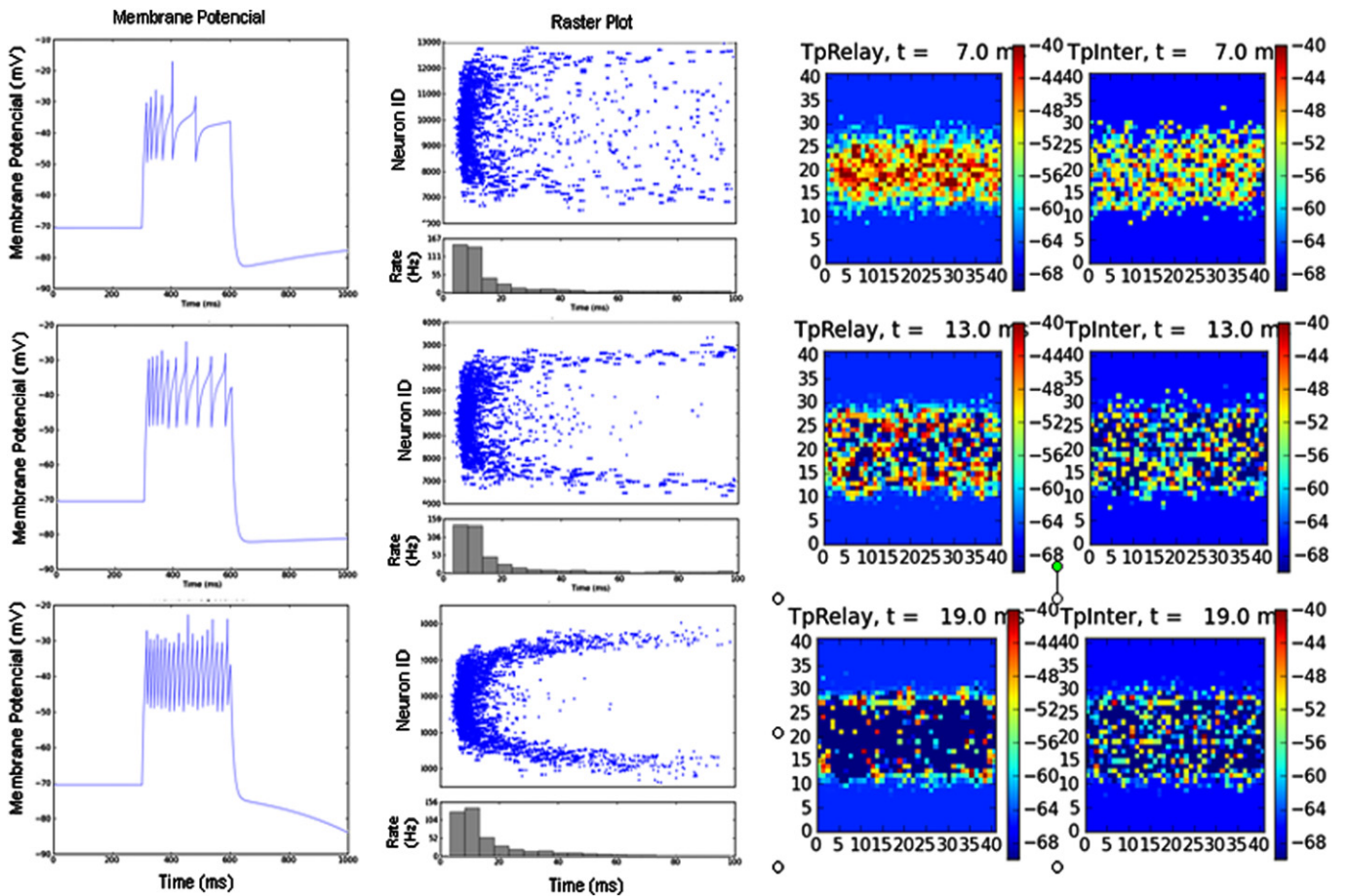

Fig. 5. Impact of tonic activity in NGL processing. The figure illustrates the membrane potential for both relay cells and interneurons (left column), the raster plot recording the activity of thalamic relay cells along a longitudinal section of the thalamic layer (middle column), and the output activity of the whole population of relay cells at some specific time (right column). When both relay cells and interneurons behave in tonic mode (lower inset) we get a better perception of the edges of our stimulus. Furthermore, both raster plots and output activity show that the time required to detect these edges is also reduced as the membrane potential of relay cells and interneurons becomes more tonic (lower inset).

w is an adaptation current with time constant τ_w and sub-threshold adaptation level set by a

$$\tau_w \frac{dw}{dt} = a(V - E_L) - w \qquad (7)$$

A spike event is triggered when the membrane potential diverges due to the exponential term. In practice, a spike is triggered when V reaches a sufficiently large value such as V_T. When a spike occurs, the membrane potential is reset to V_r and a spike adaptation b is added to the adaptation current w:

$$V \geq V_T \begin{cases} V = V_r \\ w = w + b \end{cases} \qquad (8)$$

4. Results

4.1. Impact of OFF channel inhibition in LGN processing

In the following experiment, we present a horizontal bar stimulus with and without the lateral inhibition coming from the OFF channel (Fig. 3). The following results were obtained in our simulation for both situations.
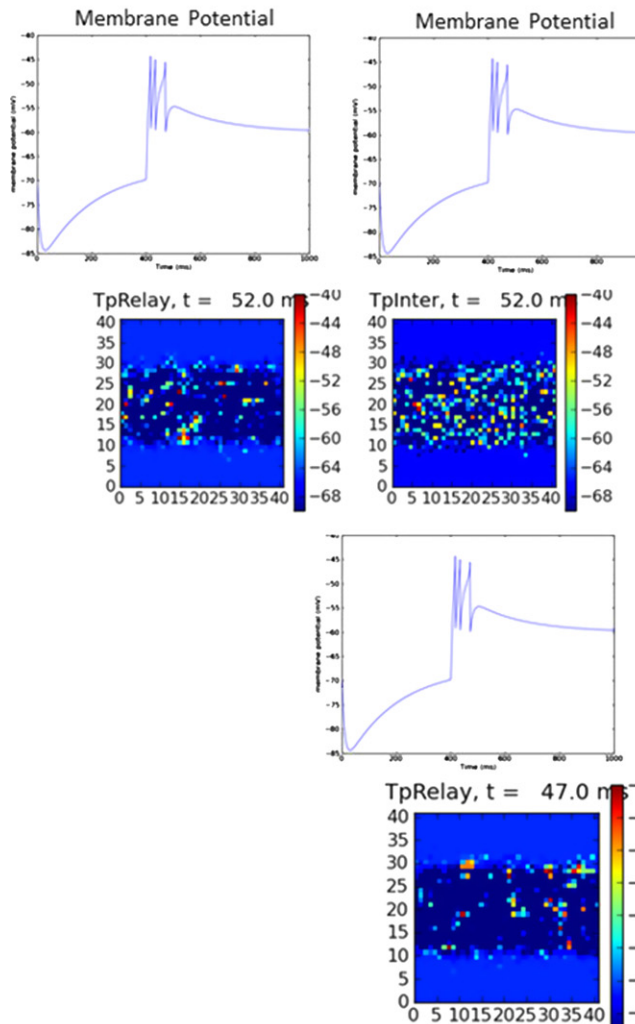
- ON Channel enabled and OFF channel disabled. The simulation shows that at time $t = 47$ ms the activity of the LGN cell population is centered mainly on the edges of the horizontal bar. Although the ON channel is detecting edges due to the structure of the receptive field DoG, we see that a significant activity remains at its center (see simulation Fig. 3).
- ON and OFF Channels enabled. If we present the same stimulus in both channels ON and OFF and we enable the inhibitory pathway coming from the OFF channel, the stimulus edges are detected more precisely (Fig. 3). Moreover, the time required to detect the edges is significantly reduced (not shown) when compared with the previous simulation.

It can be concluded that the OFF channel implements a gain control function over the retinal input reaching the ON channel relay cells with the goal of highlighting the stimulus edges.

4.2. Impact of DoG shape in LGN processing

The goal of this experiment consists on analyzing the impact of the difference-of-Gaussians shape on the detection of stimulus edges. We have tested different values of the parameter B (see Eq. (1)), which controls the balance between the contributions of the excitatory center and inhibitory surround of the ON/OFF retinal
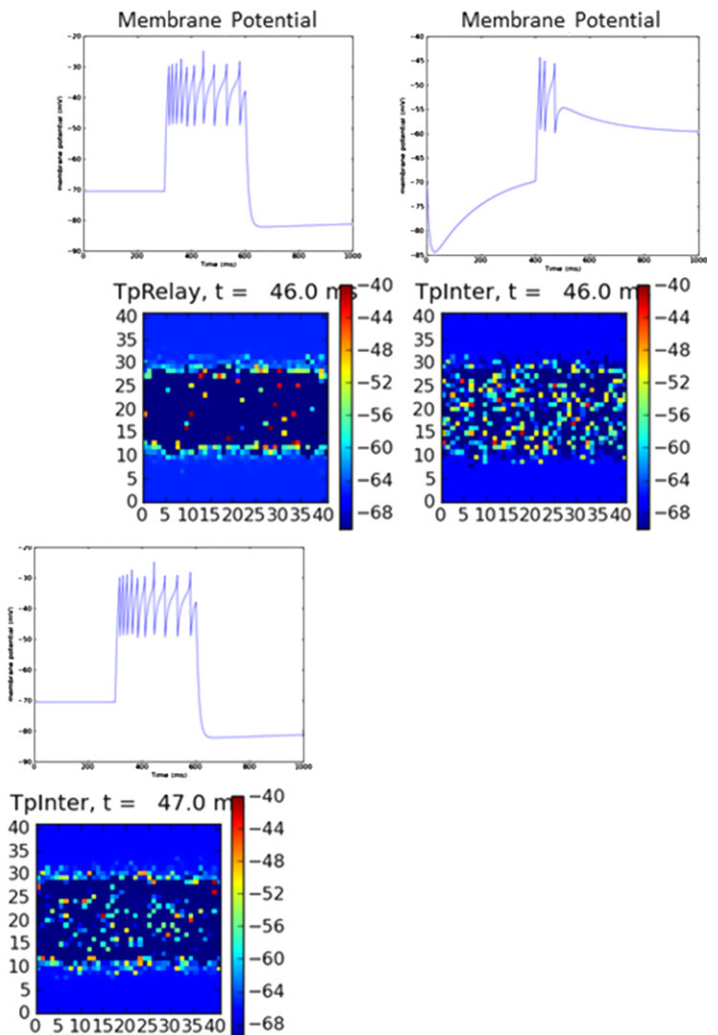

Fig. 6. Impact of bursting activity in NGL processing. The figure presents three insets showing the activity of both single cells and output activity. When relay cells and interneurons behave simultaneously in bursting mode, there is a poor detection of the stimulus edges (upper left inset). The stimulus edges are best detected when the relay cells respond in tonic mode and interneurons in bursting mode (upper right inset).

ganglion cells. Fig. 4 shows that higher values of B (right inset), generate a membrane potential activity revealing the edges of the stimulus with better accuracy.

4.3. Impact of tonic and bursting activity in LGN processing

The thalamic relay cells respond to excitatory inputs in two different modes: tonic and bursting mode. The behavior of both modes depends basically on the calcium current known as I_T.

In the bursting mode, I_T is activated and an influx of calcium causes a depolarization triggering a burst of action potentials. When the relay cell is depolarized during ~ 100 ms or more, I_T tends to be de-activated and the cell fires in tonic mode.

The aim of this experiment is to analyze what type of filtering is carried out in our LGN circuitry when the relay cell shows a tonic or a bursting activity. Modifying the parameter a in the model AEIaf, we can simulate the behavior of ion channels and therefore change the membrane potential. Values of $a > 0$ hyperpolarize (potassium current) the membrane, activating the current I_T, and therefore triggering the bursting mode. On the other side, values of $a < 0$ depolarize (low threshold current of calcium) the membrane, thus inactivating current I_T and therefore generating the tonic mode. The results obtained from our simulations follows:

Table 2
Parameter b affects detection time.

| b (interneurons)	b (relay cells)	Detection time (ms)
80.5	80.5	75
80.5	100.5	55
80.5	120.5	45
80.5	180.5	45
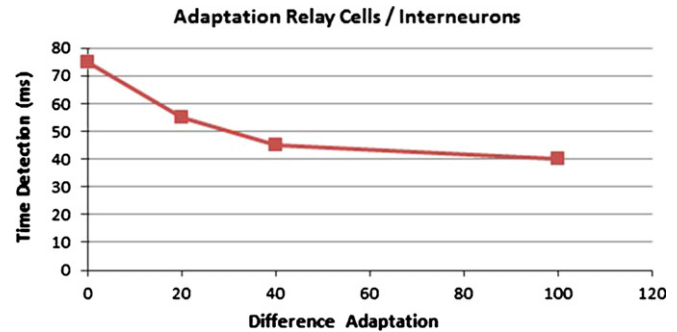
Fig. 8. Time needed for detection varies with adaptation.

Fig. 7. Impact of spike adaptation in neural activity. Membrane potentials of interneurons and relay cells for $b=80.5$ (a) and $b=120.5$ (b).
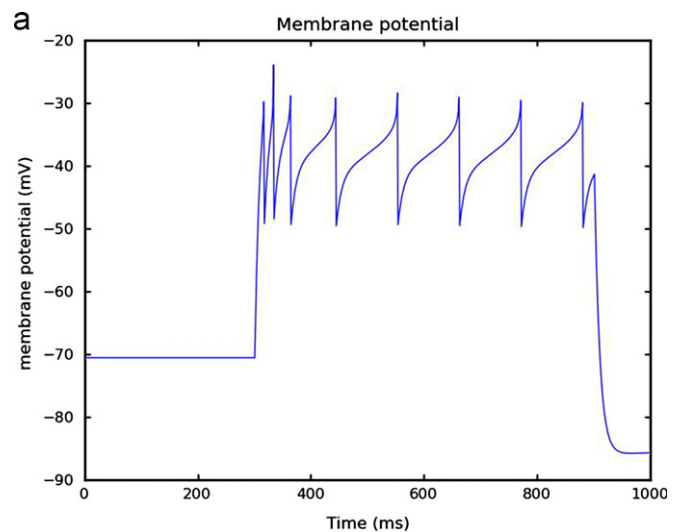

Fig. 9. Effect of depolarizing ramp on relay cells. Membrane potential after setting $\Delta_T=2$ (a) and $\Delta_T=12$ (b).

- When relay cells and interneurons show the tonic mode, we get a better detection of the edges of our stimulus (Fig. 5).
- Time detection of the edges of the stimulus is reduced as the membrane potential of relay cells and interneurons becomes more tonic (Fig. 5).
- When relay cells and interneurons behave simultaneously in the bursting mode, there is a poor detection of the stimulus edges (Fig. 6).
- When relay cells and interneurons behave on modes tonic/bursting and viceversa, the edges are best detected when the relay cells are working in tonic mode and the interneurons in bursting mode (Fig. 6).

4.4. Impact of spike adaptation in LGN processing

In the next experiment we have changed the adaptation parameter b of both relay cells and interneurons and then analyzed the behavior after these changes. Fig. 7 illustrates the membrane potential of an interneuron and a relay cell, which is the same for both types of neurons, for two different values of b. In addition, we tested

the impact of this parameter on the time required to detect the edges of the stimulus. Table 2 summarizes the obtained detection time under different combinations of parameter b for both relay cells and interneurons. Time detection is defined here as the precise moment at which the relay cells showing activity are all of them located at the edges of the stimulus. Fig. 8 plots, for a relay cell, the detection time against increasing values of parameter b. The simulations point out that the higher the value of parameter b, the shorter the time required to detect edges. Furthermore, the plot suggests the existence of a minimum detection time that cannot be reduced by simply increasing the value of parameter b.

4.5. Impact of sub-threshold depolarizing ramp in relay cells

In tonic mode and after the injection of a depolarizing stimulus, the main difference between the action potentials of relay cells and interneurons appears within the first 10–100 ms. While interneurons show a clear pattern of acceleration/de-acceleration discharge during this period, relay cells show a sub-threshold depolarizing ramp that delays their discharge. In order to analyze the impact of this delay in the behavior of the circuit, we have modified the slope of the
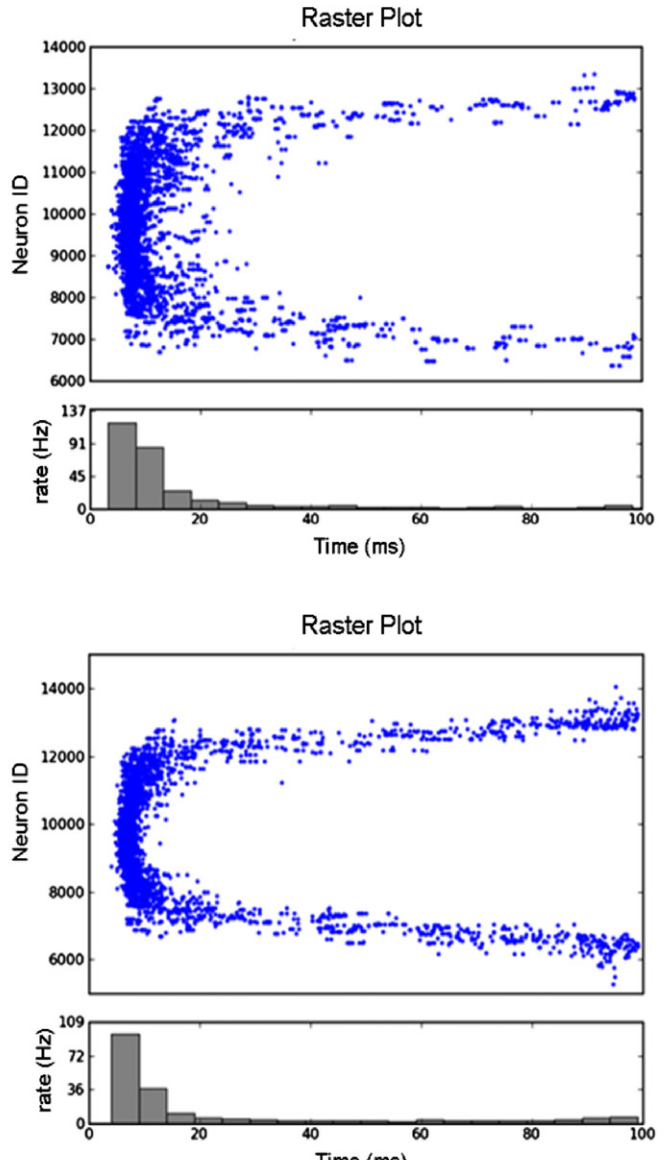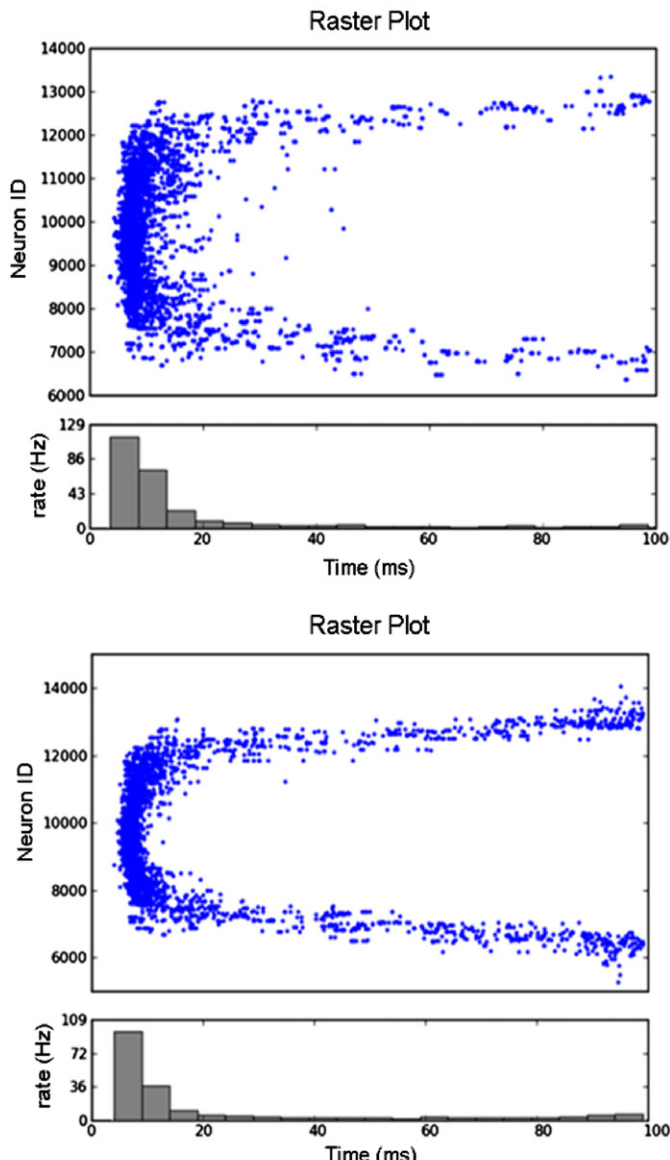

Fig. 10. Edge detection efficacy varies with depolarizing ramp values. This figure illustrates raster plots of thalamic relay cells for different values of Δ_T in interneurons: 2, 5, 10, and 15. Edges are more clearly perceived with higher values of Δ_T.
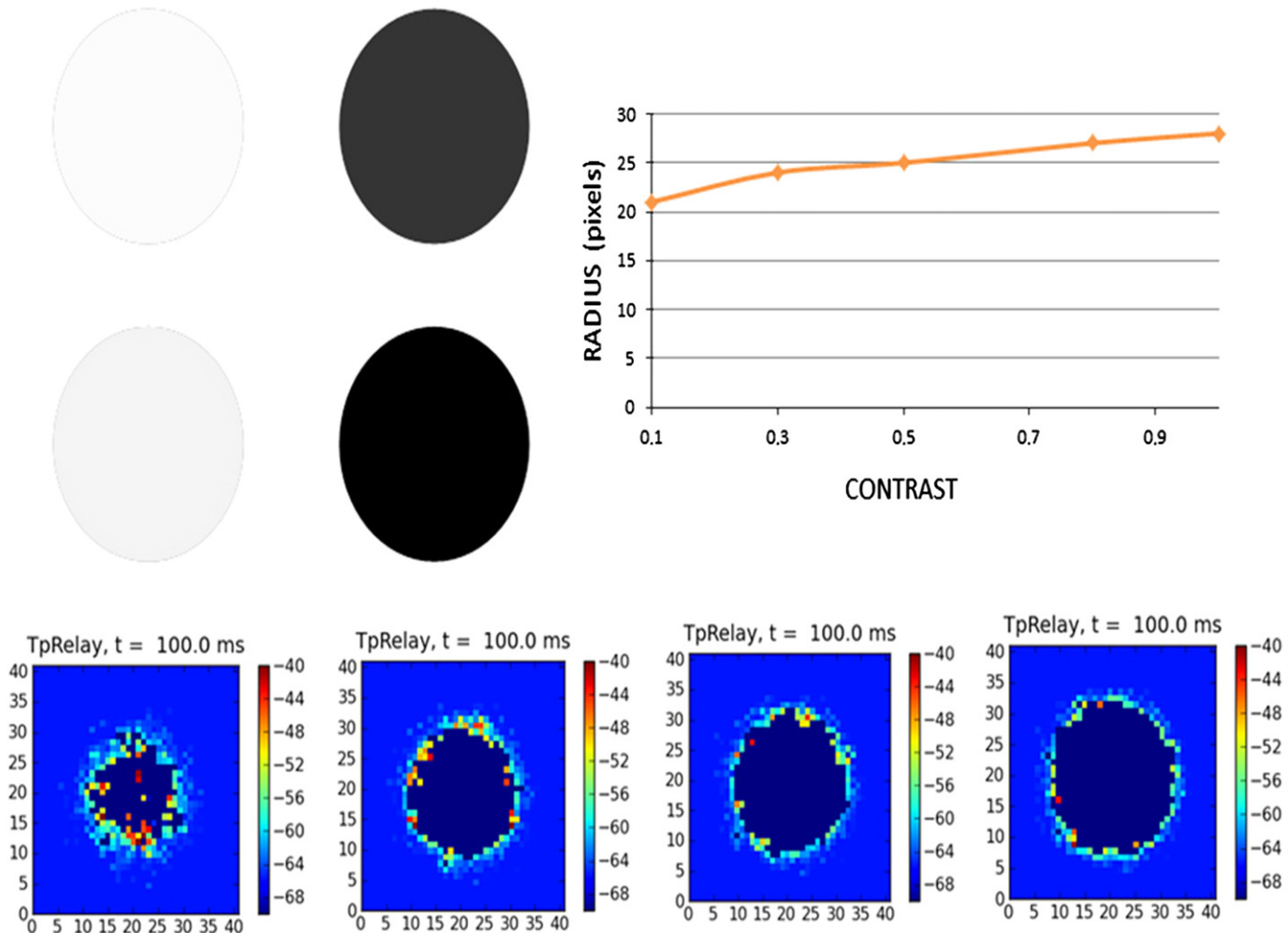
Fig. 11. LGN processing depends on contrast. Increasing values of stimulus contrast (upper left inset) lead higher values of stimulus radius perceived from the LGN (upper right inset). The output activity of the LGN shows how the LGN better perceives the circular stimulus as the contrast increases from left to right (lower inset).

interneuron's ramp by changing the parameter Δ_T included in our Exponential Integrate and Fire (AEIaF) neuron model. Fig. 9 illustrates the effect of Δ_T on the discharge pattern of interneurons. Higher values of this parameter induce higher frequencies on the generation of action potentials. With regard to the impact on the circuit behavior, we observed that higher values of Δ_T contribute to improve the efficacy of the edge detection process, by reducing the time required to perceive those edges (Fig. 10).

4.6. Perception of stimulus size depending on stimulus contrast

In the next experiment, we have generated different stimulus with varying degree of contrast between the stimulus and background (Fig. 11). The results obtained from our simulations show the perceived size of the stimulus in ON channel relay neurons increases as the contrast of the stimulus is increased (Fig. 11).

5. Discussion

Our model of the NGL indicates that this nucleus is probably performing some relevant visual information tasks. Concretely, it provides a plausible explanation of the functionality of the ON and OFF channel circuit. The center-surround receptive field of the ON channel detects changes in contrast and therefore edges

of the presented stimuli. Moreover, we found that the OFF channel (inhibition) is performing a gain control of over the ON channel retinal inputs. The efficacy of the gain control circuit is determined, not only by stimuli features, as for instance the stimulus-background contrast, but also by the activity mode of the LGN cells. Tonic activity in relay cells seems more suitable than bursting activity to detect edges in static stimulus.

The next step will consist on analyzing the difference between the model predictions and the experimental observed activity. To facilitate this future comparison and the relationship between the neural activity and the stimulus features, we are realistically modeling all the ionic channels known in both relay cells and interneurons [7,8].

Acknowledgment

References

[1] E.A. Allen, R.D. Freeman, Dynamic spatial processing originates in early visual pathways, J. Neurosci. 26 (45) (2006) 11763–11774.

[2] J.M. Alonso, C.I. Yeh, C. Weng, C. Stoelzel, Retinogeniculate connections: a balancing act between connection specificity and receptive field diversity, Prog. Brain Res. 154 (2006).

[3] R. Brette, W. Gerstner, Adaptive exponential Integrate-and-Fire model as an effective description of neuronal activity, J. Neurophysiol. 94 (5) (2005) 3637–3642.

[4] C.I. Yeh, C.R. Stoelzel, C. Weng, J.M. Alonso, Functional consequences of neural divergence within the retinogeniculate pathway, J. Neurophysiol. 101 (2009).

[5] M. Madarász, J. Gerle, F. Hajdu, G. Somogyi, T. Tömböl, Quantitative histological studies on the lateral geniculate nucleus in the cat. II. Cell numbers and densities in the several layers, J. Hirnforsch. 19 (2) (1978) 159–164.

[6] L.M. Martinez, Q. Wang, R.C. Reid, C. Pillai, J.M. Alonso, F.T. Sommer, J.A. Hirsch, Receptive field structure varies with layer in the primary visual cortex, Nat. Neurosci. 8 (3) (2005) 372–379.

[7] D.A. McCormick, J. Huguenard, A model of the electrophysiological properties of thalamocortical relay neurons, J. Neurophysiol. 68 (1992) 1384–1400.

[8] J.R. Huguenard, D.A. McCormick, Voltage clamp simulations of currents involved in rhythmic oscillations in thalamic relay neurones, J. Neurophysiol. 68 (1992) 1373–1383.

[9] M. Molano, M.M. Rodríguez, L.M. Otero, DEA. How the thalamus changes what the cat's eye tells the cat's brain, 2009.

[10] M.O. Gewaltig, M. Diesmann, Nest (neural simulation tool), Scholarpedia 2 (4) (2007) 1430.

[11] D.L. Ringach, Haphazard wiring of simple receptive fields and orientation columns in visual cortex, J. Neurophysiol. 92 (2007) 468–476.

[12] W.M. Usrey, J.B. Reppas, R.C. Reid, Specificity and strength of retinogeniculate connections, J. Neurophysiol. 82 (1999) 3527–3540.

Rubén Ferreiroa Garcia was born in Ferrol, Spain in 1973. He received his B.S., degree in Physics from the University of Santiago de Compostela in 1998, M.S. degree in Telematic from ITE Caixa Galicia/University of La Coruña, 1999 and M.S. degree in Neuroscience at the University of Santiago de Compostela in 2010. Nowadays he combines his Ph.D. with a job in Navantia Company as System Engineer Manager. His research interest is in computational models of visual system and information coding.

Eduardo M. Sánchez Vila was born in Barcelona, Spain in 1970. He received the B.S. degree in physics from the University of Santiago de Compostela in 1993, a M.S. degree in Neuroscience at the International University of Andalucía in 1996, and a M.S. degree in Computer Science at the University of Southern California in 2001. He also received the PhD in Physics in 2000 at the University of Santiago de Compostela. Nowadays, he is working as Professor of the Department of Electronics and Computer Science at the University of Santiago de Compostela. His research interest is in computational models of somatosensory and visual system, distributed computing, information coding and complex network theory.

ANEXO 2

CLASSIFICATION OF SOMATOSENSORY STIMULI ON THE BASIS OF THE TEMPORAL CODING AT THE CUNEATE NUCLEUS

Navarro, J., Sánchez, E., Ferreiroa, R., & Canedo, A.
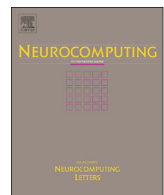
Classification of somatosensory stimuli on the basis of the temporal coding at the cuneate nucleus

Juan Navarro [a], Eduardo Sánchez [b], Rubén Ferreiroa [b], Antonio Canedo [a]

[a] Departamento de Fisiología, Facultad de Medicina, Universidad de Santiago de Compostela, 15782 Santiago de Compostela, Spain
[b] Grupo de Sistemas Inteligentes (GSI), Centro Singular de Investigación en Tecnologías de la Información (CITIUS), Universidad de Santiago de Compostela, 15782 Santiago de Compostela, Spain

ARTICLE INFO

ABSTRACT

The present study explores the capacity of a temporal code generated by the projection neurons of a realistic computational model of the cuneate nucleus to classify somesthetic stimuli. Four classification experiments were carried out with a feedforward network trained under a supervised learning algorithm in which the input is a vector including the sequence of outputs of the cuneate nucleus. The number of correct responses on each classification task varied with the complexity of the experiment, but a decrease in the number of errors was observed when presenting the optimal length of the input vector. This suggests that the cuneate nucleus might (1) transmit the appropriate information required for input classification, and (2) function as an information processing center and not merely as a relay or filtering stage.

© 2014 Published by Elsevier B.V.

1. Introduction

Our interest focuses on the information processing of the middle zone of the cuneate nucleus (CN), which is located at the dorsal column nuclei and receives input from primary afferents transmitting tactile information from cutaneous receptives located in the upper trunk. The types of cells found in the cuneate circuitry are the following [2,7]: projection or cuneothalamic cells (CT), gabaergic interneurons (GAB), and glycinergic interneurons (GLY). To date, only the structure of the receptive fields (RFs) of CT cells is known [5]. Their RFs, determined by the somatotopic organization of the afferent cells, are made up of an excitatory center as well as an inhibitory surround mediated by GAB interneurons coming from adjacent areas. Further experiments [1] suggested that CT cells also receive: (1) recurrent lateral inhibition induced by GAB interneurons, which are excited from CT cells located at non-adjacent receptive fields, and (2) recurrent disinhibition, or facilitation, mediated by GLY interneurons inhibiting GAB interneurons. After being transformed by the cuneate nucleus, the somesthetic information passes to the ventro-postero-lateral (VPL) nucleus of the thalamus [6] before reaching the primary somatosensory cortex.

The functional role of the CN is hard to assess experimentally because of some important methodological limitations: firstly, the complexity of carrying out intracellular recordings of CN cells in awaking animals, and secondly, the difficulty of setting and controlling the stimulation parameters with the required spatial and temporal accuracy. To overcome these limitations, a realistic computational model of the CN based on experimental findings was developed [14]. A scheme of the model describing the different types of neurons as well as both afferent and recurrent connections is shown in the left inset of Fig. 1. The neuron's RFs described above are also depicted in the right inset. In a previous work [9], it has been shown that this circuitry produces a spatio-temporal progressive coding that starts signaling regions with lower regularity (higher intensity contrast), and progressively covers regions with an increasing degree of regularity (lower intensity contrast) until the stimulus is filled. In order to visually explore this code evolving over time, a global output variable has been chosen. It might represent the activity of a single feature detector integrating the output of CT neurons at any given time. The temporal series of this variable reveals an oscillatory pattern showing a repeated behavior in which the oscillation's amplitude diminishes with time until a stationary state, corresponding with the end of the fill-in process, is reached. The analysis of this behavior discovered positive correlations [9] between the degree of regularity of the stimuli and some parameters of the oscillatory pattern such as (1) the duration of the fill-in effect, (2) the amplitude of the oscillatory patterns during the fill-in effect, and
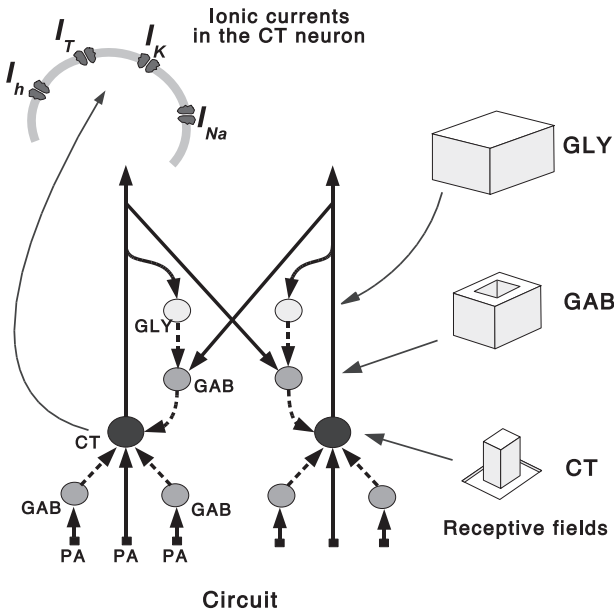
Fig. 1. Realistic model of the cuneate nucleus based on experimental findings in the cat. PA: primary afferents, CT: cuneothalamic cells, GAB: gabergic interneurons and GLY: glycinergic interneurons. Solid and dashed arrows represent excitatory and inhibitory synapses, respectively. The shape of RFs for CT, GAB and GLY cells is also shown.

(3) the amplitude of the residual oscillations when the stationary state is reached. Similar correlations were found between the size of the stimuli and the mentioned parameters of the oscillatory pattern. These findings might suggest that (1) the progressive coding built at the CN seems to encode salient features of the stimuli (such as the degree of regularity and size), and (2) the oscillatory patterns could be useful to decode and classify incoming somesthetic stimuli. This paper is aimed at testing the later hypothesis.

2. Methods

2.1. Model of cuneate nucleus

Each CT neuron n_j has been modeled in a realistic way with the following firing condition $y_j(t) = 1$ if $v_j(t) > \Theta_{spike}$, where $v_j(t)$ is the membrane potential at time t and Θ_{spike} a positive threshold value. The membrane potential is updated as follows: $v_j(t) = v_j(t-1) + I_j^{total}(t) - I_j^{ionic}(t)$, where the total afferent input $I_j^{total}(t)$ being computed by multiplying every input I_i inside its receptive field by its corresponding synaptic weight w_{ij}. The ionic current term I_j^{ionic} is a linear combination of the contributions of a sodium current, a potassium current, a hyperpolarization-activated cationic current, and a low-threshold calcium current, all currents being supported by experimental evidence [4,11,12]. The interneurons have been characterized as simple McCulloch–Pitts units, in which the output of the jth neuron is $y_j = \Psi(\sum w_{ji} x_i)$ with activation function Ψ being of the threshold type, and the strength of the synapse between neuron ith and neuron jth being described by the weight w_{ji}. As regards the circuitry, the key aspect is the recurrent loop around the cuneothalamic neurons, whose state at time t is determined by the output of other CT neurons at time $t-1$. These recurrent connections are responsible for the generation of the temporal progressive code observed as the output of CT neurons. Further details of the model and its temporal code can be found in Navarro et al. (2007) [10].

2.2. Preprocessing the oscillatory pattern of the global output variable

As described in the Introduction section, a single global output variable was initially chosen to visualize the progressive coding generated by the CN over time. The positive correlations found between some parameters of the global output oscillatory pattern (see Fig. 2 and panels B1 and B2 of Fig. 3) and salient features of the stimuli might suggest that this way of coding could be useful to classify the stimuli at later processing stages. As the oscillatory pattern of the global output presents doublets, which are repeated peak values to probably provide a robust postsynaptic response at the VPL, as well as points of time in which the CN output is silent, preprocessing was carried out in a two-stage process: the first one aimed at removing null values and repetitions of the first peak value, the second one to normalize the data. Panels C1 and C2 of Fig. 3 show two examples of this transformation.

2.3. Classification with a feedforward network and supervised learning

Our hypothesis is that the oscillatory patterns could be useful to classify incoming somesthetic stimuli. To test this idea we have been inspired by the concept of ideal observer introduced by Britten et al. (1992) [3]. In their work, an observer has to predict the motion directions in a two-alternative forced choice task on the bases of ROC curves derived from behavioral experiments with monkeys. They found that the observer could perform the discrimination tasks with a similar accuracy that the monkey did. Our
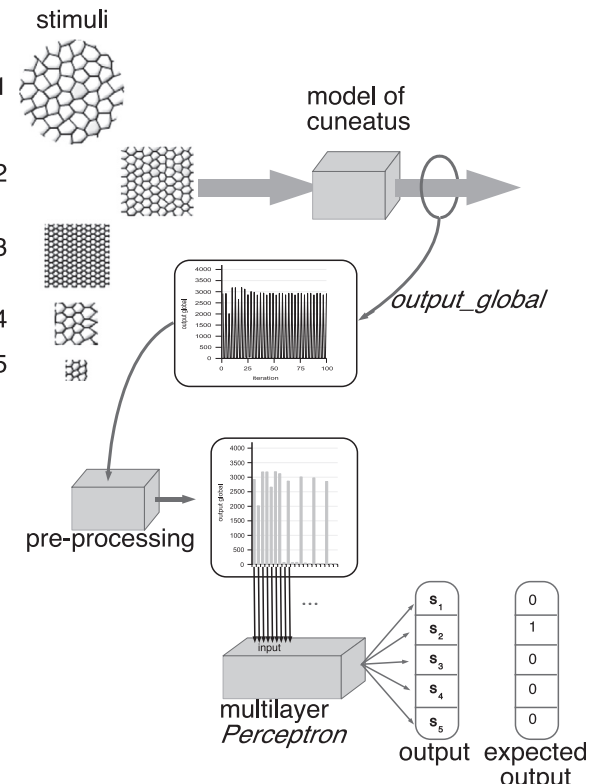
Fig. 2. Classification experiments to test the encoding capabilities of the temporal oscillatory pattern. The oscillatory pattern made up of the *output_global* variable evolving over time is pre-processed by removing zeros as well as the repeated first value. The resulting series is the input vector of the classifier. The expected output (size 2 in this example) is extracted from the training set in order to both compute the classification error and modify the appropriate learning weights. Arrows indicate the flow of data in the classification experiments.
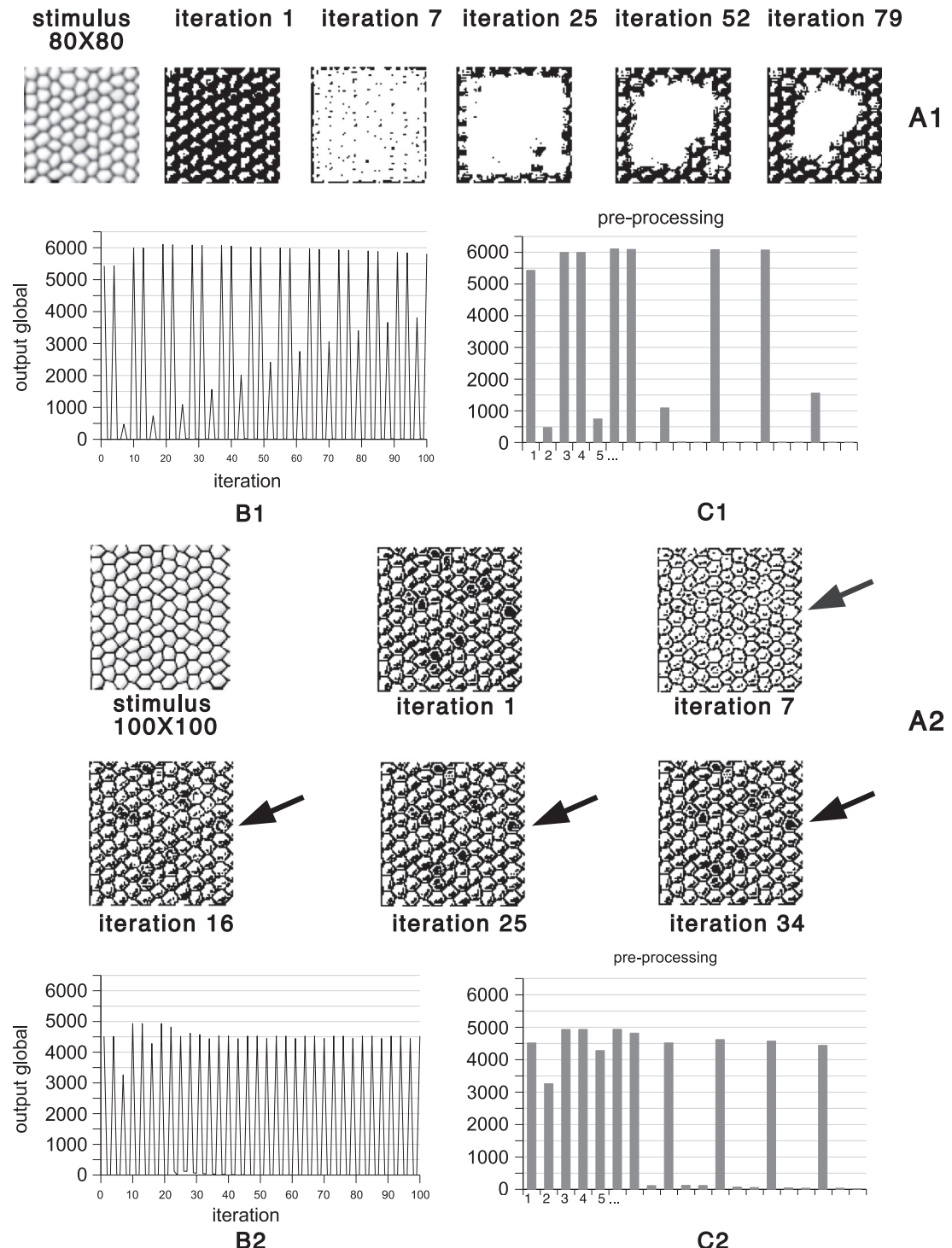
Fig. 3. Examples of progressive coding and corresponding oscillatory patterns. Panels A1 and A2 show two somesthetic inputs (first image) as well as the generated output of CT neurons over time. At the input, each dot represents the intensity of pressure; at the output, a black dot represents an action potential being generated in a CT neuron. Arrows in A2 indicate some areas where the filling of the progressive coding can be observed. Panels B1 and B2 represent the oscillatory activity of the variable *output_global* throughout the first 100 iterations. Panels C1 and C2 represent the pre-processed oscillatory pattern extracted from panels B1 and B2 after eliminating zeros and repetitions of the first value.

approach is slightly different and we have replaced the human watching at ROC curves by a classifier looking at the pre-processed oscillatory pattern. As we did not want to impose any constraint on this classifier, we have resorted to a biologically plausible feedforward network (multilayer perceptron) made up of four layers: an input layer, two intermediate or hidden layers, and an output layer. The input layer has a variable number of units that depends on the length of the input vector (the pre-processed oscillatory pattern). The two hidden layers have 50 and 10 units, respectively. Finally, the output layer presents also a variable number of units that represents the total number of labeled classes on each experiment. The activation functions were sigmoids and each ith unit is connected with every jth unit in the next layer, being each connection described through weight w_{ji}.

As our purpose is on testing the classification capabilities of the CN code, a supervised learning algorithm was applied to minimize the output error function by means of adapting the weights w_{ji}. In our case, we have resorted to the Backpropagation learning algorithm [13] though other algorithms could be used as well. The learning rate was adjusted to obtain stable results and finally set to a value between 0.05 and 0.25. No momemtum term was used during the training stage. The results of the experiments carried out with the classifier were analyzed in light of the classification error of the network, which is the percentage of stimuli that were incorrectly classified in the validation stage.

3. Results

Fig. 3 shows the spatio-temporal dynamics of the CN output in response to the stimuli illustrated in panels A1 and A2. Both stimuli are squares including a mosaic pattern but different degree of regularity: the first one being slightly smoothed by means of a Gaussian filter, the second one preserving its original intensity profile. In response to a static stimulus presented to the model, the output of the CT neurons evolves over time as shown in panels A1 and A2. The progressive fill-in coding of the stimulus surface is observed, beginning with the zones of lower regularity and progressing towards the zones of higher regularity. It is interesting to note that the zones of lower regularity in A1 are at the perimeter of the square, while in A2 are located at the inner positions of the mosaic lattice. In panel A1 the fill-in effect is quite global but in panel A2 it is of a local type affecting local regions, one of which is indicated by arrows to aid identification. When the fill-in effect ends, the output reaches a stationary state from which the transmission of the information is repeated. In summary, the CN circuitry seems to transmit information in a two-stage process, the first one comprising the fill-in effect, the second one transmitting an stable representation of the stimulus. Panels B1 and B2 show the oscillatory pattern of the global output variable during 100 iterations. In the first processing stage, in which the fill-in effect takes place, the oscillatory pattern presents an amplitude that diminishes over time. In the second processing stage, the stationary stage, a residual oscillation is maintained (see panel B2

in Fig. 3). The duration of the first stage, the maximum amplitude of the oscillatory pattern, and the amplitude of the residual oscillations, all depend on features, such as degree of regularity and size, of the presented stimulus [9,10].

Four classification experiments were carried out in order to test whether the pre-processed oscillatory activity encodes useful information to classify the stimulus. Each classification problem focuses on a single relevant stimulus feature: size, degree of regularity (contrast), shape and degree of segmentation. The classification error of each experiment is plotted against the length of the input vector presented to the classifier. The reason for this comes from the fact that the length of the input vector determines the total amount of data available to perform the classification tasks. Therefore, it is expected that the longer the input length, the higher the probability of correctly classifying the stimulus.

The first experiment dealt with classification by stimulus size in which five classes of different sizes were created and a total number of 130 stimuli were used (65 for training and 65 for validation). Some examples of each class are shown in the upper inset of Fig. 4. It can be noticed that the stimuli on each class also have different shapes, texture and degree of regularity. The classification error against input length is plotted in the lower inset of the same figure. The error reported with vector length 1 is quite low (11.69%) and further decreases until reaching the minimum value (1.69%), what happens with vector length 3. If size were the unique factor affecting the value of the global output activity, the error at length 1 should probably be lower. In reality, both the degree of regularity and shape are explanatory factors as well, what makes the classification task a little bit more complex. Fig. 2 illustrates the case comparing two stimuli. Even though the first one (panel A1) is smaller in size than the second one (panel A2), its global output is greater. The reason why this happens is because the former stimulus has a higher degree of regularity than the later one. The classifier therefore needs more data to discriminate among different sizes. In fact, this is what happens just by adding the next value of the pre-processed oscillatory pattern, which corresponds with the output of the model at the 7th iteration. The classification error then decreases to 4.3%. This trend, surprisingly, reverses at length 7 when the error increases until reaching its maximum at length 17. A possible
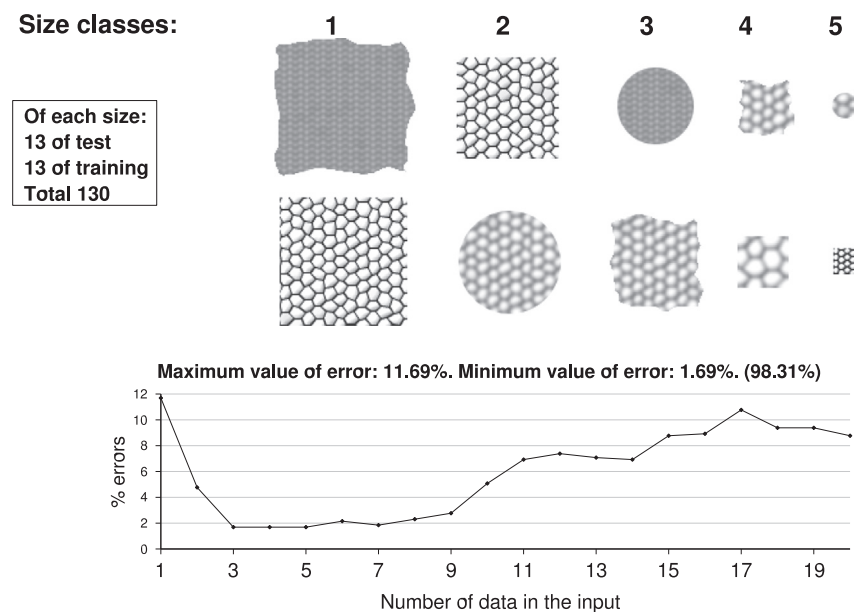

Fig. 4. Classification by stimulus size. Upper inset: five classes were identified according to their different size. For each class, 13 stimuli for training and 13 stimuli for test were generated. Lower inset: the classification error is shown for different lengths of the input vector (CN output series).

explanation is that the signal-to-noise ratio is reduced as the length exceeds some optimal value.

The second experiment was aimed at classifying stimuli by their degree of regularity (or inversely, their degree of contrast). Four classes were created: one with no smoothing, and the other three with different degree of smoothing (Gaussian filters: 2×2, 4×4 y 8×8). All samples of each class having different sizes and textures (Fig. 5). Some examples of each class are shown in the upper inset (from left to right: no smoothing, 2×2, 4×4 and 8×8 Gaussian filter). Overall, 128 different stimuli were used (64 for training and 64 for validation). The classification error, shown in the lower inset of Fig. 5, presents an initial error of 37.5% and then decreases until a minimum value of 3.65%, which is reached at vector length 9. The error slightly increases afterwards when lengths get longer than 9. Compared with the size experiment, it seems that this task is more complex and a greater amount of data is required to reach a similar classification performance.

The third experiment was focused on classification by stimulus shape. Here, nine classes corresponding with the numerical characters 1, 2, 3, 4, 6, 7, 8 and 0 were defined, and a total number of 180 stimuli were used (90 for training, and 90 for validation). The upper inset of Fig. 6 depicts some examples of the typescripts for the nine classes. The classification error is quite high at the shortest input vector length (84.13%) but it substantially decreases until reaching the minimum value (45.13%) at vector length five. As in previous experiments, the error gets worse at the vector length exceeds that value.

In the final experiment, the task was to classify stimuli by their degree of segmentation. Five classes, with number of segments ranging from 1 to 5, were set (see Fig. 7, upper inset) and a total number of 100 stimuli were used (50 for training and 50 for validation). The total surface area was kept constant in all cases. The classification error is quite high at the beginning (80%), which indicates the complexity of the task at hand, but it decreases as expected when increasing vector length until reaching the minimum value (48.33%) at length eight. It is interesting to note that in this and the previous experiment, the initial error is the same as the one produced by a predictor merely based on prior probability distributions of stimulus classes. Let M be the total number of classes and N the total number of stimuli per class. The probability that a stimulus n would belong to class m is $P(class(stimulus_n) = m) = N_m/N_{total}$,

where N_m is the total number of stimuli in class m and N_{total} the total number of stimuli in all classes. As $N_m = 10$ for all classes and $N_{total} = 50$, the prior probability $P(class(stimulus_n) = m) = 0.2$. This means that the probability of correct predictions by betting $class(stimulus_n) = m$ for all stimuli n is just 20%. In other words, the probability of incorrect predictions, the classification error, would be 80%, which is the same value obtained by our classifier when the length of input vector is just one.

4. Discussion

The errors obtained on each of the four classification problems correlate with the complexity of the task at hand: the lowest error corresponding with the stimulus size classification, the highest one with the identification of stimulus segments. However, a common pattern is observed in all the experiments: (1) the maximum error value is obtained with the shortest input vector, (2) the error decreases as the length of the input vector increases, (3) the minimum error value is reached at some intermediate length of the input vector, and (4) the error value increases as the input vector goes beyond the optimal length. The optimal classification is thus carried out during the temporal window in which the CN model transmits a representation combining both the zones of highest contrast and the progressive coding of the stimulus surface. These two components are decisive in reducing the errors in the recognition and classification of stimuli and are the result of the processing carried out by the circuitry of the cuneate nucleus. The number of correct responses increased when the learning network took into account a code specifically elaborated by the model of the nucleus. However, we have to further investigate whether the classifier could be improved by taking as input the parameters of the oscillatory pattern (duration, maximum amplitude, and amplitude of residual oscillations) rather than the raw pattern itself.

Temporal codes have been proposed in other sensory systems as well. In the auditory system, for instance, it has been reported that inner hair cells of the cochlea generate a spatio-temporal pattern encoding the tones of the incoming sound signals [15]. These patterns are processed later by the central auditory neurons in order to categorize the characteristic frequency. Moreover, in
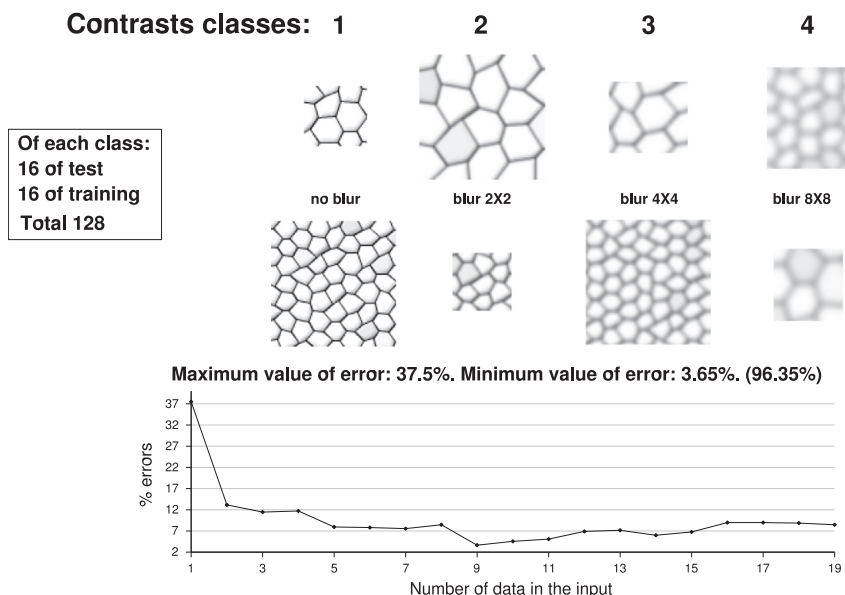

Fig. 5. Classification by stimulus regularity. Upper inset: four classes were identified according to their different degree of regularity (or inversely, their degree of contrast). For each class, 16 stimuli for training and 16 stimuli for test were generated. Lower inset: the classification error is shown for different lengths of the input vector (CN output series).
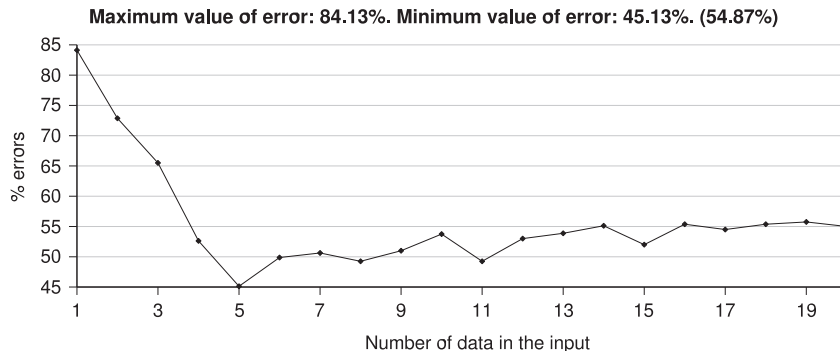
Fig. 6. Classification by stimulus shape. Upper inset: nine classes were identified according to their different shape. For each class, 10 stimuli for training and 10 stimuli for test were generated. Lower inset: the classification error is shown for different lengths of the input vector (CN output series).
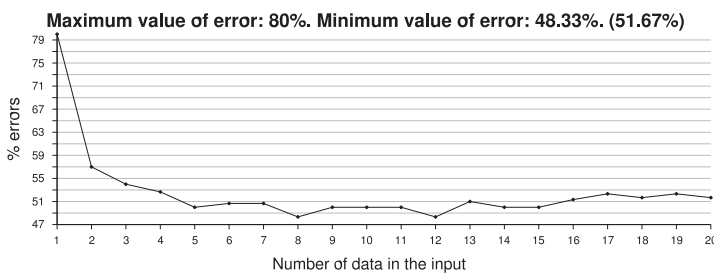

Fig. 7. Classification by degree of segmentation. Upper inset: five classes were identified according to their degree of segmentation. For each class, 10 stimuli for training and 10 stimuli for test were generated. Lower inset: the classification error is shown for different lengths of the input vector (CN output series).

the visual system, a rank-based coding has been proposed based on the order of the firing of the first spike for each neuron [16].

In short, our model predicts that the CN creates a type of spatio-temporal code, which could be similar to the codes proposed in other sensory systems, that encodes relevant information about relevant stimulus features (such as its size, shape and degree of regularity). Furthermore, it suggests that the neurons of the primary somatosensory cortex, the main candidates to play the role of observers, might receive the spatio-temporal code generated at CN and thalamus and perform the classification task. Our findings indicate that the longer the time spent by the cortex to process the incoming temporal code, the bigger the amount of data available as input, and thus the higher the accuracy on performing the classification task.

References

[1] J. Aguilar, C. Soto, C. Rivadulla, A. Canedo, The lemniscal-cuneate recurrent excitation is suppressed by strychnine and enhanced by $GABA_A$ antagonists in the anaesthetized cat, Eur. J. Neurosci. 16 (2002) 1697–1704.

[2] K.J. Berkley, R.J. Badell, A. Blomqvist, M. Bull, Output systems of the dorsal column nuclei in the cat, Brain Res. Rev. 11 (1986) 199–225.

[3] K.H. Britten, M.N. Shadlen, W.T. Newsome, J.A. Movshon, The analysis of visual motion: a comparison of neuronal and psychophysical performance, J. Neurosci. 12 (1992) 4745–4765.

[4] A. Canedo, L. Martinez, J. Mari no, Tonic and bursting activity in the cuneate nucleus of the chloralose anesthetized cat, Neuroscience 84 (2) (1998) 603–617.

[5] A. Canedo, J. Aguilar, J. Mari no, Lemniscal recurrent and transcortical influences on cuneate neurons, Neuroscience 97 (2) (2000) 317–334.

[6] H.G.J.M. Kuypers, J.D. Tuerk, The distribution of the cortical fibers within the nuclei cuneatus and gracilis in the cat, J. Anat. 98 (1964) 143–162.

[7] J.H. Lue, S.M. Luai, T.J. Wang, J.Y. Shieh, C.Y. Wen, Synaptic relationships between corticocuneate terminals and glycine-immunoreactive neurons in the rat cuneate nucleus, Brain Res. 771 (1997) 167–171.
[9] J. Navarro, E. Sánchez, A. Canedo, Spatio-temporal information coding in the cuneate nucleus, Neurocomputing 69 (16–18) (2006) 1946–1953.
[10] J. Navarro, E. Sánchez, A. Canedo, Information coding in early stages of the somatosensory system, Nat. Comput. 6 (2007) 253–267.
[11] A. Nu nez, W. Bu no, In vitro electrophysiological properties of rat dorsal column nuclei neurons, Eur. J. Neurosci. 11 (1999) 1865–1876.
[12] A. Reboreda, E. Sánchez, M. Romero, A. Lamas, Intrinsic spontaneous activity and subthreshold oscillations in neurons of the rat dorsal column nuclei in culture, J. Physiol. 551 (1) (2003) 191–205.
[13] D.E. Rumelhart, E.H. Geoffrey, R.J. Williams, Learning Internal Representations by Error Propagation, in: E. David, Rumelhart, James L. McClelland (Eds.), Parallel Distributed Processing: Explorations in the Microstructure of Cognition and the PDP Research Group, vol. 1, MIT Press, 1986.
[14] E. Sánchez, J. Aguilar, C. Rivadulla, A. Canedo, The role of glycinergic interneurons in the dorsal column nuclei, Neurocomputing 58–60 (2004) 1049–1055.
[15] S. Shamma, Spatial and temporal processing in central auditory networks, in: C. Koch, e.I. Segev (Eds.), Methods in Neuronal Modeling, 1998, pp. 411–460.
[16] S.J. Thorpe, J. Gautrais, Rank order coding: a new coding scheme for rapid processing in neural networks, in: J. Bower (Ed.), Computational Neuroscience: Trends in Research, 1998, 113–119.

Rubén Ferreiroa was born in Ferrol, Spain, in 1973. He received the B.S. degree in physics from the University of Santiago de Compostela in 1998, M.S. degree in Telematic from ITE Caixa Galicia/University of La Coruña, 1999 and M.S. degree in Neuroscience at the University of Santiago de Compostela in 2010. Currently he combines his Ph.D. with a job in Navantia Company as System Engineer Manager. His research interest is in computational models of visual system, information coding.

Antonio Canedo is a professor of Physiology at the School of Medicine, Universidad de Santiago de Compostela, Spain. He received his Ph.D. from the University of Santiago de Compostela in 1980. His main research interest is to study the mechanisms leading to sensorimotor integration at supraspinal level, using electrophysiological techniques.

Juan Navarro was born in Spain in 1953. He did his graduation in Medicine at the University of Santiago de Compostela in 1980. Currently, he is working as an Associate Professor in the Department of Physiology at the University of Santiago de Compostela. His research interest is in computational models of somatosensory system.

Eduardo Sánchez was born in Barcelona, Spain, in 1970. He received the B.S. degree in physics from the University of Santiago de Compostela in 1993, an Ms. degree in Neuroscience at the International University of Andalucía in 1996, and an Ms. degree in Computer Science at the University of Southern California in 2001. He also received the Ph.D. in Physics in 2000 at the University of Santiago de Compostela. Currently, he is working as an Associate Professor of the Department of Electronics and Computer Science at the University and as researcher of the Research Center for Information Technologies (CITIUS) of Santiago de Compostela. His research interest is in computational models of somatosensory and visual system, satisfaction models and recommender systems.

Anexo 3

Aceptado para publicación con el título pendiente de modificación por el editor

The indepence of image contrast and sharpness in the early visual pathway / Image sharpness and contrast tuning in the early visual pathway.

Sánchez, E., Ferreiroa, R., Arias, A., Martínez, L.M.

IMAGE SHARPNESS AND CONTRAST TUNING IN THE EARLY VISUAL PATHWAY

EDUARDO SÁNCHEZ

Grupo de Sistemas Inteligentes (GSI),Centro Singular de Investigación en Tecnologías de la Informacin (CITIUS), University of Santiago de Compostela, Rua Jenaro de la Fuente
Santiago de Compostela, 15782, Spain
E-mail: eduardo.sanchez.vila@usc.es
www.usc.es/citius

RUBÉN FERREIROA

Grupo de Sistemas Inteligentes (GSI),Centro Singular de Investigación en Tecnologías de la Informacin (CITIUS), University of Santiago de Compostela, Rua Jenaro de la Fuente
Santiago de Compostela, 15782, Spain
E-mail: rferreiroa@gmail.com
www.usc.es/citius

ADRIÁN ARIAS

Grupo de Sistemas Inteligentes (GSI),Centro Singular de Investigación en Tecnologías de la Informacin (CITIUS), University of Santiago de Compostela, Rua Jenaro de la Fuente
Santiago de Compostela, 15782, Spain
E-mail: adrian.arias.abreu@usc.es
www.usc.es/citius

LUIS M. MARTÍNEZ

Instituto de Neurociencias de Alicante, CSIC-Universidad Miguel Hernández
Avenida de Ramón y Cajal s/n
03550, San Juan de Alicante, Spain
E-mail: l.martinez@umh.es
in.umh.es

The center-surround organization of the receptive fields of retinal ganglion cells highlights the presence of local contrast in visual stimuli. As receptive fields of thalamic relay cells follow the same basic functional organization, it is often assumed that they contribute very little to alter the retinal output. However, in many species, thalamic relay cells largely outnumber their retinal inputs, which diverge to contact simultaneously several units at thalamic level. This gain in cell population as well as retinothalamic convergence opens the door to question how information about contrast is transformed at the thalamic stage. Here, we address this question using a realistic dynamic model of the retinothalamic circuit. Our results show that different components of the thalamic receptive field might implement the analogous of various types of well-known image processing techniques to preserve the quality of a higher resolution version of the image on its way to the primary visual cortex.

1. Introduction

Visual information reaches the brain through the activity of thousands of neurons distributed in non-random arrays across the innermost layer of the retina (Wässle et al., 1981a). Anatomical and physiological studies have shown that both the dendritic arbors and the receptive fields (RFs) of these retinal ganglion cells (RGCs) form mosaics that are coordinated to approach the theoretical resolution limit of a hexagonal lattice (Wässle et al., 1981b; Eglen et al., 2005; Gauthier et al., 2009; Liu et al., 2009). Further, it has recently been shown that these RF mosaics are established without the need of visual experience (Anishchenko et al., 2010). Given the stereotyped, optimized and hardwired nature of these retinal arrays it is often assumed that their spatial arrangement sets the limits of visual resolution, and hence image quality, before information is relayed to visual structures upstream for further processing.

On the other hand, high-resolution information about an image, which is first encoded by mosaics of RGCs of the X- or parvo-type, reaches the primary visual cortex (V1) via a relay in the lateral geniculate nucleus of the thalamus (LGN). Since relay cells in the LGN have RFs that resemble the spatiotemporal structure of the retinal RFs, i.e. built from two antagonistic and concentrically arranged subregions with the opposite preference for stimulus contrast (Kuffler, 1953; Wiesel, 1959; Hubel, 1961), most current models consider that the retinal message is not significantly altered on its way through the thalamus.

However, a closer look to the details of the retinothalamic circuit seems to suggest otherwise. First, in many species such as the cat, LGN relay cells outnumber their antecedent RGCs by at least a factor of 2 (Madarász et al., 1978; Peters and Payne, 1993). Second, in previous studies, it has been consistently shown that retinal afferents diverge profusely upon entering the LGN, in such a way that relay cells receive relatively large values of retinothalamic convergence (Cleland et al., 1971a,b; Freund et al., 1985; Mastronarde, 1992; Peters and Payne, 1993; Usrey et al., 1999; Alonso et al., 2001; Yeh et al., 2009; Martínez et al., 2014). We have recently used computational models based on experimental data and simple statistical wiring rules to show that this gain in cell population as well as retinothalamic convergence generates in the LGN an interpolated map of the retinal output that upsamples the retinal image, improving coverage of visual space, expanding information capacity and increasing signal-to-noise ratio (Martínez et al., 2014). Thus, an analysis with a Bayesian decoder (Ruderman and Bialek, 1992) shows that the LGN is, in fact, able to estimate the position of a point stimulus in noise more precisely than the retina can achieve alone (Martínez et al., 2014; Hirsch et al., 2015).

Improving visual resolution through interpolation, however, introduces spatial correlations that smooth contrast borders degrading the quality of the perceived images. Our previous physiological results show that LGN relay cells receive a particular spatial arrangement of excitatory and inhibitory inputs within the RF center that mitigates this effect by increasing the slope of contrast borders, akin to some techniques used in digital image processing (Martínez et al., 2014; Hirsch et al., 2015). These results were based on a static, topological model of the retinothalamic circuit that considered fundamentally the spatial distribution of synaptic inputs to the RF centers of LGN relay cells and interneurons. The potential contribution of the other compartments of retinal and thalamic RFs, i.e. the excitatory and inhibitory surrounds, was not explored. Here, we used a dynamic, spiking version of our previous computational model to investigate how the different cellular components of the retinothalamic circuit, with their full center-surround RFs, interact to improve spatial resolution and quality of the retinal image on its way to V1.

2. Hypothesis

The goal of this study is therefore to analyze the function of the LGN circuit and its role on the retinothalamic X pathway. The 2:1 ratio between LGN and RGC cells (Madarász et al., 1978; Peters and Payne, 1993) might suggest that an upsampling process of the input, which corresponds to RGC's output, is carried out at the LGN. In the field of image processing such type of image transformation might be accomplished by means of different types of interpolation schemes, which estimate the intensity values of the new pixels. At LGN, the interpolation operation could be successfully implemented in LGN cells through the weighted aggregation of RGCs outputs. However, interpolation is a smoothing operation that comes at the cost of blurring the

edges, thus reducing the perceived quality of the images. The issue then regards with how the LGN is capable to enhance input details in order to recover or mitigate the impact of such smoothing operation.

Two types of image processing techniques are typically used to enhance image quality: sharpening and contrast stretching (Gonzalez and Woods, 2008). The first one corresponds to the class of spatial filtering techniques, the second one to the class of intensity or luminance transformation techniques. Sharpening focuses on highlighting the edges or luminance transitions while contrast stretching aims at amplifying the difference between luminance levels. Our hypothesis states that the LGN might preserve or even enhance details to both sharpen and stretch the contrast of each local patch of the input. Moreover, sharpness and contrast could be processed independently by means of different components of the thalamic receptive field.

3. Methods

3.1. *Retina-LGN Model: Overall view*

Fig. 1 shows the overall view of the main processing elements at the different stages of our retinothalamic model. The model simulates a patch of the retinothalamic circuit corresponding with a parafoveal visual field of $8°x8°$. The retina is simulated by two layers, the first one made up of ON-center Retinal Ganglion Cells (ON-RGC), the second one with OFF-center Retinal Ganglion Cells (OFF-RGC). RGCs are modelled with a Difference-of-Gaussians (DoG) model whose output is passed through a Poisson generator to simulate the spike train of the retinal output. The LGN is then modeled by three layers: the first one containing ON-center LGN Relay

Cells (ON-LGNr), the second and the third one containing OFF-Center LGN interneurons (OFF-LGNi) and ON-Center LGN interneurons (ON-LGNi), respectively. LGN cells are then modelled as spiking Integrate-And-Fire neurons.

3.2. *Input Stimuli*

A step-type stimuli made up of a dark and a bright band connected with an abrupt (step function) transition is used in the simulations (Fig. 2). Each stimulus is represented mathematically as a bi-dimensional 130x130 matrix, the matrix coefficients indicating the degree of luminance or intensity per point $I(x, y)$. Luminance values range from 0, the minimum value, to 1, the maximum one. Two different configurations were chosen to test our models: a High-Contrast (HC), with a $0, 3 - 0, 7$ luminance profile, and a Low-Contrast (LC), with a $0, 45 - 0, 55$ luminance profile.

3.3. *Retina: DoG model*

RGCs are simulated using a Difference-of-Gaussians (DoG) model. This is made up of two Gaussians: the first one representing the excitatory center of the RF, the second one the inhibitory surround. Figure 3 shows an schematic diagram of the model as used by Enroth-Cugell and Robson (1966, 1984), with their relevant parameters: the maximum amplitudes k_c and k_s, and the radius r_c and r_s. The function is formalized as follows:

$$DoG(r) = k_c e^{-(r/r_c)^2} - k_s e^{-(r/r_s)^2} \qquad (1)$$

being the relevant parameters: the maximum amplitudes k_c and k_s, and the radius r_c and r_s. These parameters were obtained by Enroth-Cugell
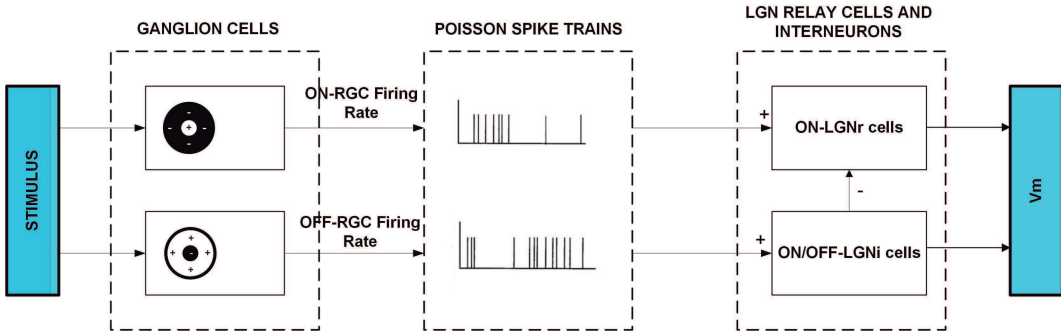
Figure 1. Overall view of the Retina-LGN model. The model is made up of RGCs, retinal Poisson generators, ON-LGNr, OFF-LGNi, and ON-LGNi.
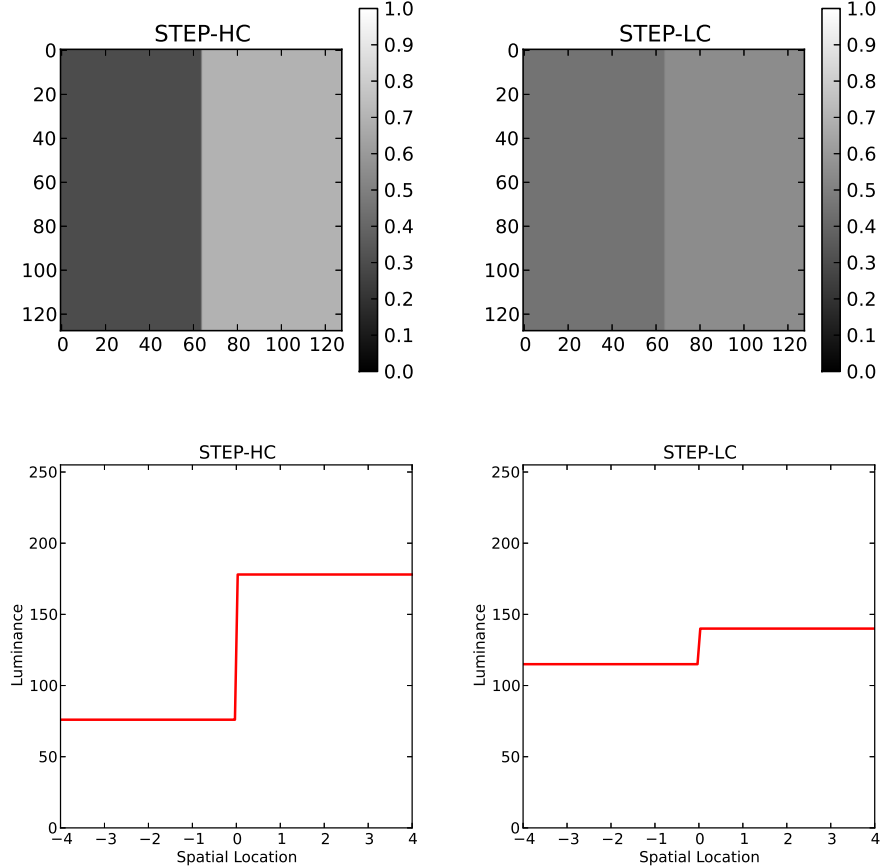
Figure 2.   Step-type stimuli. Bidimensional representation of the High-Contrast (STEP-HC) and Low-Contrast (STEP-LC) step-type stimuli (top). Luminance profile of a row chosen from the STEP-HC and STEP-LC stimuli (bottom).
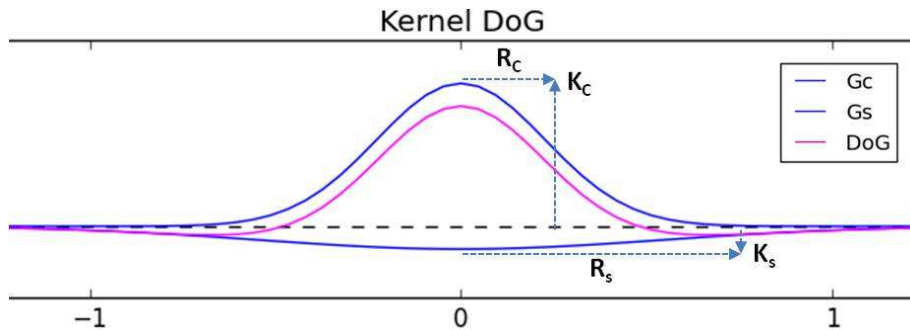
Figure 3.   The Difference-of-Gaussians model. The Gaussian describing the excitatory center (upper blue colored Gaussian) is combined with the inhibitory surround (lower blue colored Gaussian). The result is the Difference-of-Gaussian function (pink). The relevant parameters for each Gaussian, amplitudes (k_c, k_s) and radius (r_c, r_s), are also shown.

and Robson for a number of RGCs by fitting the theoretical contrast sensitivity function, derived from the DoG model, to the empirical contrast sensitivity function measured at different spatial frequencies. In this paper, we resort to these parameters (Table 1) to build realistic DoG functions that model the processing of RGCs.

DoG = f(Kc,Rc, Ks, Rs)
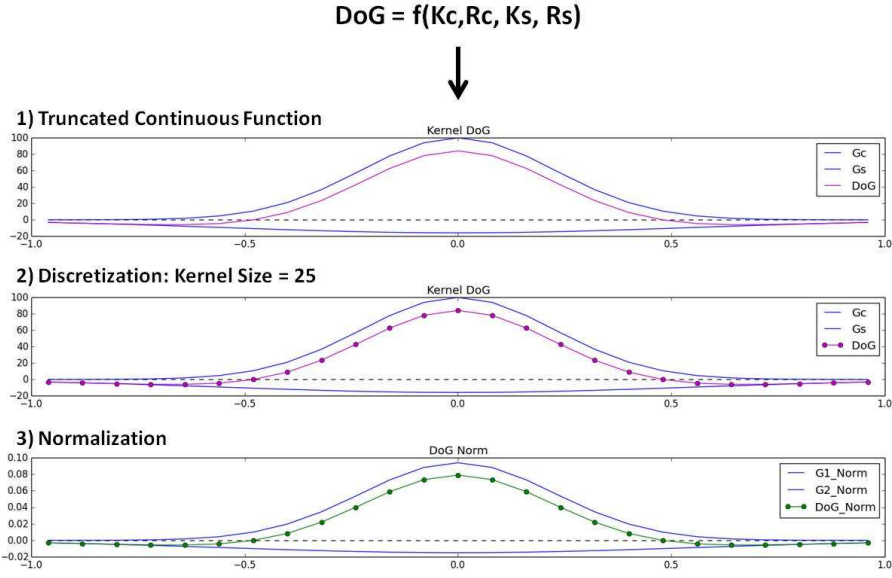
Figure 4.   Discretization of the continuous DoG model: truncation (upper inset), sampling (middle inset), and normalization (lower inset).

Table 1.   Parameters of RGC and LGN cell models. RGC parameters correspond to cell number 56, as identified by Enroth-Cugell and Robson (1966).

RGC parameters	**RGC values**	*LGN parameters*	**LGNr values**	**LGNi values**
r_c	0,14 deg	C_m	2 μF	2 μF
r_s	3,3 deg	V_r	65 mV	65 mV
r_s/r_c	23	V_t	35 mV	45 mV
$k_s r_s^2/k_c r_c^2$	0,98	a	0,02	0,1
		b	0,2	0,2
		c	-50	-65
		d	2	2

3.4.   *Retina: Discrete DoG kernels*

The continuous DoG functions fitted to experimental data has to be converted into discrete DoG kernels to operate with input images. In what follows, the four steps involved in the process are summarized. Further details can be found in Arias et al. (2015).

As the continuous function can take infinite values, the first step consisted on truncating it in order to set a finite range of values. Figure 4 describes the process in one dimension. A variable T was defined to determine the width of the truncation: $T = n_T * r_c$, where n_T is an integer and r_c the radius of the center. The second step consists on sampling the continuous function. By setting the size $N_S x N_S$ of the kernel, the number of both the elements of the kernel matrix as well as the sampling points of the continuous

DoG function are set. After the convolution of the input image with the discrete kernel, the output image has to preserve the intensity ranges of the input. The third step therefore involves the normalization of the elements of the DoG kernel matrix W_K. Each element or weight w_{ij} of the matrix is normalized as follows:

$$w_{ij}^{norm} = \frac{w_{ij}}{\Sigma_i \Sigma_j w_{ij}} \qquad (2)$$

Finally, the goodness of the discretization procedure has been assessed by fitting back the normalized discrete DoG kernel to the original continuous DoG function. The Levenberg-Marquart algorithm was chosen to solve the non-linear least squares fitting problem as its provides a good compromise between speed convergence and operating stability.

3.5. *Retina: Choice of kernels*

For each of the $23(= 17+6)$ cells reported by Enroth-Cugell and Robson (see section 3.3) a set of discrete DoG kernels were generated after varying the parameters of the discretization process being applied on the original continuous DoG function. Two discretization parameters, the integer n_T describing the width of the truncation T and the size N_S of the kernel, were modified in order to obtain each kernel of the set. The kernels were then analyzed in terms of its representation in both the spatial and frequency domains. It can be concluded that all set of kernels from all cells change with the discretization parameters in a similar fashion. On the basis of this result, the cell number 56 of Enroth-Cugell and Robson (1966) was chosen to simulate the RGCs in our model.

In our implementation the kernel properties change with the discretization parameters (Arias et al., 2015). The maximum gain (g_{max}) is the most relevant kernel parameter that determines the degree of transformation carried out in the input. Discrete kernels with negligible gains generate outputs quite similar to the inputs. On the contrary, high-gain kernels can make important changes in the input, both in terms of contrast and spatial correlation. In order to analize the LGN contribution to visual processing on a plausible range of inputs (the corresponding retinal outputs), we have chosen two kernel configurations:

- Zero-gain DoG Kernel: K_{zero}, where $g_{max} = 0$ dB. The discretization parameters for this kernel are: $n_T = 40$, and $N_S = 15$.
- Medium-gain DoG Kernel: K_{medium}, where $g_{max} = 18,13$ dB. The discretization parameters for this kernel are: $n_T = 20$, and $N_S = 35$.

A high-gain kernel was not chosen as it might saturate the output when the input contains high-contrast transitions. The saturation issue can be handled with contrast gain control mechanisms. As our focus here is on the LGN, we decided to keep the Retina model as simple as possible by not including those mechanisms.

3.6. *Retina: Output Firing Rate*

The rate R of a ganglion cell at location (x,y) is computed with a 2D discrete convolution function between the input stimulus I and the discrete DoG kernel matrix W_K:

$$R(x,y) = \sum_{s_u=1}^{N_S} \sum_{s_v=1}^{N_S} W_K(x - s_u, y - s_v) \cdot I(x,y) \quad (3)$$

where N_S represents the size of the kernel, and both s_u and s_v some indices to iterate through the rows and columns of matrix W_K.

Finally, a sequence of spikes is stochastically generated through a pulse train generator that follows the statistics of a homogeneous Poisson process:

$$P_T(n) = \frac{R(x,y)T}{n!} e^{-R(x,y)T} \quad (4)$$

3.7. *LGN: Cell types and models*

Our model of LGN is made up of three types of neurons: (1) ON-center LGN relay cells (ON-LGNr), (2) OFF-center LGN interneurons, and (3) ON-center LGN interneurons. The other processing channel, the OFF-center LGN relay cells, was not included in the presented model.

We used spiking models (Ghosh-Dastidar and Adeli, 2009) of LGN neurons. Specifically, an implementation of the Izhikevich model (Izhikevich, 2003) as implemented in the NEST simulator (Gewaltig and Diesmann, 2007) for the relay cells as well as interneurons. This model reproduces regular spiking, fast spiking and bursting behavior depending on the parameters selected in the following equations:

$$C_m \frac{dV}{dt} = -k(V - V_r) + (V - V_t) - U + I \quad (5)$$

$$\frac{dU}{dt} = a(b(V - V_r) - U) \quad (6)$$

where C_m is the capacitance, V is the membrane potential, V_r is the resting membrane potential, V_t is the instantaneous threshold potential, U is the recovery current, a is the recovery time constant, b a parameter that determines whether U is an amplifying ($b \leqslant 0$) or a resonant ($b \geqslant 0$) factor, and I the injected DC current. The dynamics of spike generation is governed by the following equation:

$$V \geqslant V_{peak} \begin{cases} V = c \\ U = U + d \end{cases} \quad (7)$$
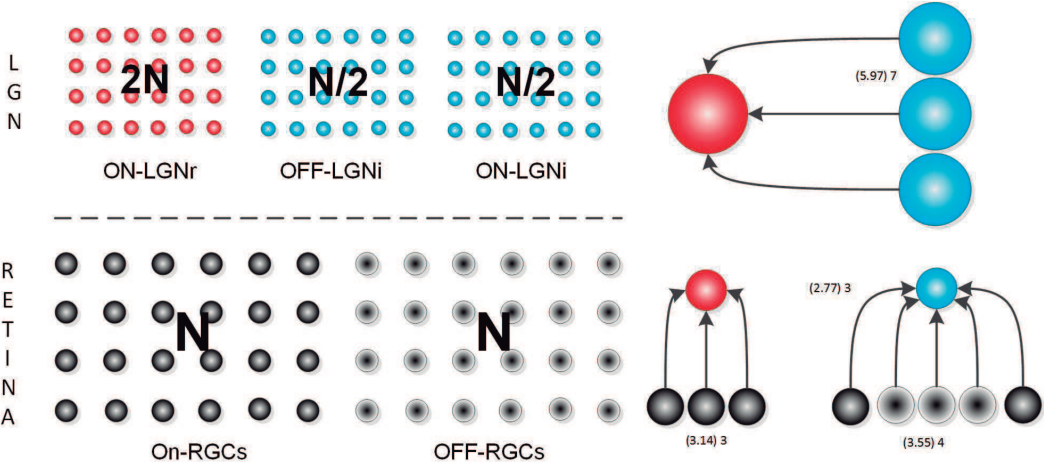
Figure 5.   Wiring of the retinothalamic circuit. The model is made up of five layers (left inset): two retinal layers representing ON and OFF-center RGCs, and three LGN layers representing ON-LGNr and both OFF-LGNi and ON-LGNi cells. The number of LGNr cells (ON plus OFF types: 2N+2N) doubles the number of RGCs (N+N), as well as follows a 4:1 ratio with LGNi cells (N/2+N/2). The mean of convergent connections was estimated by fitting a model with empirical data (right inset), but the model computes a sample mean (in brackets) of those connections each time the model is built.

where V_{peak} is the spike cutoff value, c the voltage reset value, and d describes the total amount of outward minus inward currents activated during the spike and affecting the after-spike behavior.

All these parameters (see Table 1) were fitted to simulate both relay cells and interneurons.

3.8.   *LGN: Wiring*

The retina was simulated with two rectangular layers of 80x80 point locations, the first one containing ON-RGCs, and the second OFF-RGCs. The LGN, in turn, is described with three rectangular layers: the first one with dimensions 115x115 containing ON-LGNr; the second and the third with dimensions 60x60 and made up of OFF-LGNi and ON-LGNi, respectively (Fig. 5). These dimensions were set to preserve the 2:1 ratio between LGNr and RGCs as well as the 1:2 ratio between LGNi and RGCs, which means a 4:1 ratio between LGNr and LGNi (Martínez et al., 2014). The total number of cells on each layer satisfying these constraints is shown in Fig. 5.

LGN cells receive both retinal and thalamic input according to the following structure:

- Inputs of ON-LGNr:
  (1) Center Retinal Input: ON-RGCs
  (2) Surround Retinal Input: OFF-RGCs
  (3) Center LGN Input: OFF-LGNi

- Inputs of OFF-LGNi:
  (1) Center Retinal Input: OFF-RGCs
  (2) Surround Retinal Input: ON-RGCs
  (3) Center LGN Input: ON-LGNi

- Inputs of ON-LGNi:
  (1) Center Retinal Input: ON-RGCs
  (2) Surround Retinal Input: OFF-RGCs

Each LGN cell was first connected to its nearest neighbor in the retinal layer, i.e. the one from which its polarity was inherited. The probability of each LGN cell, re-centered at retinal coordinates at the (x,y) position of its first retinal input, being connected with a RGC located at the (x',y') position follows a Gaussian function of their relative distance (Martínez et al., 2014; Alonso et al., 2001). The synaptic strength of the connections was also assumed to be a Gaussian function of the distance between the receptive-field centers (Martínez et al., 2014; Alonso et al., 2001). The function for both connection probability and strength is as follows:

$$P = p_{max}e^{-(x-y)^2/2\sigma_{cen}^2} \qquad (8)$$

Furthermore, the convergence between cell types were estimated by fitting a wiring model with empirical data (Martínez et al., 2014). Those estimated values were used in the current model and are also illustrated in Fig. 5.
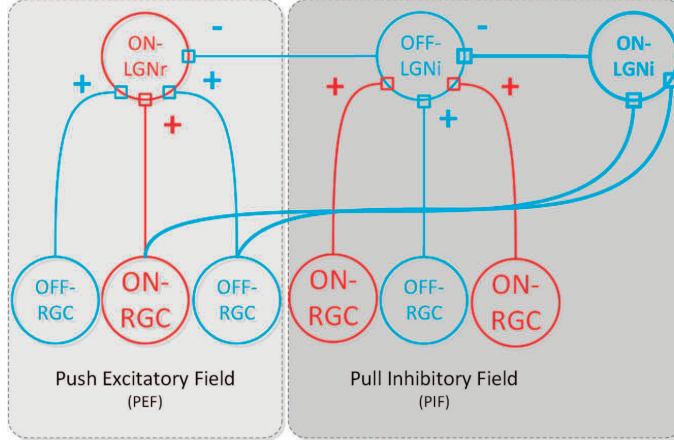
Figure 6.   LGN full push-pull circuit. The two main components of the circuit, the push excitatory field (PEF) as well as the pull inhibitory field (PIF), are highlighted.

3.9.   *LGN: Full push-pull circuit*

The wiring of the LGN cells configures a push-pull circuit (Martínez et al., 2014; Hirsch et al., 2015) with the following components (Fig. 6):

- Push Excitatory Field (PEF): ON-LGNr cells with ON-RGCs and OFF-RGCs as Center and Surround Retinal Inputs, respectively.
- Pull Inhibitory Field (PIF): OFF-LGNi cells with OFF-RGCs and ON-RGCs as Center and Surround Retinal Inputs, as well as ON-LGNi as Center LGN input.

In order to analyze the role played on visual processing by each element of the LGN we have built the full circuit step by step.

3.10.   *Contrast, sharpness and Image Quality*

In visual perception, contrast is determined as the difference between the light intensities of two adjacent regions of the visual field. However, the formal definition of contrast may have different instances, ranging from Weber, Michelson, RMS, and GLCM contrast, among others. In this paper we consider the unnormalized version of Michelson contrast, thus the difference between the maximum and the minimum levels of steady intensity of the visual or image representation (Fig. 7). Formally, it is described as follows:

$$C = I_{max}^{steady} - I_{min}^{steady} \quad (intensity \quad units) \quad (9)$$

where I_{max}^{steady} represents either the steady level of maximum luminance of an input stimulus or its corresponding spike rate at LGN output, and I_{min}^{steady} the equivalent for the minimum luminance.

Sharpness (S) is determined by the height of the peaks that a filter generates at the edges or intensity transitions of the input stimuli. On any transition, two peaks could be generated corresponding to the maximum and minimum levels of luminance. Therefore:

$$S = S_{max} + S_{min} \quad (intensity \quad units) \quad (10)$$

where,

$$S_{max} = \left| I_{max}^{peak} - I_{max}^{steady} \right| \quad (11)$$

$$S_{min} = \left| I_{min}^{peak} - I_{min}^{steady} \right| \quad (12)$$

A measure of Image Quality (IQ), suitable for the specific case of an image with a single transition, is proposed as follows (Fig. 7):

$$IQ = \tan \alpha = \frac{C + S}{TW} \quad \left(\frac{intensity \quad units}{spatial \quad units}\right) \quad (13)$$

where C and S stand for the contrast and sharpness found on the transition of the image, and TW, or Transition Width, represents the width of the transition in spatial units:
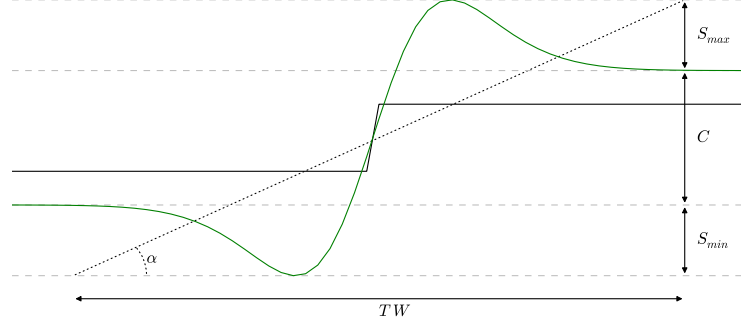
Figure 7.   Contrast (C), Maximum Sharpness (S_{max}), Minimum Sharpness (S_{min}), Transition Width (TW) and Image Quality ($\tan \alpha$).

$$TW = \left| x_{I=I_{max}^{level}} - x_{I=I_{min}^{level}} \right| \quad (spatial \quad units)$$

$$(14)$$

4.   Results

4.1.   *Retina*

HC and LC input stimuli were convolved with the two chosen kernels K_{zero} and K_{medium} to estimate the output of ON-RGCs. In parallel, the negative images of those inputs were also convolved with the same kernels to generate the output of OFF-RGCs. The plots shown in Fig. 8 illustrate the symmetry of OFF-RGCs responses (gray curves) compared with the ones of ON-RGCs (yellow curves). This fact is relevant in our study as the LGN takes as inputs both ON and OFF-RGC responses.

As K_{zero} and K_{medium} kernels might represent two different modes of operation in the Retina, it is interesting to point out the differences in their output. The responses Kzero-HC and Kzero-LC in Fig. 8 basically resemble the step stimuli presented as visual input (Fig. 2). The minor change is on the transitions, which are less abrupt in Retina than in the input, the reason probably being on the spike-based coding implemented in the model. On the other hand, the responses Kmedium-HC and Kmedium-LC significantly change the input. While preserving the intensity levels at both sides of the step, which explains why contrast (C) remains the same compared with K_{zero} kernels (Table 2), two new peaks are generated at both HC and LC transitions. These peaks are produced by the inhibitory surround of the dis-

crete DoG kernels. This process highlights the edges by sharpening the transitions, thus suggesting that the Medium-gain DoG Kernel K_{medium} might work as a sharpening filter. The sharpness generated by such filter is quantified in column S of Table 2. It can be observed that the sharpening process has the effect of doubling the difference of intensity at the transition $(C + S)$ when compared with the output of K_{zero} kernels.

Sharpening is an image processing technique aimed at improving the quality of the image by highlighting the edges of an image. In our model, if the baseline for intensity differences is just provided by the contrast parameter, we found that the sharpening process enhance the difference more than 100%, which might result in a significant improvement in terms of perception. However, this effect is reduced by means of an increase in transition width, which results in K_{zero} kernels showing higher IQs than K_{medium} ones. So, the sharpening carried out by K_{medium} filters may improve perception if and only if the sharpness enhancement does not come at a cost of stretching the transition width too much.

4.2.   *LGN: Push Excitatory Field*

The Push Excitatory Field (PEF) is made up of the retinal inputs received by ON-LGNr, on both its RF center and surround. The center input originates from ON-RGCs while the surround from OFF-RGCs (Fig. 6). We focus first on the effect of the center input and proceed then by including the surround.
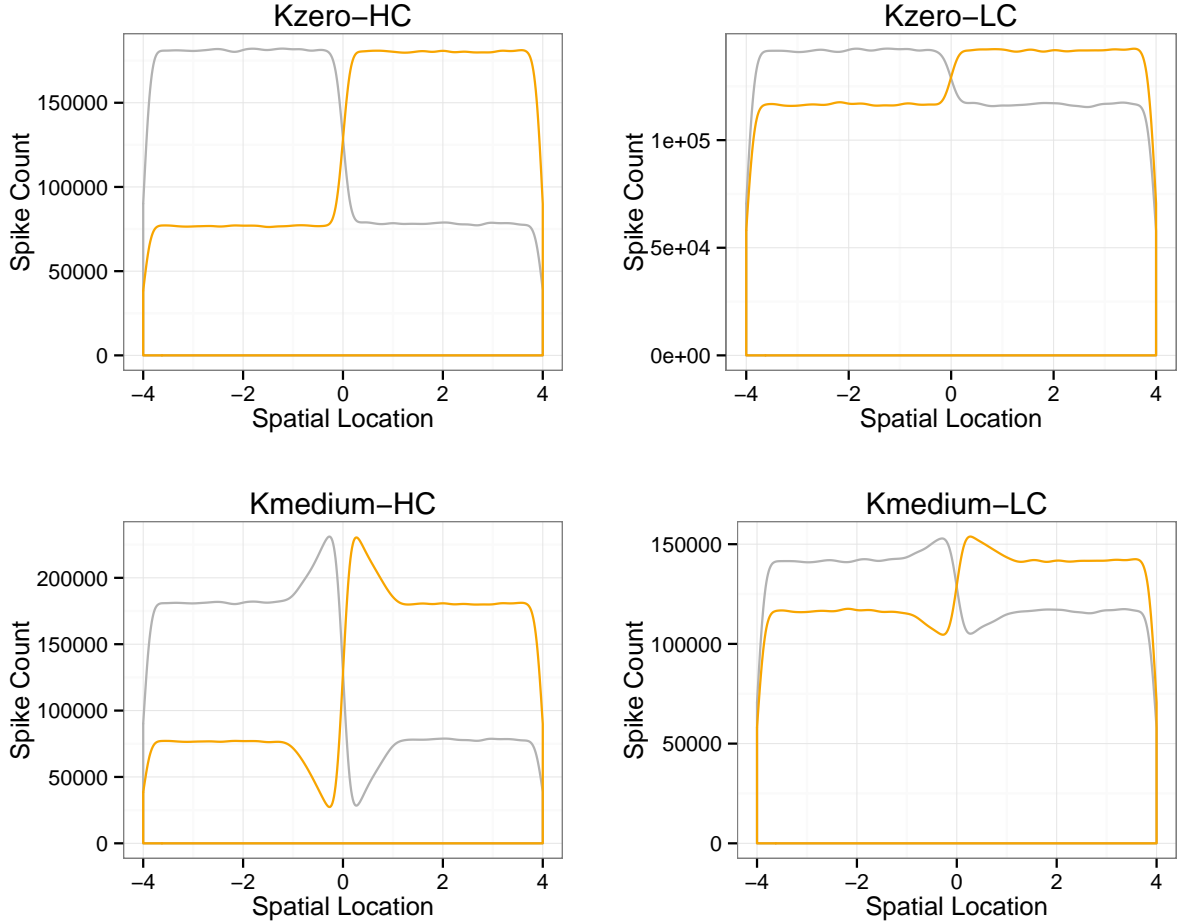
Figure 8.   Retina: RGCs responses induced by stimulus input. The spike-count of RGCs measured at different spatial locations is plotted during a 100 ms interval after stimulus presentation. On each plot, both ON-RGC (yellow curve) and OFF-RGC (gray curve) are shown. Kzero-HC and Kzero-LC: HC and LC stimulus convolved with K_{zero} kernel. Kmedium-HC and Kmedium-LC: HC and LC stimulus convolved with K_{medium} kernel.

Table 2.   Retina: Effect of center-surround arrangement on RGC output. The output is described in terms of the following parameters: Contrast (C), sharpness (S), Transition Width (TW) and Image Quality (IQ).

Retinal Kernel	Stimulus	C	S	TW	IQ
K_{zero}	HC	103.778	0	0,21	494.181
K_{zero}	LC	25.277	0	0.36	70.213
K_{medium}	HC	103.718	121.900	2.49	90.637
K_{medium}	LC	25.277	29.800	2.57	21.451

4.2.1.   *Center-alone effect*

The 2:1 ratio between LGNr and RGCs points out to an increase of spatial resolution at the LGN, and the mean value of convergent connections (3, see section 3.8) suggests that LGNr cells compute the weighted average of its ON-RGCs inputs. The profiles of responses are very similar to the ones observed in Retina but slightly smoothed (Fig. 9). The smoothing effect is quantified by considering the Transition Widths (TW) shown in Table 3. Their values are

Table 3. PEF-Center-Alone: Effect of center-alone arrangement on LGN processing. The LGN response is described in terms of the following parameters: Contrast (C), sharpness (S), Transition Width (TW), and Image Quality (IQ).

Arrangement	Retinal Kernel	Stimulus	C	S	TW	IQ
PEF-Center-Alone	K_{zero}	HC	72.764	0	1,13	64.219
PEF-Center-Alone	K_{zero}	LC	18.428	0	0,65	28.026
PEF-Center-Alone	K_{medium}	HC	70.563	70.228	2,74	51.389
PEF-Center-Alone	K_{medium}	LC	17.006	18.484	2,68	13.218

higher than those of Retina for all input configurations, specifically K_{zero} kernels. This is because the increase in sharpness present only in response to K_{medium} inputs, rises the transition slope and thus reduces the increase in width of the smoothing process. On the other hand, the contrast C as well as sharpness S for K_{medium} inputs are both substantially reduced, compared to the Retina. The analysis of the spiking behavior indicates that the firing rate of LGN-r cells is also lower than in the Retina, a result that has been experimentally observed before (Carandini et al., 2007), and that can be a consequence of the coincident firing of convergent aferents.

The overall impact of increased TWs and reduced Cs and Ss can be observed in the IQ values of Table 3. IQs are drastically reduced compared with Retinal values, therefore indicating that the quality of the image at the output of LGN is seriously affected by the transition carried out by the center of the push excitatory field established between ON-RGC and ON-LGNr layers. As expected, the upsampling process that expands the spatial representation of the image comes at a cost of reducing its perceived quality.

4.2.2. *Center-Surround effect*

The contribution of the excitatory surround is intriguing as this is the first time, as far as we know, that this type of input on LGN processing has been specifically analyzed. As no empirical data about these connections is still available, an arrangement similar to the center-surround organization of the Retina was assumed. Otherwise, wiring probability followed the same principle as the one used between ON-RGCs and ON-LGNr (see section 3.8).

When the surround is added to the center, some relevant changes arise compared with the center-alone configuration. First, the difference between the

intensities at each step level is notably reduced for all input configurations (Fig. 9). The output of OFF-RGCs is stronger on the left than on the right side of the step (see Fig. 8, gray curve), thus increasing significantly the excitatory drive received by the left part of the LGN circuit. The net effect is a reduction in contrast (C) in all input configurations as shown in Table 4. Second, a mild increase in sharpness appears already in response to K_{zero} inputs, as quantified in column S of Table 4. The sharpening operation carried out by the surround is accompanied by a reduction in TW values, except in the case of Kzero-LC, when compared with those of the center-alone configuration. The generation of the peaks around the luminance transition in the case of K_{zero} inputs, and the slight sharpening of the existing peaks in the case of K_{medium} inputs, both modify the slope of the intensity profile at the transition of the biphasic stimulus, thus reducing its width.

It was totally unexpected that the full Push Excitatory Field, with no inhibitory connections, could operate as a classical sharpening filter. Some basic formal analysis, however, can account for this result. Let $R_{ON}(x, y)$ be response intentity at the output of ON-RGCs of the Retina. If it is assumed that the negative representation of the image is processed by the OFF channel, then $R_{OFF}(x, y)$ is roughly:

$$R_{OFF}(x, y) = 1 - R_{ON}(x, y) \qquad (15)$$

Now, both responses are modulated by a Gaussian function that represents the RGC-LGN connections. These means that $R_{ON}(x, y)$ and $R_{OFF}(x, y)$ are low-pass filtered by the center and surround Gaussian connectivity, respectively. As a result, the input of the LGN circuit is:

$$I_{LGN}(x, y) = \langle R_{ON}(x, y) \rangle_{Gc} + \langle R_{OFF}(x, y) \rangle_{Gs} \qquad (16)$$

Table 4. PEF-Center-Surround: Effect of center-surround arrangement on LGN processing. The LGN response is described in terms of the following parameters: Contrast (C), sharpness (S), Transition Width (TW) and Image Quality (IQ).

| Arrangement	Retinal Kernel	Stimulus	C	S	TW	IQ
PEF-Center-Surround	K_{zero}	HC	29.601	3.020	0,73	44.442
PEF-Center-Surround	K_{zero}	LC	7.497	1.093	0,80	10.737
PEF-Center-Surround	K_{medium}	HC	29.993	40.605	2,54	27.836
PEF-Center-Surround	K_{medium}	LC	7.934	8.593	2,04	8.121
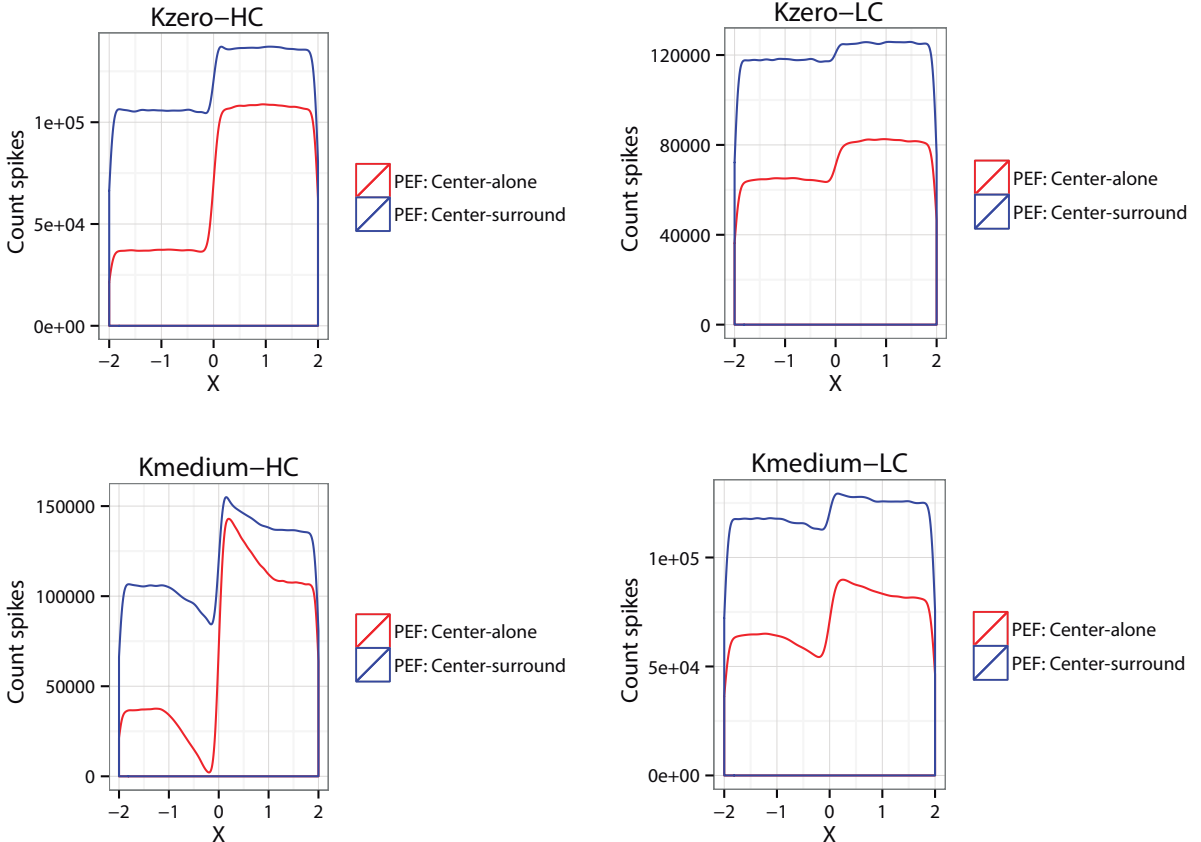
Figure 9. Push Excitatory Field (PEF): ON-LGNr responses under the effect of the center-alone as well as the combined effect of center-surround excitatory input are shown. The spike-count is plotted at different spatial locations being measured during a 100 ms interval after stimulus presentation. Kzero-HC and Kzero-LC: ON-LGNr responses after HC and LC stimulus being convolved with K_{zero} kernel. Kmedium-HC and Kmedium-LC: ON-LGNr responses after HC and LC stimulus being convolved with K_{medium} kernel.

where $\langle...\rangle$ denotes the low-pass filtering, and Gc and Gs the center and surround Gaussians. Substituting equation 15 in equation 16:

$$I_{LGN}(x,y) = 1 + \langle R_{ON}(x,y)\rangle_{Gc} - \langle R_{ON}(x,y)\rangle_{Gs} \tag{17}$$

Hence, if we assume that $Gs > Gc$ then a certain amount of low-frequency components is substracted from $\langle R_{ON}(x,y)\rangle_{Gc}$, or in other words, the high frequency components will be enhanced. The overall process can be understood as a sharpening operation by means of removing a number of low-frequency components of the input at the center of each ON-

LGNr cells.

However, the sharpening process cannot compensate the reduction in contrast, which results in lower IQs than those obtained with the center-alone arrangement.

4.3. *LGN: Pull Inhibitory Field*

The Pull Inhibitory Field (PIF) includes three main components (Fig. 6): OFF-LGNi cells receiving excitatory center input from OFF-RGCs, which, in turn, make inhibitory synapses on ON-LGNr cells; the excitatory surround input of OFF-LGNi coming from ON-RGCs; and finally, ON-LGNi cells evoking inhibition on OFF-LGNi neurons (interneurons with opposite polarity). As in the previous section, we will proceed to analyze the effect of each component by adding them to the circuit one at a time.

4.3.1. *Center-alone effect*

The processing carried out by this wiring has been analyzed by Martínez et al. (2014) (see also Hirsch et al., 2015) by means of a linear model. They found that the pull component with center-alone arrangement could improve the subjective appearence of an image by changing the slope or derivative of the intensity profile at luminace borders. We have tested their prediction by using our non-linear spiking version of the retinothalamic model.

The simulations show that the intensity levels are reduced at both sides of the transition (Fig. 10, green curve). The effect of the OFF-LGNi inhibitory input is to decrease the overall activity of ON-LGNr cells. However, the effect is larger on the left side, where the output of OFF-RGCs is stronger, than on the right side. The asymmetry of inhibition causes an increase of contrast, or difference between the intensity levels, which not only recovers but overtakes the values obtained with the Push Excitory Field under the center-alone configuration. In addition, the widths TW are higher than PEF-Center-Surround but lower than PEF-Center-Alone. The results shown in Table 4 indicate that the IQs of the PIF-Center-Alone configuration are superior to those of PEF-Center-Surround and PEF-Center-Alone (except in the case of Kzero-LC). Compared to PEF-Center-Surround, this improvement is explained by means of the increase in contrast; while regarding to PEF-Center-Alone, it is explained be-

cause of the lower TWs.

The downside is the loss of sharpness with Kzero-HC and Kzero-LC inputs as shown in Table 4. The reason lies on the fact that the OFF-LGNi layer has a much lower spatial resolution than the ON-LGNr one. Recall that the ratio of OFF-LGNi per OFF-RGC is just 1:2, whereas the ratio of ON-LGNr per ON-RGC is 2:1. A lower spatial resolution shapes the inhibitory profile, which is strong over the positive peak at the right side of the transition while weak on the negative peak at the left side (plots not shown). As a result, the peaks of the Kzero-HC and the Kzero-LC profiles of the PEF-Center-Surround circuit are suppressed.

Thus, contrast and sharpness enhancement seem to be at odds. While PEF-Center-Surround enhances image sharpness at the cost of reducing contrast, PIF-Center-Alone does the opposite, amplifying contrast at the cost of image sharpness.

4.3.2. *Center-Surround Effect*

This arrangement now includes the full center-surround receptive field of OFF-LGNi cells. The receptive field arrangement was assumed to be similar to the center-surround organization of the RGCs. In addition, connection probability followed the same wiring rules used between ON-RGCs and ON-LGNr (see section 3.8). The results shown in Fig. 10 illustrate that PIF-Center-Surround configuration generate responses that are smoothed versions of the ones obtained with PIF-Center-alone. In that regard, the behavior of the circuit resembles the one observed in PEF-Center-Surround when compared with the output of PEF-Center-Alone. The difference between levels is substantially reduced due to the increase of overall input to OFF-LGNi cells coming from the excitatory surround, which is higher on the right than on the left side of the biphasic stimulus. Inhibition is thus stronger on the right side, further reducing the difference, or contrast, in the response of ON- LGNr cells around the luminance transition. However, contrary to what happened with PEF-Center-Surround, no sharpness improvement is generated in this case. This is explained by considering the 1:2 ratio between OFF-LGNi and OFF-RGC. This reduction in spatial resolution impedes the sharpening process, thus avoiding the possibility of generating the side peaks in the OFF-LGNi responses.

Table 5. PIF-Center-Alone: Effect of center-alone arrangement on LGN processing. The LGN response is described in terms of the following parameters: Contrast (C), sharpness (S), Transition Width (TW) and Image Quality (IQ).

| Arrangement	Retinal Kernel	Stimulus	C	S	TW	IQ
PIF-Center-Alone	K_{zero}	HC	79.624	0	0,88	89.939
PIF-Center-Alone	K_{zero}	LC	21.574	0	0,79	27.423
PIF-Center-Alone	K_{medium}	HC	78.754	60.184	2,59	53.623
PIF-Center-Alone	K_{medium}	LC	21.192	19.108	2,58	15.601
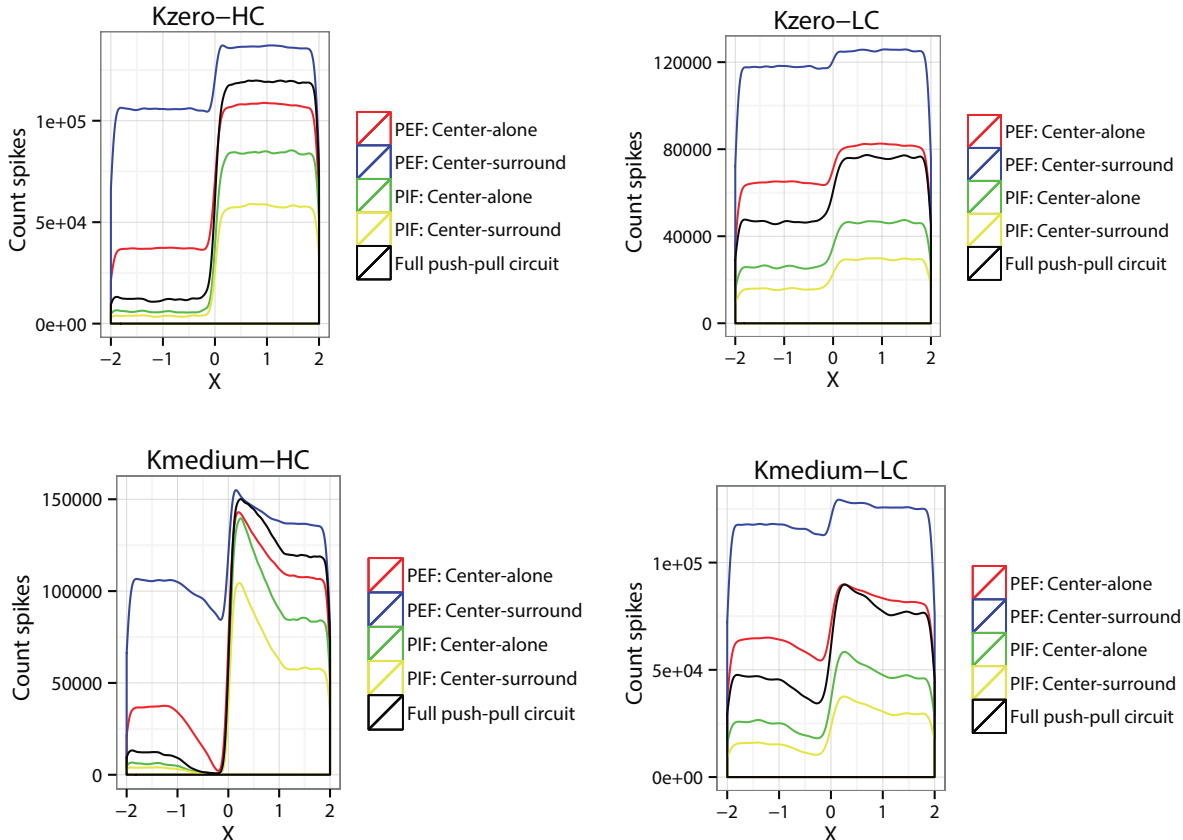
Figure 10. Full push-pull circuit: ON-LGNr responses under the effect of the PEF as well the PIF components of the full circuit are shown. The spike-count is plotted at different spatial locations being measured during a 100 ms interval after stimulus presentation. Kzero-HC and Kzero-LC: ON-LGNr responses after HC and LC stimulus being convolved with K_{zero} kernel. Kmedium-HC and Kmedium-LC: ON-LGNr responses after HC and LC stimulus being convolved with K_{medium} kernel.

Overall, the quality of the image representations with PIF-Center-Surround is markedly reduced. The values shown in Table 5 are clearly lower than those obtained with the Center-Alone arrangement. So, it seems that this circuit would not contribute with an improvement or a recovery of the details lost by the smoothing operation of the Center-Alone effect in PEF.

4.3.3. *Full push-pull circuit*

By adding the opposite-polarity interneuron the full push-pull circuit is completed (Fig. 6). The mutual interaction between LGNi cells of different polari-

Table 6. PIF-Center-Surround: Effect of center-surround arrangement on LGN processing. The LGN response is described in terms of the following parameters: Contrast (C), sharpness (S), Transition Width (TW) and Image Quality (IQ).

Arrangement	Retinal Kernel	Stimulus	C	S	TW	IQ
PIF-Center-Surround	K_{zero}	HC	53.944	0	0,99	54.489
PIF-Center-Surround	K_{zero}	LC	13.967	0	0,75	18.734
PIF-Center-Surround	K_{medium}	HC	54.362	60.185	2,58	40.173
PIF-Center-Surround	K_{medium}	LC	13.679	13.486	2,64	10.297

ties is included, assuming that ON-LGNi interneurons show a similar receptive field arrangement as ON-LGNr cells. The plots showing the output of the Full-push-pull circuit compared to those of other configurations are shown in Fig. 10. The parameters C, S, TW and IQ for all arrangements are presented in Table 6.

The plots show a major improvement in terms of contrast for all input configurations. A key aspect of the Full-push-pull circuit is the asymmetrical inhibition evoked by ON-LGNi on OFF-LGNi cells. This inhibition is stronger where the activity of ON-RGCs is higher, thus causing a disinhibitory effect. The circuit thus preserves the activity profile on the side of the stimulus with the highest luminance, the right side in this case, while reducing the output of the LGN cells with receptive fields on the other side of the luminance border. The disinhibitory mechanism, built from inhibitory synapses between LGNi cells, is similar to a winner-take-all process, in which the most active elements suppress the activity of lower intensity neighbouring units. By removing the inhibition on the right side, the pull works mainly on the left side, thus drastically increasing the slope of the intensity profile at the transition. This results is a substantial increase in contrast (see Table 6) for all the Full-push-pull circuit's inputs. The increase is so dramatic that it overtakes in all cases the contrast values coming out of the Retinal representation. This explains why the full circuit achieves the best IQs in three out of four input configurations. The only exception is the Kmedium-HC input, in which the IQ is on the same range but somewhat lower than for the equivalent PIF-Center-Alone arrangement. This is probably because, in that particular case, TW (2.83) is disproportionally large compared to the evolution of TWs among all the circuits we have tested. If it were on a similar range, Full-push-pull would also yield the best IQ value of all circuit configurations.

However, TWs do not recover the low values obtained in Retina, what explains why the overall IQs of Full-push-pull, except in the case of Kmedium-LC, never approach the quality of the image at the Retinal output.

5. Discussion

Stereotyped mosaics of RGCs encode high-resolution information about a visual image and send it out for further processing to V1 via a relay in the LGN. Both the retina and the LGN form complete and orderly arrangedmaps of visual space. Since LGN relay cells largely outnumber their retinal inputs, the thalamus forms a more densely packed, interpolated map that improves the spatial representation of visual stimuli in the presence of sensor noise (Martínez et al., 2014). Interpolation, however, introduces image blur compromising the quality of edge perception. Using a simple topological model of the retinothalamic connection we have recently found that very specific arrangements of excitation and inhibition within the RF-centers of LGN relay cells can counteract these side effects of interpolation by effectively increasing the slope of the luminance transitions at an edge (Martínez et al., 2014). Our previous work, however, only considered the synaptic structure of the centers of retinal and thalamic RFs; and LGN RFs are spatially complex, showing a double opponent structure. Both in the center and the surround, stimuli of the opposite polarities evoke responses of the opposite sign. Thus, white squares flashed in the RF-center of an On-center cell evoke depolarization while dark squares presented to the same location evoke inhibition (operating as a push-pull mechanism); and the opposite is true for stimuli flashed in the surround. A complementary spatial arrangement of excitatory and inhibitory responses is found in Off-center cells (Hirsch et al., 2015). Excitatory inputs onto each

Table 7. Full push-pull circuit: The response of all arrangements are compared in terms of Contrast (C), sharpness (S), Transition Width (TW) and Image Quality (IQ).

Arrangement	Retinal Kernel	Stimulus	C	S	TW	IQ
Retina	K_{zero}	HC	103.778	0	0,21	494.181
PEF-Center-Alone	K_{zero}	HC	72.764	0	1,13	64.219
PEF-Center-Surround	K_{zero}	HC	29.601	3.020	0,73	44.442
PIF-Center-Alone	K_{zero}	HC	79.624	0	0,88	89.939
PIF-Center-Surround	K_{zero}	HC	53.944	0	0,99	54.489
Full push-pull	K_{zero}	HC	107.201	0	0,99	**108.047**
Retina	K_{zero}	LC	25.277	0	0.36	70.213
PEF-Center-Alone	K_{zero}	LC	18.428	0	0,65	28.026
PEF-Center-Surround	K_{zero}	LC	7.497	1.093	0,80	10.737
PIF-Center-Alone	K_{zero}	LC	21.574	0	0,79	27.423
PIF-Center-Surround	K_{zero}	LC	13.967	0	0,75	18.734
Full push-pull	K_{zero}	LC	29.705	0	0,78	**38.044**
Retina	K_{medium}	HC	103.718	121.900	2.49	90.637
PEF-Center-Alone	K_{medium}	HC	70.563	70.228	2,74	51.389
PEF-Center-Surround	K_{medium}	HC	29.993	40.605	2,54	27.836
PIF-Center-Alone	K_{medium}	HC	78.754	60.184	2,59	53.623
PIF-Center-Surround	K_{medium}	HC	54.362	60.185	2,58	40.173
Full push-pull	K_{medium}	HC	106.204	43.103	2,83	**52.837**
Retina	K_{medium}	LC	25.277	29.800	2.57	21.451
PEF-Center-Alone	K_{medium}	LC	17.006	18.484	2,68	13.218
PEF-Center-Surround	K_{medium}	LC	7.934	8.593	2,04	8.121
PIF-Center-Alone	K_{medium}	LC	21.192	19.108	2,58	15.601
PIF-Center-Surround	K_{medium}	LC	13.679	13.486	2,64	10.297
Full push-pull	K_{medium}	LC	29.301	26.090	2,60	**21.314**

compartment of the LGN RF come from RGCs of the proper center sign (On or Off), whereas inhibition is routed through local interneurons driven by RGCs of the opposite center sign. Using a dynamic spiking model, here we asked how the different cellular components of the retinothalamic circuit, with their full center-surround RFs, might contribute to high-resolution visual processing. Our results show that the LGN uses the analogous of two types of image processing techniques to enhance the fine details in the input that might have been lost in the interpolation process. First, a sharpening process to highlight the edges or luminance transitions. And, second, a contrast stretching operation to amplify and linearize the difference in response to the luminance levels on both sides of a border. Interestingly, we have found that sharpness improvement (or acutance) and contrast enhancement are produced independently by different components of the thalamic RF. Excitation of opposite-sign in both the RF-center and surround interact to improve image acutance, while push-pull inhibition in the RF-center, as previously reported (Martínez et al., 2014; Hirsch et al., 2015), stretches

contrast increasing the dynamic range of visual responses

5.1. *The retinal output*

According to the efficient coding hypothesis, the goal of the retina is to transform the spatially correlated input into a set of decorrelated retinal outputs (Barlow, 1961; Srinivasan et al, 1982; Atick and Redlich, 1992; Dan et al., 1996; Wang et al., 2010). Thus, the best discretization of the continuous DoG function would be the Medium-gain DoG Kernel described in section 3.4, whose sharpening operation reduces the spatial correlation. However, the early visual pathway must also maximize the reliability of the message it sends to the cortex by increasing the mutual information between the visual stimuli and the responses they evoke (Linsker, 1987; Van Hateren, 1992). Taking this into account, the best kernel would be the one that preserved the response as similar as possible to the stimulus; in this case, the Zero-gain DoG kernel. Given this tradeoff between efficiency and reliability, the properties of the retinal kernel could change dynamically depending on the properties of

the input (signal-to-noise, average luminance, contrast, etc) and it could do so independently in different regions of the visual image.

5.2. *Contribution of LGN wiring to image coding*

The upsampling process between Retina and LGN in combination with the interpolation operation through the weighted aggregation of RGC outputs determines that the message of each RGC unit is relayed to a number of LGN units (Martínez et al., 2014). This arrangement distributes the same message throughout different channels, thus adding redundancy and increasing the reliability of the code generated by the LGN. However, the increase of redundancy is significantly constrained by the statistical random wiring of the retinothalamic circuit which favours the diversity of LGN RFs, therefore reducing the dependency among LGN units (Martínez et al., 2014) and thus improving the efficiency of the code. Interestingly, in line with the retinal processing discussed above, the retinothalamic circuit seems to be subject to a similar tradeoff between reliability and efficiency.

5.3. *Sharpening through opposite-sign excitation in LGNr cells*

Sharpening is a popular technique in digital photography and related forms of signal processing to detect and highlight the edges of an image. Various operators and algorithms have been proposed to carry out this operation (Gonzalez and Woods, 2008): first and second-order derivatives, unsharp masking filters, Canny operator, and so on. However, none of them include lateral opposite-sign excitatory interactions. The most popular approach is probably the Marr-Hildreth algorithm that uses a Laplacian of Gaussian functions as a kernel to detect edges or luminance transitions. The discrete version of this function is a matrix with positive coefficients at the center and negative ones at the surround. This concentric positive-negative arrangement of coefficients resembles the spatial profile of the Difference-of-Gaussian function, the paradigm used to model RFs in the retina and the LGN. This similarity supported the idea that neurons in the early visual pathway perform sharpening or edge detection operations. In our model of the retinothalamic network, however,

sharpening is implemented in a different way by the interaction of an excitatory center and an excitatory opposite-sign surround in the push circuit (PEF-Center-Surround, see Fig. 6). This unexpected result is explained by the fact that the excitatory surround is originated from OFF-RGC responses.

5.4. *Image sharpness (acutance) and contrast in the LGN*

The sharpening mechanism discussed in the previous section could be a form of local sharpness enhancement (LSE). On the other hand, our previous results (Martínez et al., 2014) show that opposite-sign (or pull) inhibition in the RF center covers a larger region of visual space than does the excitation (or push), reflecting a highly convergent retinal input onto thalamic interneurons (Montero, 1981; Van Horn et al., 2000) and the fact that LGNr's are supplied by several local inhibitory neurons (Hamos et al., 1985; Crunelli et al., 1988; Blitz and Regehr, 2005; Martínez et al., 2014; Hirsch et al., 2015). Our current results, with this dynamic version of the same model, corroborate that the push-pull structure in the RF center allows for interaction between the On and Off channels in the LGN, increasing the dynamic range of the circuit (Barlow, 1981; Pouille et al., 2009; Martínez et al., 2014), at once removing the redundancy introduced by the interpolation process and enhancing local contrast around the luminance transitions. This operation is conceptually equivalent to local contrast enhancement (LCE) by morphological filters in signal processing and digital photography.

In essence, the LGN operates as a local difference enhancement center. It is important to note that both LCE and LSE operations are carried out locally and to some extent independently of each other. The local nature of these operations would allow, in principle, to adjust the acutance independently in different patches of the visual image. This possibility is very interesting for two main reasons: first, because the slope of luminance transitions can differ markedly in natural images, given the reported independence of luminance and contrast (Mante et al., 2005); and, second, because the structure and relative density of the retinal and LGN mosaics, and hence the strength of the interpolation process, can also vary substantially in different locations of the retinothalamic network (Ringach, 2007; Martínez et

al., 2014). In addition, the independence of LCE and LSE makes it possible to apply them at different temporal windows. If we assume that the push is activated before the pull, the visual cortex would then receive first a version of the visual input with enhanced sharpness followed by a representation with enhanced contrast. Interestingly, both forms of local difference enhancement cannot be easily tuned up together at the LGN, as PIF-Center-Alone tends to remove the positive and negative peaks introduced by PEF-Center-Surround around the luminance transitions. There must be, therefore, a critical interplay between the retina and the LGN in order to optimize the behavior of both circuits.

Images require both high acutance and resolution to be perceived as critically sharp. It seems that the early visual pathway, through a very precise spatial distribution of excitatory and inhibitory circuits, is specially designed to achieve exactly that.

Acknowledgments

Bibliography

1. Alonso, J. M., W. M. Usrey, et al. (2001) Rules of connectivity between geniculate cells and simple cells in cat primary visual cortex. J Neurosci 21:4002-4015.
2. Anishchenko, A., Greschner, M., Elstrott, J., Sher, M., Litke, A.M., Feller, M.B. and Chichilnisky, E.J. (2010) Receptive Field Mosaics of Retinal Ganglion Cells Are Established Without Visual Experience. J Neurophysiol. 103:18561864.
3. Arias, A., Sánchez, E., Martínez, L. (2015) Retinal DoG filters: effects of the discretization process. Artificial Computation in Biology and Medicine. Lecture Notes in Computer Science. 9107:249-257.
4. Atick, J. J., and Redlich, A. N. (1992). What does the retina know about natural scenes?. Neural computation, 4(2), 196-210.
5. Barlow, H. B. (1961). Possible principles underlying the transformations of sensory messages. 217-234.
6. Blitz, D.M., and Regehr, W.G. (2005).Timing and specificity of feed-forward inhibition within the LGN. Neuron 45:917-28.
7. Carandini, M., Horton, J. C., and Sincich, L. C. (2007). Thalamic filtering of retinal spike trains by postsynaptic summation. Journal of Vision, 7(14), 20.
8. Cleland, B.G., Dubin, M.W., and Levick, W.R. (1971).Sustained and transient neurones in the cat's retina and lateral geniculate nucleus.J.Physiol. 217:473-496.
9. Crunelli, V. Haby, M., Jassik-Gerschenfeld, D., Leresche, N., and Pirchio, M. (1988).Cl- - and K+- dependent inhibitory postsynaptic potentials evoked by interneurons of the rat lateral geniculate nucleus. J. Physiol. 399:153-176.
10. Dan, Y., Atick, J.J., and Reid, R.C. (1996). Efficient coding of natural scenes in the lateral geniculate nucleus: experimental test of a computational theory. J. Neurosci.16:3351-62.
11. Eglen, S. J., Diggle, P. J., and Troy, J.B. (2005). Homotypic constraints dominate positioning of on- and off-center beta retinal ganglion cells. Vis. Neurosci. 22:859-71.
12. Enroth-Cugell C, Robson JG. (1966). The Contrast Sensitivity of Retinal Ganglion Cells of the Cat. J Physiol. 187: 517-523.
13. Enroth-Cugell C, Robson JG. (1984). Functional characteristics and diversity of cat retinal ganglion cells. Basic characteristics and quantitative description. IOVS. 25: 250-67.
14. Freund, T. F., K. A. Martin, et al. (1985). Innervation of cat visual areas 17 and 18 by physiologically identified X- and Y- type thalamic afferents. I. Arborization patterns and quantitative distribution of postsynaptic elements.J. Comp. Neurol. 242:263-274.
15. Gauthier, J. L., Field, G. D., Sher, A., Greschner, M., Shlens, J., Litke, A. M., and Chichilnisky, E. J. (2009). Receptive fields in primate retina are coordinated to sample visual space more uniformly. PLoS biology, 7(4), 747.
16. Gewaltig, M.O., Diesmann, M. (2007). Nest (neural simulation tool). Scholarpedia 2(4):1430.
17. Ghosh-Dastidar, S., Adeli, H. (2009). Spiking neural networks. International journal of neural systems, 19(04), 295-308.
18. Gonzalez R, and Woods R. (2008). Digital Image Processing. Prentice Hall.
19. Hamos, J.E., Van Horn, S.C., Raczkowski, D., Uhlrich, D.J., and Sherman SM. (1985).Synaptic

connectivity of a local circuit neurone in lateral geniculate nucleus of the cat. Nature317:618-21.

20. Hirsch, J.A., Wang, X., Sommer, F.T. and Martínez, L.M. (2015) How inhibitory circuits in the thalamus serve vision.Annu. Rev. Neurosci. 38:309-329.

21. Hubel, D.H. and Wiesel, T.N. (1961) Integrative action in the cat's lateral geniculate body. J. Physiol. 155:385-398.

22. Izhikevich, E. M. (2003). Simple model of spiking neurons. IEEE Transactions on neural networks, 14(6), 1569-1572.

23. Kuffler, S.W. (1953) Discharge patterns and functional organization of the mammalian retina. J. Neurophysiol. 16:37-68.

24. LeVay, S., and Ferster D. (1979).Proportion of interneurons in the cat's lateral geniculate nucleus. Brain Res. 164:304-8.

25. Linsker, R. (1988). Self-organization in a perceptual network. Computer, 21(3), 105-117.

26. Liu, Y.S., Stevens, C.F., and Sharpee, T.O. (2009).Predictable irregularities in retinal receptive fields.Proc. Natl. Acad. Sci. USA. 106:16499-504.

27. Madar´sz, M., Gerle, J., Hajdu, F., Somogyi, G., and Tmbl, T. (1978).Quantitative histological studies on the lateral geniculate nucleus in the cat. II. Cell numbers and densities in the several layers. J. Hirnforsch. 19:159-64.

28. Mante, V., Frazor, R.A., Bonin, V., Geisler, W.S. and Carandini, M. (2005) Independence of luminance and contrast in natural scenes and in the early visual system. Nat Neurosci. 8:1690-1697.

29. Martínez, L.M., Molano-Mazón, M., Wang, X., Sommer, F.T. and Hirsch, J.A. (2014) Statistical wiring of thalamic receptive fields optimizes spatial sampling of the retinal image. Neuron 81:943-956.

30. Mastronarde, D.N. (1992). Nonlagged relay cells and interneurons in the cat lateral geniculate nucleus: receptive-field properties and retinal inputs. Vis. Neurosci. 8:407-41.

31. Montero, V.M. (1991).A quantitative study of synaptic contacts on interneurons and relay cells of the cat lateral geniculate nucleus. Exp. Brain Res. 86:7-270.

32. Peters, A. and B. R. Payne (1993).Numerical relationships between geniculocortical afferents and pyramidal cell modules in cat primary visual cortex.Cereb Cortex 3:69-78.

33. Pouille, F., Marin-Burgin, A., Adesnik, H., Atallah, B.V., and Scanziani, M. (2009). Input normalization by global feedforward inhibition expands cortical dynamic range. Nat. Neurosci. 12:1577-85.

34. Ringach, D.L. (2007). On the origin of the functional architecture of the cortex.PLoS One 2, e251.

35. Srinivasan, M. V., Laughlin, S. B., and Dubs, A. (1982). Predictive coding: a fresh view of inhibition in the retina. Proceedings of the Royal Society of London B: Biological Sciences, 216(1205), 427-459.

36. Ruderman, D.L. and Bialek, W. (1992) Seeing beyond the Nyquist limit. Neural Comput. 4:682-690.

37. Stone, J., and Campion, J.E. (1978). Estimate of the number of myelinated axons in the cat's optic nerve. J. Comp. Neurol. 180:799-806.

38. Usrey, W. M., Reppas, J.B. and Reid, R.C. (1999).Specificity and strength of retinogeniculate connections.J Neurophysiol 82:3527-3540.

39. Van Hateren, J. H. (1992). A theory of maximizing sensory information. Biological cybernetics, 68(1), 23-29.

40. Van Horn, S.C., Erisir, A., and Sherman, S.M. (2000).Relative distribution of synapses in the A-laminae of the lateral geniculate nucleus of the cat. J. Comp. Neurol. 416:509-520.

41. Wang, X., Hirsch, J.A., and Sommer, F.T. (2010).Recoding of sensory information across the retinothalamic synapse. J. Neurosci. 30:13567-13577.

42. Wässle, H., Boycott, B.B., and IllingR.B.(1981a). Morphology and mosaic of on- and off-beta cells in the cat retina and some functional considerations. Proc. R. Soc. Lond. B Biol. Sci. 212:177-95.

43. Wässle, H., Peichl, L., and Boycott, B.B. (1981b). Dendritic territories of cat retinal ganglion cells. Nature 292:344-5.

44. Wiesel, T.N. (1959) Recording inhibition and excitation in the cats retinal ganglion cells with intracellular electrodes. Nature 183:264-265.

45. Yeh, C. I., Stoelzel, C.R., Weng, C. and Alonso, J.M. (2009).Functional consequences of neuronal divergence within the retinogeniculate pathway. J Neurophysiol 101:2166-2185.